

Teemu Pukkila

DETRENDED FLUCTUATION ANALYSIS OF HEART RATE VARIABILITY DURING DRIVING

Faculty of Engineering and Natural Sciences
Master's Thesis
May 2021

ABSTRACT

Teemu Pukkila: Detrended fluctuation analysis of heart rate variability during driving
Master's Thesis
Tampere University
Science and Engineering, MSc
May 2021

Wearable heart rate devices are becoming more accurate and widespread in daily life. These devices can measure the time between successive heart beats called RR intervals, which are used to study heart rate variability (HRV). The increased availability of HRV data from different activities has increased the interest in heart rate variability analysis. One worthwhile target for HRV analysis is driving, since it is a very common everyday task that is also both psychically and motorically multidimensional task, and all the physiological effects of driving are not known yet.

The physiology of driving has been studied before, but this thesis focuses on using new technique, that aims to broaden previous knowledge. This technique is called Dynamic detrended fluctuation analysis (DDFA). It is utilized to detect real time changes in the HRV during driving in real world experiments in order to find HRV behavior that is specific to driving. Dynamic detrended fluctuation analysis improves conventional detrended fluctuation analysis by allowing calculation of scaling exponent as function of both the scale and time.

In this thesis multiparameter data with RR intervals from several subjects is utilized. The data includes electrocardiogram from the subjects during both rest and drive sections. This data is used to calculate the HRV measures. Results from the DDFA calculations are compared to the conventional HRV measures and different analysis methods are applied to find differences between the rest and drive sections. Finally, the results are used in classification between the sections. The aim of the classification is to compare the performance of the DDFA measures against conventional HRV measures and examine how well the different sections can be identified from each other.

This thesis showed that utilizing the DDFA method gives valuable additional information about the differences between the rest and drive sections. A reasonable next step would be analyzing larger data sets with clearly labeled sections of different activities in order to make statistically accurate conclusion about the physiology of driving.

Keywords: Detrended fluctuation analysis, driving, heart rate variability, classification

The originality of this thesis has been checked using the Turnitin OriginalityCheck service.

TIIVISTELMÄ

Teemu Pukkila: Dynaaminen trendit poistava flukтуаatioanalyysi sykevälivaihtelulle autoa ajettaessa
Diplomityö
Tampereen yliopisto
Teknis-luonnontieteellinen, DI
Toukokuu 2021

Puettavat sykemittarit ovat entistä tarkempia ja yleisempiä jokapäiväisessä käytössä. Näillä laitteilla pystytään mittamaan peräkkäisten sydämenlyöntien aikavälejä eli RR intervaleja, joita käytetään sykevälivaihteluiden tutkimisessa. Lisääntynyt sykevälivaihteludata erilaisten aktiviteettien aikana on lisännyt kiinnostusta sykevälivaihteluanalyysille. Yksi kiinnostava kohde sykevälivaihtelu analyysille on autolla ajaminen, sillä se on erittäin yleinen ja toisaalta psyykkisesti ja motorisesti moniulotteinen arkielämän aktiviteetti, jonka fysiologisia vaikutuksia ei vielä tarkasti tunneta.

Ajamisen vaikutuksia sykevälivaihteluun on tutkittu jonkin verran aikaisemmin, mutta tämä diplomityö keskittyy uuteen menetelmään, jonka avulla aiempaa tietämystä pyritään syventämään. Menetelmä on nimeltään dynaaminen trendit poistava flukтуаatioanalyysi (Dynamic Detrended Fluctuation Analysis, DDFA). Sitä hyödynnetään sykevälivaihtelun reaaliaikaisten muutosten havaitsemiseen todellisissa ajotilanteissa, tarkoituksena löytää ajamiselle ominaista sykevälivaihteluiden käytöstä. DDFA parantaa perinteistä trendit poistavaa flukтуаatioanalyysiä mahdollistamalla sykevälivaihtelun skaalautumisen tutkimisen sekä itse skaalan että ajan funktiona.

Tässä diplomityössä käytetään moniparametrasta dataa, joka sisältää RR intervallit useilta eri henkilöiltä. Data sisältää koehenkilöiden sydänsähkökäyrän sekä levon, että ajon aikana. Tätä dataa hyödynnetään sykevälivaihteluparametrien laskemiseen. DDFA-tuloksia verrataan perinteisillä sykevälivaihtelumittareilla laskettuihin tuloksiin, ja erilaisia analyysimenetelmiä hyödynnetään lepo- ja ajojaksojen erotteliseksi toisistaan. Lopuksi tuloksia käytetään myös lepo- ja ajojaksojen luokitteluun. Luokittelun tarkoituksena on vertailla DDFA-tuloksia perinteisiin sykeväivaihteluparametreihin sekä tarkastella kuinka hyvin eri jaksot voidaan erottaa toisistaan.

Diplomityö osoittaa, DDFA-menetelmän hyödyntäminen sykevälivaihtelun tutkimisessa antaa arvokasta lisätietoa lepo- ja ajojaksojen eroavuuksista. Looginen seuraava askel olisi analyysi suuremmalla datajoukolla erilaisista ja selkeästi jaotelluista aktiviteeteista, jotta voitaisiin vetää tilastollisesti tarkkoja johtopäätöksiä autolla ajamisen fysiologisista vaikutuksista.

Avainsanat: ajaminen, trendit poistava flukтуаatioanalyysi, sykevälivaihtelu, luokittelu

Tämän julkaisun alkuperäisyys on tarkastettu Turnitin OriginalityCheck –ohjelmalla.

CONTENTS

1.INTRODUCTION	1
2.THEORY	3
2.1 Heart rate variability	3
2.2 Time series analysis.....	4
3.DATA AND PREPROCESSING	6
3.1 Dataset	6
3.2 Data preparation	8
4.METHODS.....	11
4.1 Conventional methods for heart rate variability analysis	11
4.1.1 Time-domain analysis	11
4.1.2 Frequency-domain analysis	12
4.1.3 Detrended fluctuation analysis	13
4.1.4 Implementation of conventional methods	16
4.2 Dynamic detrended fluctuation analysis methods.....	18
4.2.1 Alpha distribution	19
4.2.2 Significance comparison of different scale ranges.....	19
4.3 Classification.....	20
4.3.1 Feature preparation	22
4.3.2 Classification methods	23
5.RESULTS	25
5.1 Conventional methods	25
5.2 Dynamic detrended fluctuation analysis	29
5.2.1 DDFA alpha distribution	33
5.2.2 Significance comparison of different scales.....	35
5.3 Classification.....	38
5.4 Comparison to previous studies	41
6.CONCLUSION	43
REFERENCES.....	44
APPENDIX A: DDFA ALPHA SURFACE PLOTS	49
APPENDIX B: DDFA ALPHA DISTRIBUTION.....	54
APPENDIX C: DDFA ALPHA MEAN AND STANDARD DEVIATION AS FUNCTION OF SCALE.....	73

LIST OF FIGURES

Figure 1: Example of interbeat interval calculated from the R-peaks of the successive heart beats.	4
Figure 2: Example of electrocardiography recording with detected R peaks.	7
Figure 3: Example of removing incorrect peaks from the RR intervals.	8
Figure 4: Example of different steps in calculating detrended fluctuation analysis.	15
Figure 5: Detrending data from the first rest section of Subject09 with smoothness priors method using different smoothing parameters λ	17
Figure 6: Example of binary classification.	21
Figure 7: Visualization of two dimensional principal component analysis calculation.	22
Figure 8: Relative change of HRV time-domain measures.	26
Figure 9: Relative change of HRV time-domain measures between the second and first rest sections.	27
Figure 10: Difference in (a) alpha-1 and (b) alpha-2 between different sections for all the Subjects as boxplots.	27
Figure 11: Relative change of HRV frequency-domain measures.	28
Figure 12: HRV frequency domain measures for each section and Subject separately as a line plot.	28
Figure 13: DDFA alpha values as functions of time and scale presented as a colormap.	30
Figure 14: Zoomed plots of the Subject08 DDFA alpha values in the first rest section.	31
Figure 15: Zoomed plots of the Subject12 DDFA alpha values in the first rest section.	32
Figure 16: Zoomed DDFA alpha values in drive segments for (a) Subject08 and (b) Subject12.	33
Figure 17: Aggregation distribution of DDFA scaling exponents as function of scale for the whole data (upper left) and each segment separately.	34
Figure 18: Subject13 distribution of DDFA scaling exponents as function of scale for the whole data (upper left) and each segment separately.	35
Figure 19: Aggregation box plot of normalized alpha mean values at different scale ranges in rest and drive sections.	36
Figure 20: Aggregation box plot of normalized alpha standard deviations at different scale ranges in rest and drive sections.	37
Figure 21: Mean (upper panel) and standard deviation (lower panel) of the DFA scaling exponent α for Subject04 at different scales.	38
Figure 22: Area under curve (AUC) values for different features.	39
Figure 23: Correct classification proportions of the support vector machine classification algorithm.	40

LIST OF SYMBOLS AND ABBREVIATIONS

ANS	Autonomic nervous system
AUC	Area under curve
CV	Coefficient of variation
DDFA	Dynamic detrended fluctuation analysis
DFA	Detrended fluctuation analysis
ECG	Electrocardiogram
EMG	Electromyogram
GSR	Galvanic skin response
HR	Heart rate
HRV	Heart rate variability
IBI	Interbeat interval
NN	Normal-to-normal
PCA	Principal component analysis
PNS	Parasympathetic nervous system
PSD	Power spectral density
ROC	Receiver operating characteristics
RRI	RR interval
SDNN	The standard deviation of the IBI of normal sinus beats
SNS	Sympathetic nervous system
SVM	Support vector machine
α	Detrended fluctuation analysis scaling exponent
λ	Smoothing parameter
$B(i)$	Interbeat time series
$B(i)_{stat}$	stationary Interbeat time series
$\langle B \rangle$	Arithmetic mean of B
C	Grid search parameter
Cov	Covariance
D_2	The second-order difference matrix
$F(n)$	Fluctuation function
\tilde{F}_t	Logarithmic fluctuation function
H	Hurst exponent
h	time step
h_-	Logarithmic backward difference

h_+	Logarithmic forward difference
I	Identity matrix
$l(s)$	Segment lengths in DDFA calculations
\log	Base-10 logarithm
$P_x(\omega)$	Power spectral density
τ	Lomb-scargle periodogram inner function
ω	Angular frequency
$y(k)$	Integrated time series
$y_n(k)$	Values of linear fits in DFA calculations
y_t	Observation at time t
X_j	Time series

1. INTRODUCTION

Wearable heart rate (HR) devices are becoming highly accurate and widespread in daily life. These devices can measure successive heart beats called RR intervals, which are used to study heart rate variability (HRV). The increased availability of HRV data from different activities has increased the interest in HRV analysis. It has been previously applied to detect cardiac autonomic neuropathy in cardiology, to study stress and recovery during physical activity and to detect stress [1-3]. These studies have established the possibilities of HRV analysis in understanding the physiology behind these complex physiological functions.

Driving is a worthwhile target for HRV analysis since it is a complex and common task. In driving, different sensory, motor and cognitive functions are needed simultaneously [4]. Due to traffic collisions, driving is also a dangerous activity and about 90% of the collisions are related to driver errors [5]. Finding and detecting physiological changes during driving could have relevant applications in road traffic safety. Therefore, studying and learning human behavior during driving is an important research topic. The physiology of driving has been studied before, but this thesis focuses on new dynamic methods of analyzing HRV during driving. These new methods and easy availability of HRV data make this approach to analysis sensible.

Conventionally, HRV has been studied with time domain measures calculated from the RR intervals and frequency domain measures calculated from the power spectrum of the time series. HRV has also been studied with nonlinear methods quantifying the complexity and unpredictability of the RR intervals. Detrended fluctuation analysis (DFA) is a commonly used nonlinear method describing HRV behavior on different time scales [6]. This thesis focuses on using new method called dynamic DFA (DDFA). It can detect real time changes in the HRV during driving to find HRV behavior that is specific to driving [7]. DDFA improves conventional DFA by allowing the calculation of the scaling exponent as functions of both scale and time. DDFA has been previously used to study running and sleeping with promising results [7, 8].

In this thesis, multiparameter data with RR intervals from several subjects while they are resting in the car, and while they are driving, are used to calculate the HRV measures. The results from the DDFA calculations are compared to the conventional HRV measures. Furthermore, different analysis methods are applied to find differences between the rest and drive sections. Finally, the results are used to classify these sections. The aim of the classification is to compare the performance of the DDFA measures against conventional HRV measures and examine how well the different sections can be identified from each other.

This thesis begins with the basic theory of HRV and time series analysis in Ch. 2. This is followed by describing the dataset and explaining the preprocessing methods for the data in Ch. 3. Chapter 4 focuses on the theory and implementation of analysis methods. In Ch. 5 the calculated results are presented and described. Finally, Ch. 6 concludes the thesis by briefly discussing the results and giving a further outlook.

2. THEORY

2.1 Heart rate variability

A human heart is a complex system and there are many factors affecting the heartbeat. Even in homeostasis a healthy heart has many complex and constantly changing fluctuations in the RR intervals. This constantly changing behavior allows the heart to quickly adjust to environmental and psychological changes affecting homeostasis [6, 9]. The heart consists of two atria and two ventricles that are mainly controlled by the sinoatrial node (SA) and atrioventricular (AV) node. An electrocardiogram (ECG) records the electrical activation caused by SA and AV nodes and allows to study the electrical activity of the heart. Typical ECG recordings contain multiple peaks from different phases of the heartbeat. R-peaks of the QRS complex shown in Fig. 1 are generally the most prominent features in the ECG and determine the heartbeat [10]. The fluctuation in time between subsequent beats, called interbeat intervals (IBIs), is called HRV.

Even when the average HR is relatively stable, there is variability in the IBIs. On beat-to-beat basis the irregular behavior of the RR intervals (RRI) is clearly visible from the RR interval time series [9]. These fluctuations of the HR on different time scales are caused by heart-brain interactions and dynamic nonlinear autonomic nervous system (ANS) [6]. The changes in HRV can provide valuable information about changes in ANS through the parasympathetic nervous system (PNS) and sympathetic nervous system (SNS). The PNS is dominating at rest conditions, conserving and storing energy, while maintaining the basic body functions such as digestion. The sympathetic nervous system on the other hand is dominating in “fight-or-flight” reactions and during physical exercise. It is preparing the body for physical activity by increasing blood flow into skeletal muscles [11]. PNS lowers the HR and SNS increases it. Normally, there is a dynamic relative balance between the nervous systems causing homeostasis [10].

HRV measures can indicate health problems and changes in physiological states. A small HRV is associated with health problems and it is also observed in patients with autonomic dysfunction, for example in anxiety and stress [3, 10]. On the other hand, too much variability has negative effects on physiological functioning and energy utilization [10]. HRV can be utilized as a marker for diseases and adaptability to changing social and environmental demands [10].

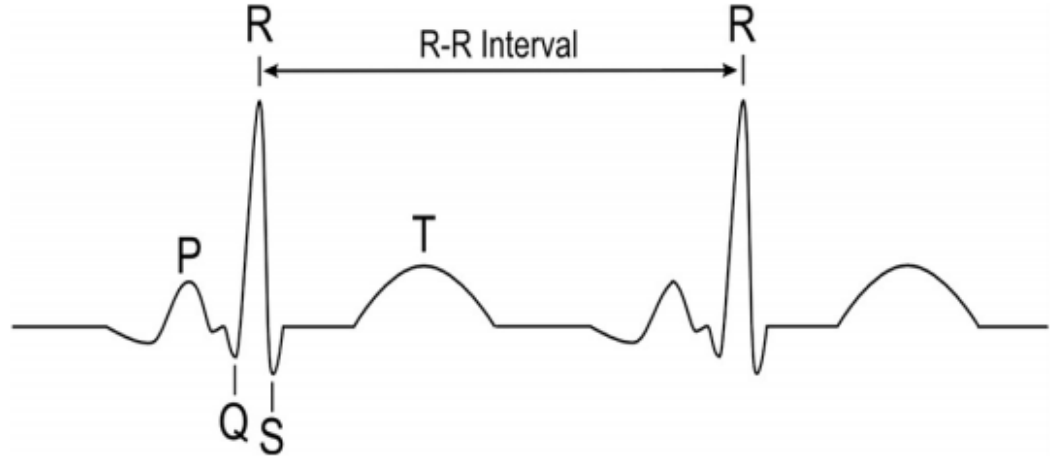


Figure 1: Example of interbeat interval calculated from the R-peaks of the successive heart beats. Figure depicted from Ref. [12].

2.2 Time series analysis

A time series is an ordered list of values with time stamps. Different types of time series can represent information from stock market indices in finance to temperature charts in climatology and so forth, including various physiological signals [13]. Time series X can formally be expressed as

$$X = \{x_1, x_2, x_3, \dots, x_T\}, \quad (2.1)$$

where x_t is the value at time point t , and T is the number of time points [14]. There are many different types of time series and different ways to classify them. The time points can be regularly or irregularly spaced. Regularly spaced time series have a constant time interval between the points of observation, and they are easier to analyze than irregular time series. However, missing observations can cause irregularity into regular time series. Different techniques have been developed to solve problems with irregularity and missing data, and in this thesis these problems are solved with Lomb-Scargle periodogram [15]. The time can also be a continuous variable, but here the focus is on time series with discrete time values [13].

Stationarity is another way to classify time series. In stationary time series the statistical characteristics are preserved over time, and there is an autocovariance function

$$y(h) = \text{Cov}(y_t, y_{t+h}) \quad (2.2)$$

between two observations y_t and y_{t+h} that does not depend on time. Stationary time series have a constant mean and variance in time. On the other hand, nonstationary time series exhibit features like trends and seasonality that change the mean and variance of

the time series over time. Some of the conventional methods developed for analyzing time series are only viable for stationary data, but most real-life time series exhibit nonstationarities. Therefore, nonstationary data needs to be transformed into stationary form [13]. This transformation into stationary time series can be achieved by removing the nonstationary trends with detrending methods [16].

Using the values measured at different time points t is not the only way to create time series from data. Sometimes other values, such as differences between successive measured values calculated as $x_t - x_{t-1}$ can provide more information than the measured values themselves [14].

The time series analysis methods can be split into linear and nonlinear methods. In linear methods, the relationship between variables can be represented as a straight line [6]. The methods and analyses used in this thesis are presented in Ch. 4.

3. DATA AND PREPROCESSING

This chapter focuses on the measurement data obtained from Physionet database [17]. The first section describes the measurements behind the dataset. The second section focuses on the preprocessing methods of the data to get the desired time series for further analysis.

3.1 Dataset

Data used in this thesis are originally published in “*Detecting Stress During Real-World Driving Tasks Using Physiological Sensors*” [18] and they are stored in the public Physionet database “*Stress Recognition in Automobile Drivers*” [17]. The database contains multiparameter recordings from healthy volunteers while they are driving a car on open roads [17].

The experimental protocol included 15 min resting periods before and after the driving activity as the baseline measurements. During the rest periods the subjects sat in the car with their eyes closed, while the car was idling in the garage. The actual drive was a 32-kilometer loop on open roads in Boston. The drive included periods of both city and highway driving on a predefined route. To keep the drives consistent, a map of the route was shown to subjects beforehand, and instructions were given. There was also an instructor on the backseat of the car to respond to possible questions. All drives were completed during midmorning or midafternoon during light traffic, but since the experiment was on open roads the traffic conditions affected the total durations of the measurements. They ranged from 65 to 93 minutes [17, 18].

The physiological measurements included galvanic skin response (GSR), electrocardiogram (ECG), electromyogram (EMG) and chest cavity expansion with an elastic Hall effect sensor for respiration. The GSR was measured from the hand and leg with electrodes. In the ECG recording, a modified lead II configuration was used to maximize the R-peak detection. The EMG was measured from the trapezoid muscle. The sampling rates of the signals captured by the FlexComp analog-to-digital converter are shown in Table 1 [18]. The ECG signal was recorded with high sampling rate of 496 Hz providing smooth and accurate results.

Table 1 Sampling rates of the sensors used in the measurement.

sensor	sampling rate (Hz)
GSR	31
ECG	496
EMG	15.5
Respiration	31

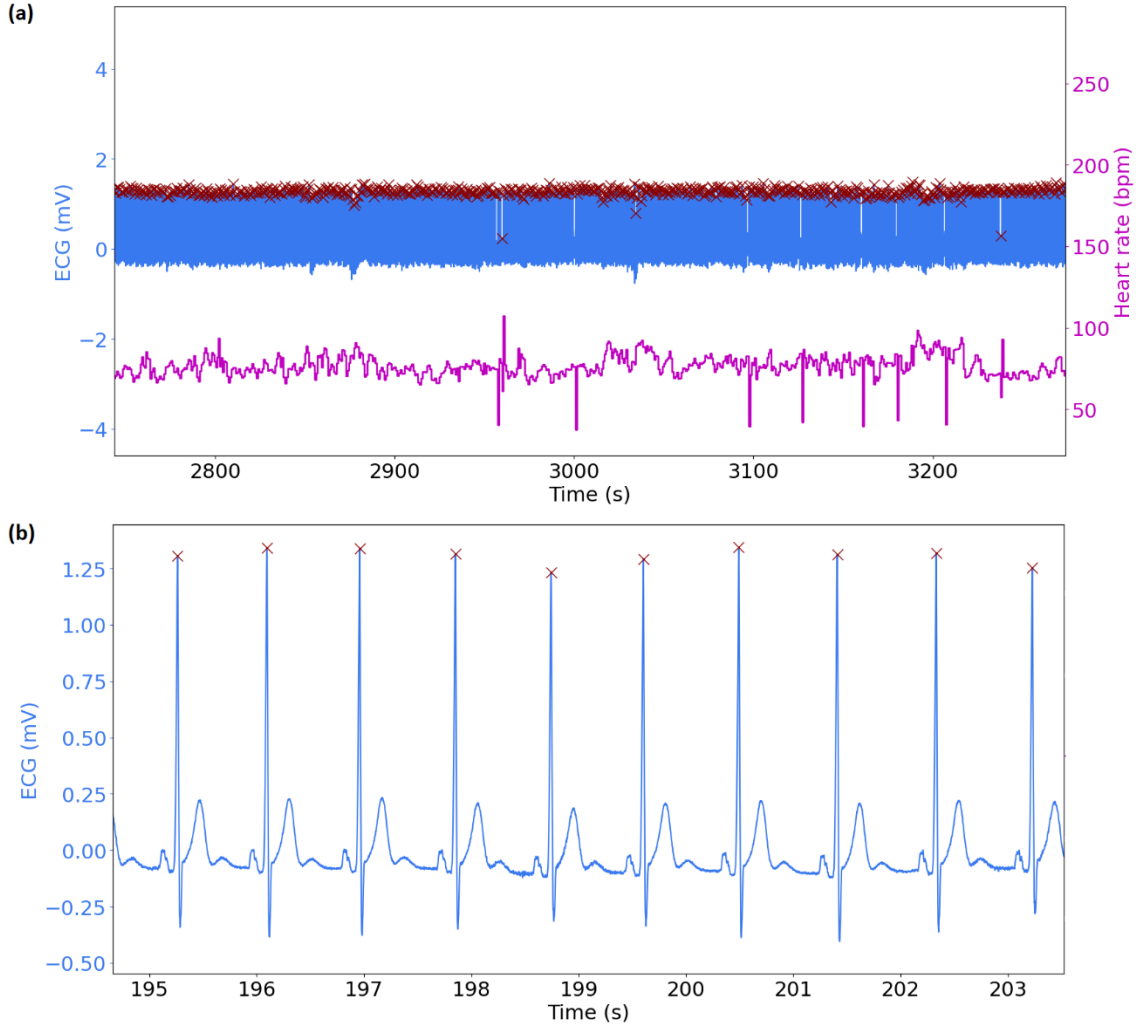


Figure 2: Example of electrocardiography recording with detected R peaks. (a) ECG recording of the whole sample including all the detected R peaks and instantaneous heart rate calculated from RR intervals. (b) Nine-second period of the ECG signal showing the quality of the ECG and the peak finding algorithm.

The dataset contains 16 complete records, and the 17th record is split into two halves [17]. Records 13 and 14 are identical, so only one of them is used. Also record 5 is missing some ECG data in the middle of the experiment. Therefore, records 5 and 17 are not included in the HRV calculations that compare or classify different sections. In addition, some of the recordings are missing some of the sensor data or they have poor quality.

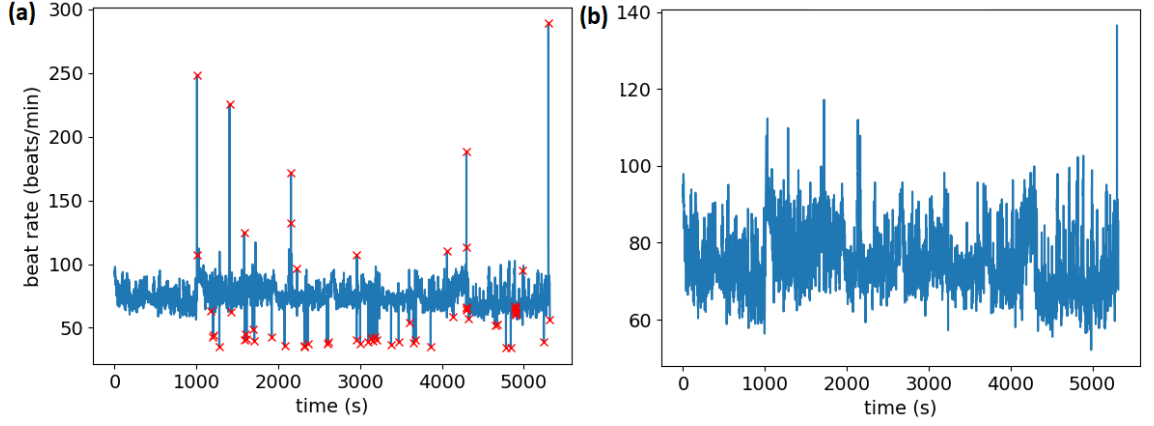


Figure 3: Example of removing incorrect peaks from the RR intervals. (a) All the RR intervals, where the red crosses mark the false peaks detected by the algorithm. (b) Fixed RR intervals, where the false peaks have been removed.

3.2 Data preparation

The data quality of the ECG recordings is very good for a large fraction of the samples, and the calculated heart rates look plausible as shown in Fig. 2. The R-peaks are marked with red crosses and the HR with a purple line. There are some marked peaks that are clearly incorrect as can be seen in their position on the y-axis, as well as in the abnormal behavior of the HR at the same time.

The R-peaks were detected with “WFDB” software package for Python using the “GQRS” algorithm [19]. The detection was limited to finding peaks between the maximum and minimum beat rates to filter out the number of incorrect peaks detected by the algorithm. The maximum beat rate was chosen to be 230 BPM and minimum 20 BPM. These values are the default ones that are loose enough not to miss any real beats but still removing the unrealistic values for healthy subjects. The labeled beats were manually inspected to ensure that the algorithm worked well. The detection algorithm worked as expected and only occasional incorrect peaks were detected. These incorrect peaks usually occurred when the recording had significant noise during one of the peaks.

Additional incorrect RR intervals were removed from the RR interval time series with an algorithm checking if the difference between the mean of the last five real RR intervals and the following RR interval exceeded a chosen threshold value. This algorithm was also manually inspected, and the parameters were corrected to ensure that only the incorrect RR intervals are removed from the time series. Based on manual inspections 250 ms was chosen as the threshold value. The incorrect RR intervals were removed without modifying the time stamps of the original time series to keep the correct peak occurrence times. The peak removing algorithm is only removing technical artifacts, e.g., missed beats, and not utilizing ECG to remove peaks based on physiological criteria. Technical artifacts, such as missed beats and unusually high HR values, can be detected

and removed from the time series with reasonable certainty without profound study of the physiological artifacts. The removal of the technical artifacts has also been utilized in previous DDFA calculations [7].

Figure 3 visualizes the peak removing algorithm. Most of the removed RR intervals are missed beats. Detecting these missed beats is straightforward, since they result into spikes that have the heart rate reduced to approximately half of the normal values. In Fig. 3 (a) the missed beats resulted into a beat rate of about 40 BPM, making them easily detectable from the overall trend of the HR.

As can be seen in Fig. 3 (b) there are still some suspicious peaks in the fixed RR intervals. These peaks are not single unusual RR intervals, but they consist of several RR intervals in a row that differ greatly from the intervals close to them. These successive unusual RR intervals were not removed from the time series, since isolating them is not straightforward, and removing multiple successive beats would affect the continuousness of the time series. The last RR intervals in Fig. 3 exemplify these successive unusual RR intervals. In Fig. 3(a) the HR is over 250 BPM but even when this peak is removed there are still RR intervals increasing the HR to over 130 BPM in Fig. 3 (b) even though the difference between the successive RR intervals does not exceed 250 ms.

Table 2: Number of removed incorrect RR intervals and their proportion of the sample.

Subject	Number of removed RR intervals	Total number of RR intervals	Percentage of removed RR intervals
01	326	5680	5.7
02	208	5832	3.6
03	127	6930	1.8
04	129	6004	2.2
05	53	5760	0.9
05a	25	2262	1.1
05b	28	3497	0.8
06	74	7243	1.0
07	61	6634	0.9
08	65	5191	1.3
09	51	4910	1.0
10	107	6406	1.7
11	138	5217	2.7
12	42	5120	0.8
13	69	7691	0.9
14	69	7691	0.9
15	44	4923	0.9
16	248	6418	3.9
17a	19	2097	0.9
17b	20	1817	1.1

Table 2 shows the number of removed RR intervals and their percentages from the total number of intervals. Most of the subjects had only a few abnormal peaks in the RR data, and the percentage of removed intervals is small, around 1 %. But there were also a few subjects with substantial regimes of abnormal intervals leading to a significant percentage of removed intervals, especially subjects 01, 02 and 16. The missing RR intervals can have an impact to the results calculated from the time series, but in this thesis, as most of the samples have a reasonably small amount of RR intervals missing, the influence of this is not studied further.

4. METHODS

This chapter introduces the time-series methods used to analyze the RR intervals. The first section focuses on the conventional methods used in the HRV analysis. This creates a basis for further analysis with nonlinear methods described in the second section. All the methods were implemented with Python.

4.1 Conventional methods for heart rate variability analysis

This section describes the conventional methods of HRV analysis that are used in this thesis and their implementations. The methods used are: time domain analysis, frequency domain analysis and conventional DFA.

4.1.1 Time-domain analysis

HRV time-domain measures quantify the amount of variability in the RR intervals time series. Table 1 introduces all the time-domain measures utilized in this thesis [6].

Table 1 *Time-domain measures for heart rate variability.*

Abbreviation	Unit	Description
mRR	ms	mean value of the RR intervals
stdRR	ms	standard deviation of the RR intervals
cvRR	ms	coefficient of variation, defined as standard deviation divided by the mean value
rmssdRR	ms	root mean square of successive RR intervals differences
pRR20	%	percentage of successive RR intervals that differ by more than 20 ms
pRR50	%	percentage of successive RR intervals that differ by more than 50 ms

The mean value of RR intervals (mRR) describes the average time between successive heart beats. It is inversely proportional to the average HR, which makes it a widely used measure. However, the HR varies a lot due to, e.g., mental stress and physical activity [20]. The mean value can be calculated from different lengths of recording based on the situation. For example, during alternating intensities of physical activity shorter segments are beneficial. On the other hand, the mean HR while sleeping can be monitored in longer periods of time.

One of the simplest ways to measure variation in RR intervals is the standard deviation of RR intervals (stdRR) usually measured in long term 24h recordings or short term (5min) recordings. StdRR measured from normal-to-normal (NN) intervals, which are RR intervals with all the artificial peaks removed, is called the standard deviation of the IBI

of normal sinus beats (SDNN). It is the measurement standard for stratification of cardiac risk in long term recordings [6, 21]. Having a low SDNN value over 24h recording increases the risk of dying after having a heart attack. SDNN values under 50 ms are considered to be unhealthy and values over 100 ms are considered healthy. The risk of mortality during a follow-up period of 31 months after heart attack is 5.3 times lower for people with healthy SDNN compared to those with unhealthy SDNN [21, 22].

Both sympathetic nervous system (SNS) and parasympathetic nervous system (PNS) affect SDNN, but this connection is dependable on the measurement conditions. In short term recordings the main source of variation is parasympathetically-mediated respiratory sinus arrhythmia (RSA), which is synchrony of HRV and respiration [6, 10, 23].

The coefficient of variation (CV) of RR intervals, defined as a quotient of stdRR and mRR is used together with mRR to detect fatigue in sports [24]. CvRR represents perturbations in HRV that can be caused by, for example, stress and recovery [25].

RmssdRR, pRR50 and pRR20 are measures that are calculated from the differences between successive heart beats. First, each successive time difference between RR intervals is calculated and then the measures are calculated from these new time series. pRR50 is defined as the percentage of successive heart beats that differ by more than 50 ms. Respectively, pRR20 is the percentage of successive heart beats that differ by more than 20 ms. PRR50 has correlations with PNS activity [26]. RmssdRR is obtained by first calculating the squares of successive heart beats and then the mean of the squared values [6]. The square root of this mean is rmssdRR. These successive heartbeat measures estimate high-frequency correlations, and they are correlated with each other. RmssdRR is the most common of these measures, since it usually gives the best estimate of the RSA [6, 10].

4.1.2 Frequency-domain analysis

HRV frequency-domain or power spectral density (PSD) analysis can be used to study the power distribution of the signal as function of frequency [10]. The frequency domain measures used in this study are presented in Table 2.

Table 2 Frequency-domain measures for heart rate variability [6].

Abbreviation	Unit	Description
HF power	ms ²	Absolute power of the high frequency band (0.15-0.4 Hz)
LF power	ms ²	Absolute power of the low frequency band (0.04-0.15 Hz)
LF/HF	%	Ratio of LF-to-HF power

Absolute powers in both LF and HF bands are calculated by first transforming the time series from time domain into frequency domain and then integrating the power spectral density (PSD) over the bands [21]. The LF power is normally recorded for periods longer than two minutes and it is produced by both the PNS and SNS activity, but in resting conditions it is mainly reflecting the baroreflex activity [6, 21].

The HF power band, also known as respiration band, is normally recorded for periods longer than one minute and it reflects the PNS activity [6]. HF band power is also correlating with rmssdRR and pRR50 time domain measurements, and it corresponds to HRV caused by respiratory cycles [21]. The HR is normally slowing down during expiration and increasing during inspiration. The normal respiration rates at rest are between 12 and 15 times per minute so they fall into the HF band [6, 27].

The LF/HF ratio is a widely used but controversial measure. It was intended to estimate the PNS and SNS activity, assuming that PNS is generated by HF and SNS by LF bands. Based on this model, a high LF/HF ratio indicates sympathetic dominance, whereas a low LF/HF ratio indicates parasympathetic dominance. But since the LF and HF bands are not caused purely by the SNS and PNS activity, and their interactions are complex and nonlinear, the LF/HF ratio has gained some criticism. Also, the testing conditions and the length of the measurements can affect the LF/HF ratio [6].

4.1.3 Detrended fluctuation analysis

Since HRV is irregular and nonstationary, nonlinear methods are useful tools to study it [6]. Detrended fluctuation analysis (DFA) was first developed by Peng et al. [28] to study long range power-law correlations of DNA sequences, but it was then quickly extended to study long-range correlations in nonstationary physiological time series [29].

The problem in conventional fluctuation analysis is that they do not generally work well with nonstationarities and trends. The nonstationarities in the signal can also be caused by environmental conditions that have little to do with the actual system [29]. DFA gives a solution to this problem with a well understood method that takes into account the nonstationarities and trends. For different noisy and nonstationary signals, DFA is found to be working better than conventional fluctuation analysis methods for a wide range of scales and different nonstationarities [30, 31].

The algorithm for calculating DFA for interbeat time series of length N consist of the following steps [29, 32].

Step 1: Integrate the time series $B(i)$ into series

$$y(k) = \sum_{i=1}^k (B(i) - \langle B \rangle), \quad (4.1)$$

where $\langle B \rangle$ is the mean value of the original time series $B(i)$.

Step 2: Split $y(k)$ into equally wide non-overlapping segments of length n . The trend in each of these boxes is then calculated by least-squares fitting a polynomial of first order into the segments. The y-coordinates of these lines are denoted as $y_n(k)$, and the integrated time series $y(k)$ is detrended by subtracting the linear trend from the time series.

Step 3: Calculate the squared fluctuations $F_w^2(n)$ for each window w as the variance from local trend with the equation

$$F_w^2(n) = \frac{1}{N} \sum_{k \in w} (y(k) - y_n(k))^2. \quad (4.2)$$

Step 4: Then the fluctuation function is calculated by averaging over the windows and taking the square root of this averaged value. This fluctuation function is given by

$$F(n) = \sqrt{\langle F_n^2(n) \rangle}. \quad (4.3)$$

The calculations of the fluctuation function $F(n)$ are repeated for different scales (lengths of the segment n), and the logarithm of the average fluctuation function $\log(F(n))$ is plotted as function of the logarithmic scale $\log(n)$.

Step 5: Determine the scaling exponent α from the slope of the log-log graph as [29, 32, 33]

$$F(n) \sim n^\alpha. \quad (4.4)$$

Figure 4 presents an example of a time series and the determination of the short-scale scaling exponent α from the log-log graph.

The obtained scaling exponent describes the autocorrelation properties of the signal [34]. The interpretation of the exponent is a generalization of Hurst exponent (H), where $\alpha = H$ for values $0 < \alpha < 1$, and $\alpha = 1 + H$ for larger values of $\alpha > 1$ [7, 29, 35]. These interpretations for α are presented in Table 3.

When studying HRV, the scaling exponent is conventionally calculated separately for short scales $4 \leq n \leq 16$ and long scales $16 \leq n \leq 64$. They are called α_1 and α_2 , respectively [6, 29]. The reasons behind this separation of the scaling exponent arises from commonly observed differences between healthy and pathologic data. When calculating DFA the log-log graph shows crossover points between scales 10 and 20 for

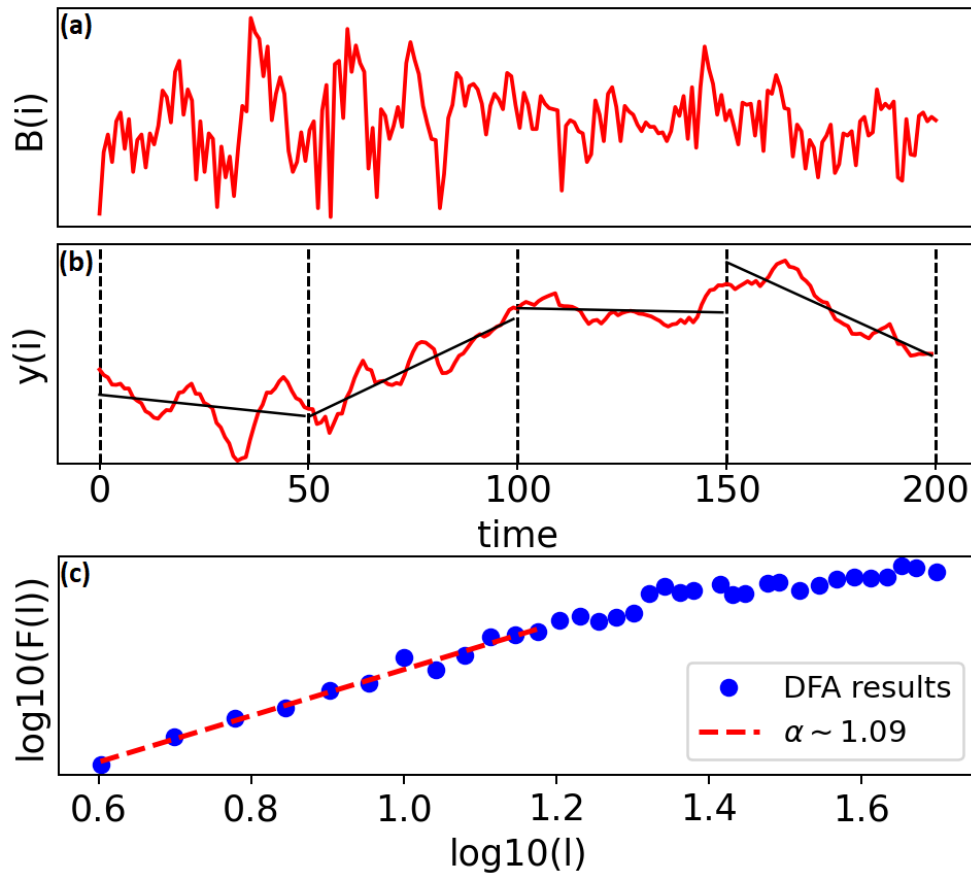


Figure 4: Example of different steps in detrended fluctuation analysis. (a) Example of HRV time series from the start of Subject01 first rest section. (b) Integrated time series from (a) with least-squares fitted first order polynomial into non overlapping windows of length 50. (c) Determination of the short-scale scaling exponent with detrended fluctuation analysis.

Table 3 Interpretation of the scaling exponent α of detrended fluctuation analysis. [7]

Scaling exponent	Interpretation	Stationarity
$0 < \alpha < 1/2$	anti-correlated	stationary
$\alpha = 1/2$	white noise	
$1/2 < \alpha < 1$	correlated	
$\alpha = 1$	$1/f$ (pink) noise	
$1 < \alpha < 3/2$	anti-correlated increments	nonstationary, stationary increments
$\alpha = 3/2$	Brownian noise	
$3/2 < \alpha < 2$	correlated increments	

both healthy and pathologic data. The scaling exponents in the regions above and below these crossover points are typically different [29].

4.1.4 Implementation of conventional methods

Algorithm 1 explains how the time domain measures are calculated in practice for the experimental protocol described in section 3.1.

Algorithm 1 Time domain measures from the rest and drive sections

1. Split RR intervals into the rest and drive sections.
 2. Calculate the time domain measures in each section using rolling window segments with segment length of 300 and step of 10 RR intervals.
 3. Calculate the means of these rolling window segments to get a single value for each measure in each section.
 4. Calculate the percentage change of measures between different sections.
 5. Combine the percentage changes of all subjects into a group and present them as a box plot.
-

The segment length of 300 RR intervals was chosen as it corresponds to the 5 min short term recording at HR of 60 BPM. A segment step of 10 RR intervals was used to have a significant overlap.

The frequency domain measures were calculated with the same algorithm as the time domain measures. But since the RR intervals are not evenly spaced, the calculation of the frequency domain measures requires some extra steps. In particular, a Fourier transform can only be used for evenly spaced series or, in other words, we need a constant sampling rate. Since the RR intervals are unevenly spaced, the time series needs to be modified to get an even sampling rate, or we need to use some other transformations.

A Lomb-Scargle periodogram [36] was used for calculating the PSD. It is the most often used algorithm for unevenly spaced data. The basic implementation of the algorithm for calculating PSD $P_x(\omega)$ for time series X measured at times t_j can be expressed as

$$P_x(\omega) = \frac{1}{2} \left\{ \frac{[\sum_j X \cos \omega(t_j - \tau)]^2}{\sum_j \cos^2 \omega(t_j - \tau)} + \frac{[\sum_j X \sin \omega(t_j - \tau)]^2}{\sum_j \sin^2 \omega(t_j - \tau)} \right\} \quad (4.5)$$

and

$$\tau = \left(\frac{1}{2\pi} \right) \tan^{-1} \left[\frac{\sum_j \sin 2\omega t_j}{\sum_j \cos 2\omega t_j} \right], \quad (4.6)$$

where ω is the angular frequency [36]. Townsend [15, 37] has refactored these equations into a form that is faster to calculate. We use this faster algorithm in the thesis.

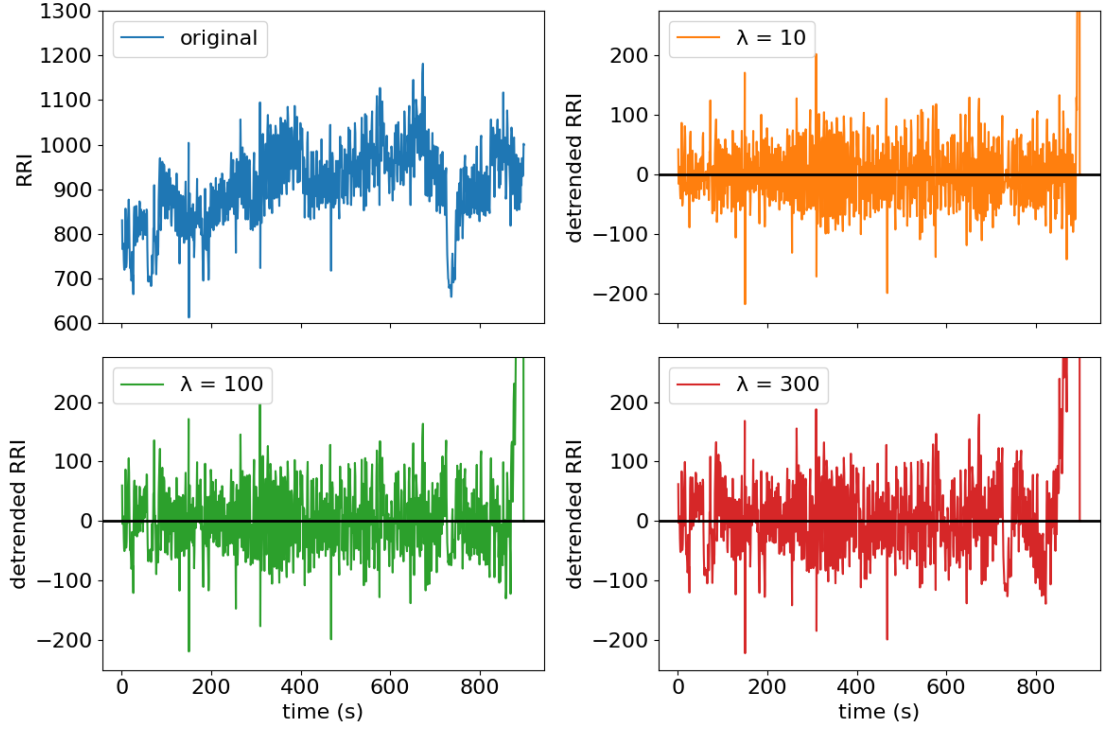


Figure 5: Detrending data from the first rest section of Subject09 with smoothness priors method using different smoothing parameters λ .

The Lomb-Scargle periodogram also requires the data to be at least weakly stationary. In this thesis the data was detrended with a method designed specifically for HRV analysis by Tarvainen et al. in Ref [16]. The method is called “smoothness priors method” and the stationary time series $B(i)_{\text{stat}}$ can be written as

$$B(i)_{\text{stat}} = [I - (I + \lambda^2 D_2^T D_2)^{-1}] B(i), \quad (4.7)$$

where D_2 is the second-order difference matrix

$$D_2 = \begin{pmatrix} 1 & -2 & 1 & 0 & \cdots & 0 \\ 0 & 1 & -2 & 1 & \ddots & \vdots \\ \vdots & \ddots & \ddots & \ddots & \ddots & 0 \\ 0 & \cdots & 0 & 1 & -2 & 1 \end{pmatrix}, \quad (4.8)$$

I is the Identity matrix and λ is a smoothing parameter. Larger smoothing parameter values reduce the cut-off frequency of the filter. Figure 5 shows the detrended data with different smoothing parameters. In this thesis $\lambda = 10$ is used as the smoothing parameter based on the quality of the detrending with different parameters. In order to keep the low frequency components of the HRV the smoothing parameter is chosen to be small, but large enough to detrend the data smoothly [16].

For the DFA measures, α_1 and α_2 scaling exponents were calculated for each rest and drive section of the experiment described in Ch. 3. The values of the scaling exponents were then compared to each other and presented in similar box plots as the other conventional methods.

4.2 Dynamic detrended fluctuation analysis methods

This section introduces dynamic detrended fluctuation analysis (DDFA) and the different methods of analyzing the DDFA results calculated from the data. We focus on finding differences in the scaling exponents between the drive and rest sections of the measurement.

Real-world HRV data has a lot of nonstationarity, and the ordinary short- and long-range DFA scaling exponents are generally not sufficient. DDFA was developed to overcome these shortcomings. DDFA determines the scaling exponent as function of time and scale with high temporal resolution [7].

The long- and short-range scaling exponents based on the different crossover patterns between healthy and pathologic HRV data discovered by Peng et al. [29] are generally not sufficient to characterize different physiological phenomena in detail [29]. In order to calculate the scaling exponent as function of scale, the local noise affecting local slope variability needs to be small enough for calculating accurate alpha values. In ordinary DFA, large intermittent bursts and strong long-range correlations cause noise affecting local slope variability [38]. Effects of the local noise can be reduced by utilizing overlapping segments in the DFA calculations. The overlapping DFA segments are moved point-by-point one RR intervals at a time. In contrast, in ordinary DFA each segment does not contain RR intervals from the previous segment. The overlapping windows method is more accurate but also has a drawback with increased computational cost [38].

Performing the calculations in moving temporal segments allows dynamic examination of the time series. Furthermore, allowing different dynamic segment lengths for different scales results in better temporal resolution for smaller scales. The segment lengths $l(s)$ as a function of scale s are calculated simply as [7]

$$l(s) = as, \quad (4.9)$$

where a is a constant that can be chosen separately for each scale. Small values of a increase the resolution but also the noise of the results. The value $a = 5$ has been previously found to yield good results. It is also used in all the DDFA calculations in this thesis [7].

The dynamic scaling exponents $\alpha(t, s)$ are calculated using the finite difference method as

$$\alpha(t, s) \approx \frac{[h_-^2 \tilde{F}_t(s+1) + (h_+^2 - h_-^2) \tilde{F}_t(s) - h_+^2 \tilde{F}_t(s-1)]}{[h_- h_+ (h_+ + h_-)]}, \quad (4.10)$$

where $h_- = \log(s) - \log(s-1)$ and $h_+ = \log(s+1) - \log(s)$ are the logarithmic backward and forward differences. \tilde{F}_t is the logarithm of the fluctuation functions

computed for each segment at scales $\{s - 1, s, s + 1\}$ utilizing overlapping windows, called the logarithmic fluctuation function. Using maximally overlapping windows leads to sufficiently smooth results to enable direct utilization of the finite difference method [7].

The alpha values are usually visualized with a surface plot as function of both the time and scale. This allows us to study the changes in alpha over time on different scales. The surface plot visualizes the complex structure of the HRV into an easily interpretable form, where the possible correlations and anticorrelations can be detected.

4.2.1 Alpha distribution

To study and to better understand the differences between the rest and drive sections, the alpha distribution as a function of scale is analyzed. This does not show the time dependence inside the sections but allows us to examine the possible differences between the sections. The DDFA alpha distribution graphs are created with Algorithm 2 described below.

Algorithm 2 DDFA alpha distribution

1. Split RR intervals into the rest and drive sections.
 2. Calculate DDFA for each section and for the whole data separately, using scales defined by the shortest section (across every subject).
 3. Split alpha into 50 equally wide bins.
 4. Calculate the number of alphas in each bin for each scale.
 5. Calculate the normalized density of alphas by comparing the number of alphas in each bin to the total number of alphas in each scale.
 6. Plot the density as functions of the scale and alpha.
-

The distribution of the scaling exponent is calculated separately for each subject and also as an aggregate distribution of all the subjects. The objective of the subject specific plots is to study the variations in each subject and the differences between the subjects. The aggregation plot is created to find general correlations that could be utilized for detecting universal differences in HRV during driving and resting.

4.2.2 Significance comparison of different scale ranges

Dynamically calculated alpha values can be easily studied at all the different scales. This can be utilized to find the best possible scales for separating rest and drive sections. To find out which scales are the most significant, the alpha values are binned into different scale ranges. Both the mean and standard deviation of the alpha values in each section

are calculated in these bins and compared to each other. Algorithm 3 explains how these scale ranges are created and how the measures are compared between the rest and drive sections. The objective is to find the scales that give the largest separation between the rest and drive sections.

Algorithm 3 Scale area segment separation

1. Split RR intervals into rest and drive sections.
 2. Calculate the logarithmic fluctuation functions of DFA in sliding windows for each section separately.
 3. Define the values of alpha for different ranges of scales as a linear fit to the fluctuation function.
 4. Normalize all alphas by subtracting the DFA alpha-1 values from the first rest period from all the alphas.
 5. Calculate the mean and standard deviation of alphas in each section for each range of scales.
 6. Visualize the mean and standard deviation with line plots for separate subjects and box plots for the aggregation results.
-

Since different subjects have different alpha values under similar conditions, some normalization is required to get valuable comparison between the subjects. The normalization is done with subtracting the alpha values by the DFA alpha-1 value calculated from the first rest section. This normalization is chosen, because the DFA alpha-1 value is widely utilized, and the first rest period is the logical baseline for the measurement. The implementation of normalization and its effects to the results are important topics that require further studies, but they are not discussed in this thesis.

4.3 Classification

This section describes the classification methods that are used to characterize the changes in different measures between the rest and drive section. All the calculations are performed with the Scikit-learn Python package [39].

Classification in machine learning is a subcategory of supervised learning. In supervised learning the machine learning algorithm learns a model for classifying data based on labeled training data. This model based on labeled training data can then be used to predict labels for unseen data [40, 41].

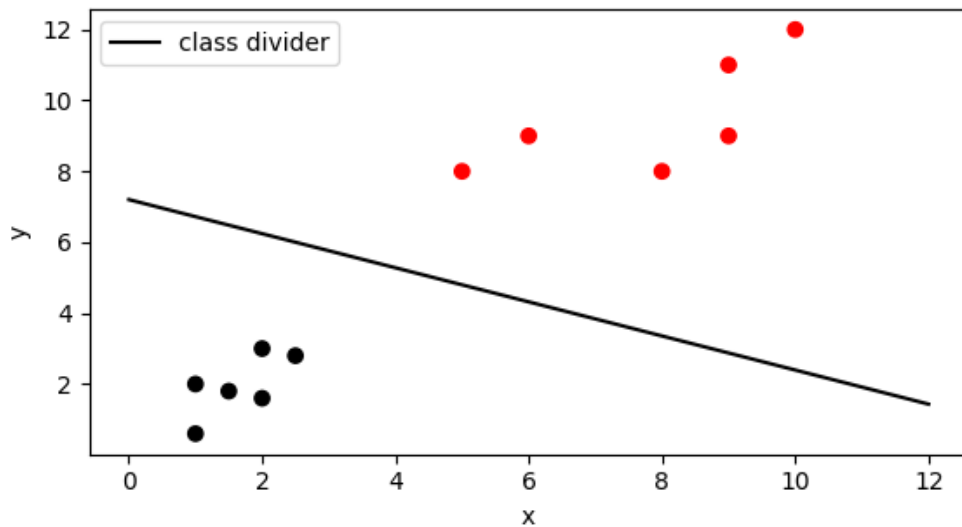


Figure 6: Example of binary classification. This example has two distinct classes illustrated by black and red dots, representing small coordinates and big coordinates, respectively. Using these six examples from each class, a simple linear machine learning algorithm can find a decision boundary or class divider shown as a line.

Figure 6 visualizes how a simple linear machine learning algorithm can find a decision boundary separating the data based on different labels. The decision boundary is chosen so that it maximizes the margin of error. In other words, the distance of the closest points of each class is maximized. This decision boundary line can then be used to label previously unseen data. If unseen data has coordinates below the line it is labeled as black, and if the unseen data has coordinates above the line it is labeled as red [40, 41]. Classification is not only limited to binary data with two labels. There can also be multilabel classifications, where the number of classes is greater than two. It is not always possible to separate the classes linearly. Kernel functions offer a possible solution to this problem. They are functions that map the training data into higher dimensional space to find linear separations between the classes [42].

Features of the data are important in classification. They are the predictor variables, and in the example shown in Fig. 6 they are the x and y coordinates. It is not always beneficial to have a lot of different features, since it can cause overfitting. In overfitting the model fits well into the training dataset, but the fitting parameters are so complex and specific that they do not generalize well for unseen data. This problem can be reduced by either feature selection or dimensionality reduction. In feature selection, only the best features for classification are chosen, based on performance in chosen feature selection algorithms. In dimensionality reduction, the features are transformed into a new set of features with smaller dimensionality, while trying to maintain as much relevant information as possible [40].

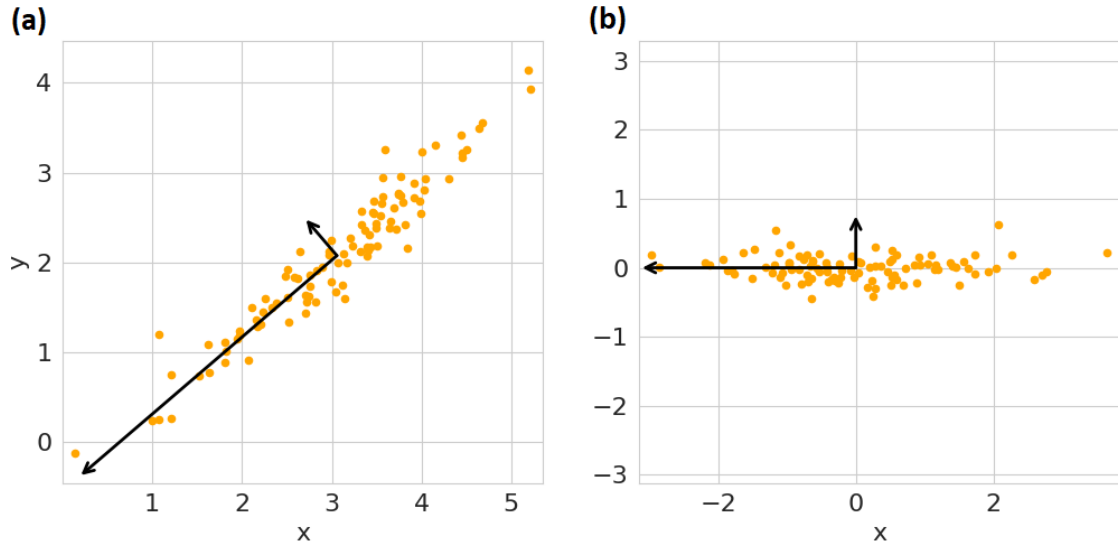


Figure 7: Visualization of two-dimensional principal component analysis calculation. Orange dots illustrate two-dimensional dataset and black vectors are illustrating the principal components. (a) Original two-dimensional dataset with the principal components. (b) Data projected to the principal axis.

4.3.1 Feature preparation

This subsection explains how the features are calculated and prepared for the classification in this thesis. The features are calculated from the data in maximally overlapping windows of length 200 RR intervals. First, the calculated features are normalized using quantile transform. Each feature is separately mapped into uniform distribution and then mapped into 10 quantiles. This transform is not linear and thus may distort linear correlations, but since the features used have very different scales, quantile transform makes them more easily comparable.

To compare how well each of the features can separate different rest and drive sections, the quantile transformed data is utilized by calculating the area under curve (AUC) receiver operating characteristics (ROC) curve for each feature. In AUC ROC curve, ROC is a probability curve and AUC describes the degree of separability [43]. AUC – ROC curve is an important metric describing the performance of the classification. The values for the curve are between 0.5 and 1. If the AUC value is high the model is good in distinguishing different classes [43].

The number of features utilized in the classification is reduced by principal component analysis (PCA). PCA increases the interpretability of the dataset by reducing the number of dimensions while minimizing the data loss. Figure 7 visualizes a simple two-dimensional PCA calculation. In PCA the first principal axis is a linear combination of variables with the most variance. In Fig. 7 the first principal axis is illustrated with the longest arrow, where length describes the amount of variance in the direction of the axis.

The second principal axis is orthogonal to the first one and has the highest amount of variance. This sequence is continued until the dimension of the data is reached. Finally, the data is projected into new principal axis. The new axis can then be sorted out based on their percentages of the total variance accounted, and then the number of features can be reduced by removing the new features with the least amount of variance. In this thesis the number of features was chosen so that 90 % of the variance is kept. Usually, the calculation of PCA is done by solving an eigenvalue problem. The methods for this procedure can be found in literature [44-46].

4.3.2 Classification methods

The classifications are done with support vector machines (SVMs) because they provide effectivity in high dimensions and also versatility with different kernel functions [47], making them a widely used tool in classification. Support vectors are the points nearest to the separation boundary of the classes. SVMs try to find an optimal hyperplane for the separation boundary so that it maximizes the margin of error. In other words, the hyperplane is chosen so that the distance of the support vectors is maximized from the separation boundary [48].

Choosing optimal parameters and kernel function for the SVM is done separately for each subject and method, using grid search with 5-fold cross-validation. In grid search all the possible combinations of chosen parameters are used to teach the model. The best parameters are then chosen based on their performance in cross-validation. In the cross-validation the training data is split into subsets. Each subset is used as a test data one by one while the other subsets are used as training data [49].

The parameters for the grid search are shown in Table 4, where parameter C is inversely proportional to regulation strength, adding penalty to too complex models. Different kernel functions map the data into different high-dimensional space in order to find better separation between the different classes [42].

Table 4 *Kernel functions and parameters used in grid search.*

Parameter	Values
C parameter	0.1, 1, 10, 100
Kernel functions	Linear, Poly, Rbf, Sigmoid

Classification is done with two different methods. First the subjects are classified independently without information from another subjects, using 70 % of the data from both rest and drive sections as training set and the remaining 30 % as testing set. The data are shuffled so that the distribution of different sections is consistent between the

training and testing datasets. The second method is the leave-one-subject-out, where one of the subjects is used as a testing data and rest of the subjects are used as training data. The leave-one-subject-out method was repeated for all the subjects.

Since the classes have different amounts of samples, balanced accuracy is used as the performance metrics in all the classification calculations. In balanced accuracy each sample is weighted based on the inverse prevalence of the samples class, giving better results for imbalanced datasets.

5. RESULTS

5.1 Conventional methods

The results obtained with the conventional HRV methods described in Ch. 4 are the baseline for analyzing the potential benefits of DDFA. Figures 8 and 9 compare the time-domain HRV measures from different rest and drive sections to each other. Figure 8 shows the differences between the rest and drive sections, whereas Fig. 9 presents the differences between the rest sections.

The rest sections do not have clear overall trends in the measures when compared to each other. There are differences when looking at individuals, but overall the time domain measures are similar in the two rest sections. The pRR50 has one outlier value with over 200 % change. It is caused by the low number of successive peaks varying more than 50ms and thus making the proportional change very large.

In the comparison between the rest and drive sections, mRR and all the measures calculated from successive RR intervals are lower in drive sections than in the rest sections. The decrease in mRR corresponds to a higher HR, and since it is at its lowest while resting, the result is plausible [50, 51]. All the measures from successive RR intervals are correlated with each other as expected. Since the pRR50 is correlated with the PNS activity, the reduction in the PNS activity can be caused by increased stress level stimulation during driving [52].

The standard deviation and coefficient of variation do not show significant changes in the median of the overall distribution, but there is significant variation between the subjects. For individual subjects there are noticeable variations in both measures. Therefore, these measures can be useful for studying certain individuals, but the results do not generalize into other subjects.

The alpha-1 values calculated with conventional DFA show similar consistency. There are no clearly distinguishable differences between the rest sections when compared to the behavior of the time-domain measures. The differences in the median of alphas presented in Fig. 10 are almost 0.1 units smaller when comparing the rest and drive sections. In other words, the alpha values are larger during the drive section than during the rest sections. However, the differences between the subjects are again significant. Figure 10 also shows significant variety when comparing the rest sections. There is 0.4 increase in alpha for some subjects and 0.4 decrease for another subject. These changes are prominent since the alpha values normally vary between zero and two and most of the measured alpha values are between 0.5 and 1.5. So even the difference

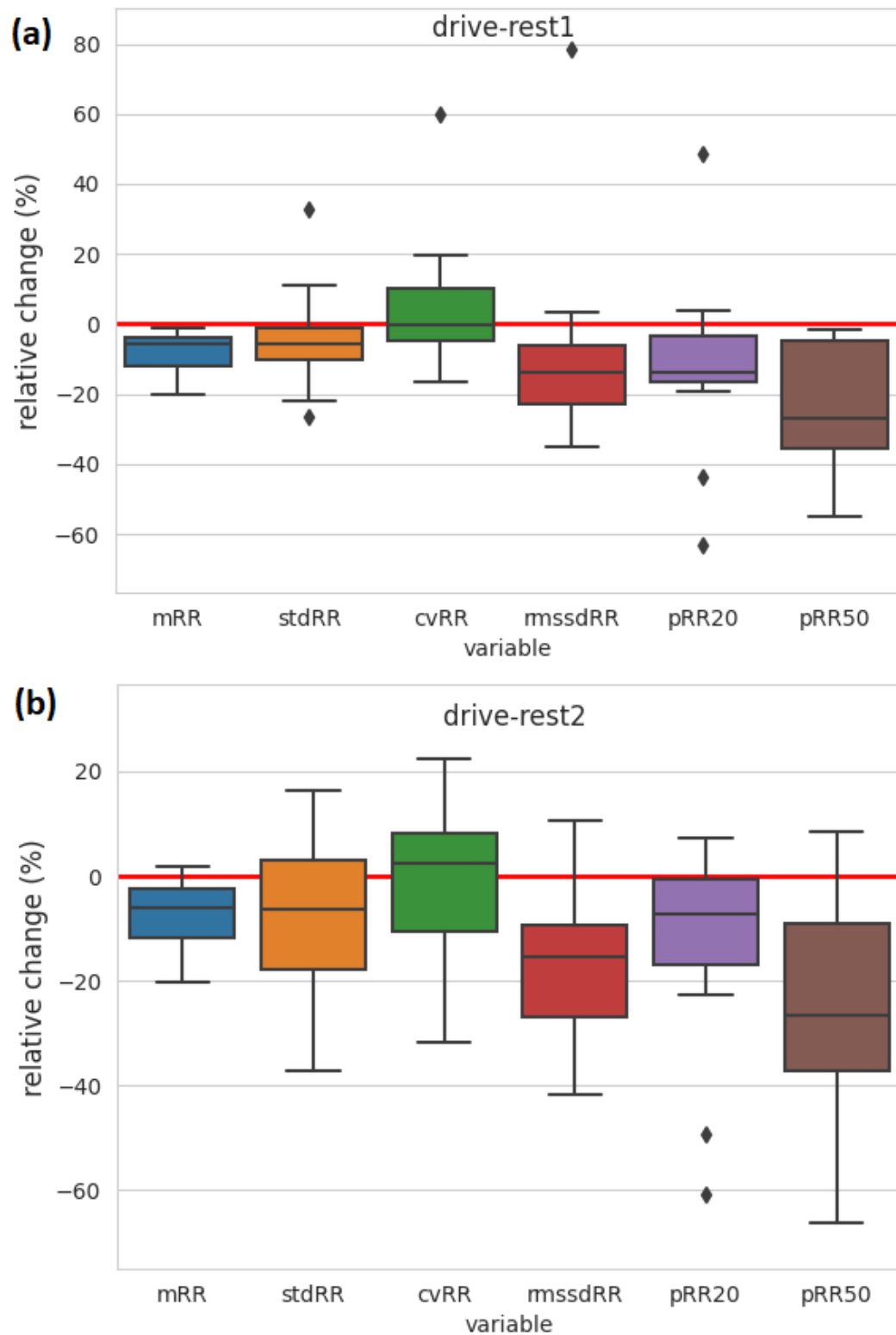


Figure 8: Relative change of HRV time-domain measures, where the change is (a) drive section compared to the first rest section and (b) drive section compared to the second rest section. The relative change was calculated for every subject. The boxes represent the quartiles of the data, and the whiskers show the rest of the distribution apart from the outliers that do not fit into 1.5 times the interquartile range, which is the maximum size of the whiskers [53]. pRR50 has one outlier that is not shown in the figure with values of 210 % for (a) and 110 % for (b).

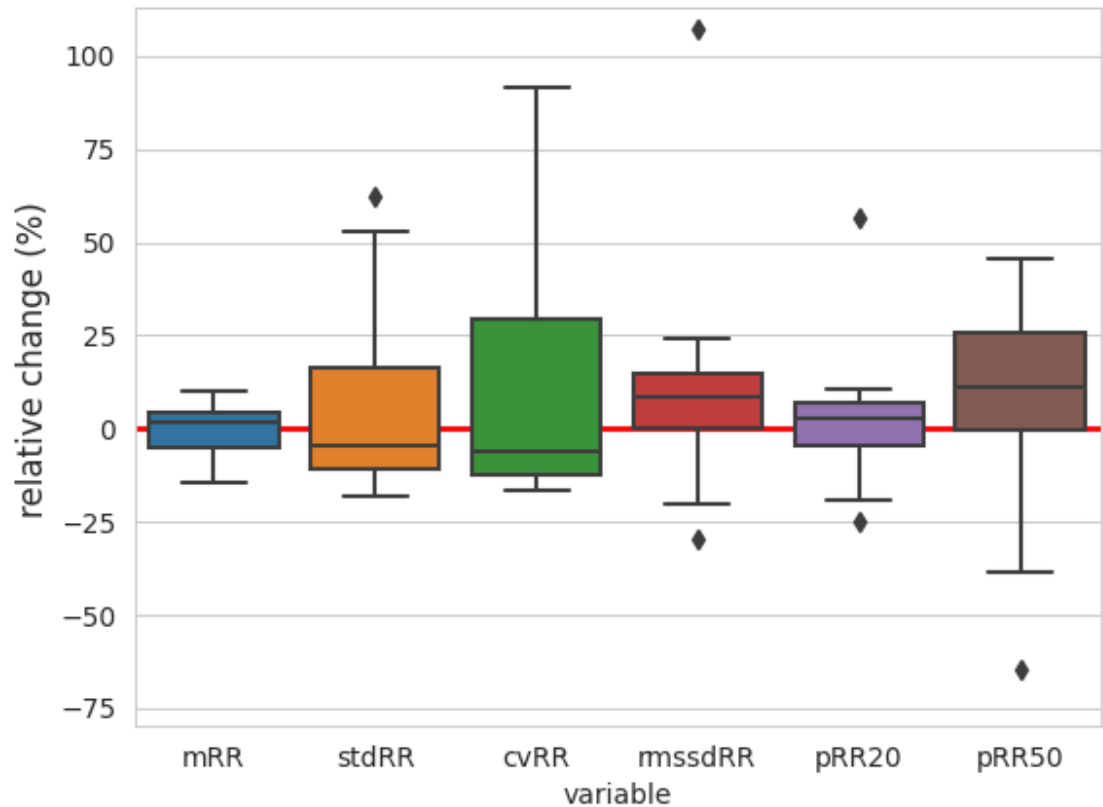


Figure 9: Relative change of HRV time-domain measures between the second and first rest sections. The relative change was calculated for every subject. pRR50 has one outlier that is not shown in the figure with a value of 240 %.

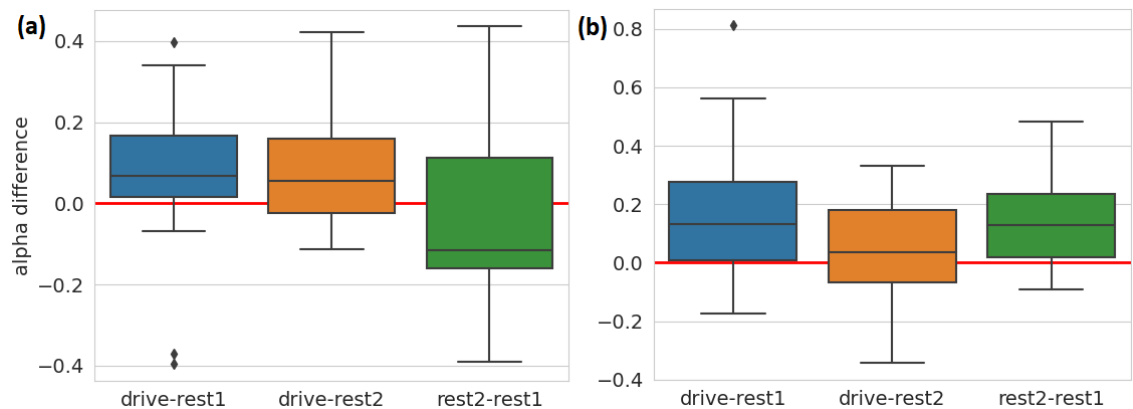


Figure 10: Difference in (a) alpha-1 and (b) alpha-2 between the different sections for all the subjects. There is a huge variation in the values between different subjects, but the overall trend shows slightly larger absolute values in alpha-1 for the rest-drive sections compared to the rest-rest sections. The alpha-2 values do not show significant changes between the sections.

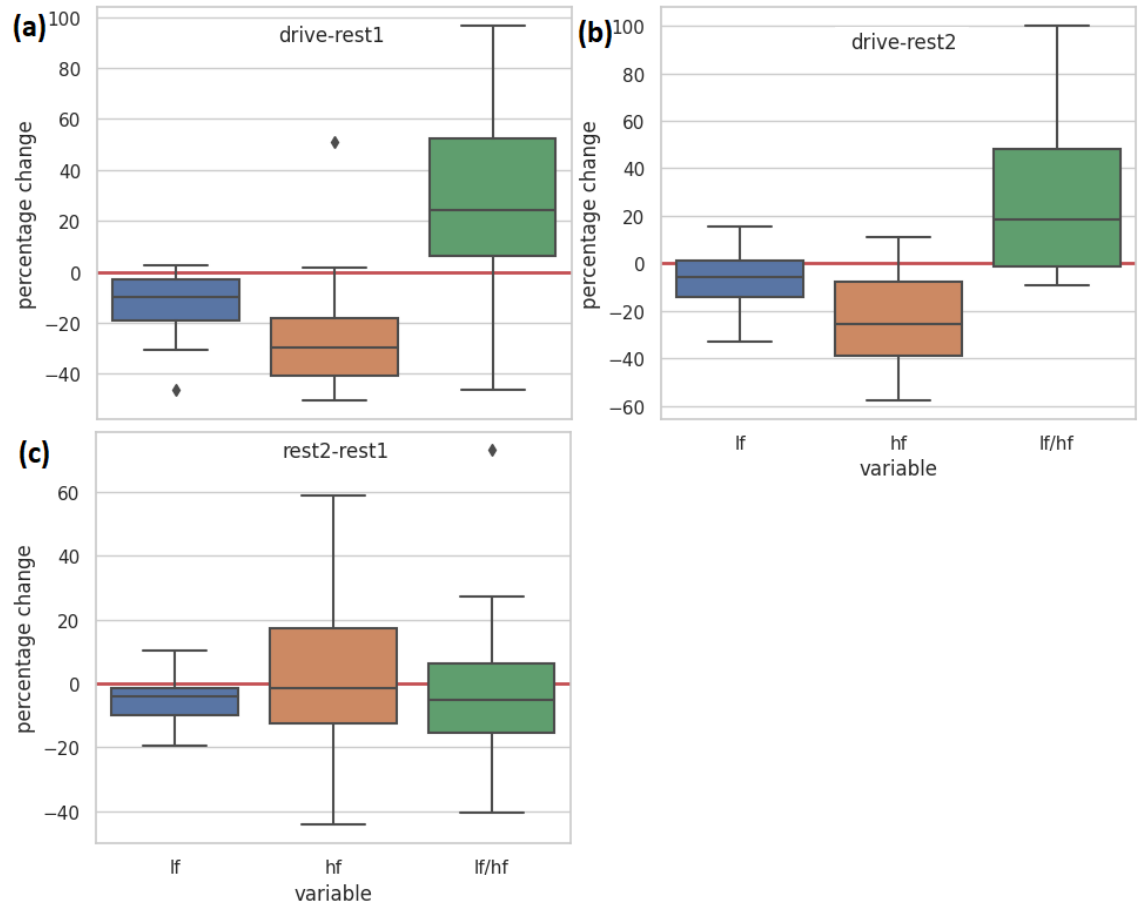


Figure 11: Relative change of HRV frequency-domain measures. (a) Difference between the first rest and drive sections. (b) Difference between the second rest and drive sections. (c) Difference between the rest sections. The relative change was calculated for every subject.

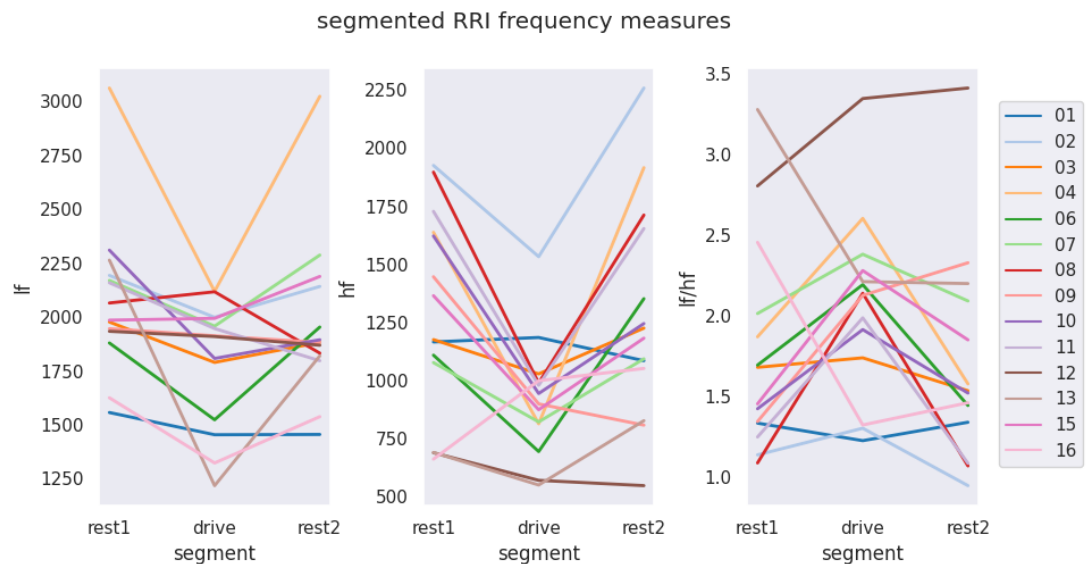


Figure 12: HRV frequency domain measures for each section and subject separately.

of 0.1 is easily noticeable. We also remind that alphas below and above 0.5 correspond to anticorrelated and correlated behavior, respectively. However, a detailed statistical analysis of the results is outside the scope of this thesis.

DFA alpha-2 values show similar behavior to alpha-1 values when comparing the first rest section and drive section, but there are some differences in the other comparisons. The relation between the rest sections is similar to that between the first rest section and drive section. This difference in rest sections is also noticeable in the rest-drive comparison. However, the changes in drive-rest2 are not as distinguishable as the changes in drive-rest1.

Figure 11 shows the frequency domain measures in a similar manner as the time-domain measures in Figs. 8 and 9. The frequency domain measures show consistent behavior between the two rest sections. However, there is prominent variability between the subjects in the HF and LF/HF measures.

The rest and drive sections show also similar results when compared to each other. There is decrease in the high-frequency absolute power indicating reduced PNS activity during driving. The same physiological change can also be seen as an increase in the LF/HF measure. These changes indicate a shift into more dominant SNS while driving compared to resting. The LF band does not show as prominent differences between the sections, but there is noticeable decrease in the LF band when comparing the first rest and drive sections,

The behavior of the frequency domain measures is rather consistent between the subjects as can be seen in Fig. 12. Especially the changes between rest and drive sections are very distinguishable in the HF and LF/HF measures for all the subjects, except for subjects 01 and 16. The changes in the LF band are not considerable in general, but there are several subjects with noticeable changes.

5.2 Dynamic detrended fluctuation analysis

Here we present the DDFA alpha values as functions of both time and scale. This visual presentation of the HRV correlations shows interesting behavior. Certain subjects (08, 09, 13, 15 and 17) show significant anticorrelations with alpha values below 0.5 in the rest periods. An example of these anticorrelations is presented in Fig. 13, which shows two subjects with very different DDFA behavior. For Subject01 the changes between the rest and drive sections are not noticeable neither in the beat rate nor in the alpha values, apart from small increases in beat rate at the end of the first rest section and the start of

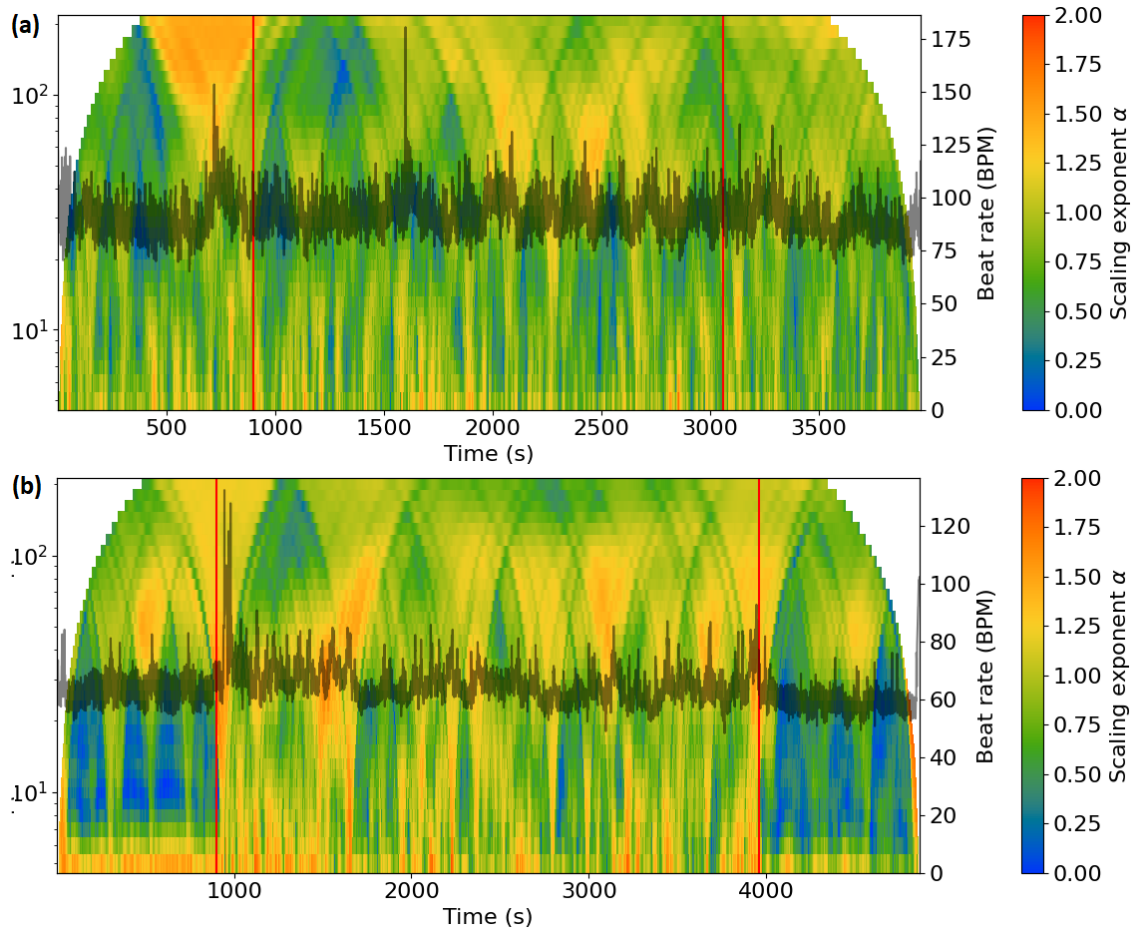


Figure 13: DDFA alpha values as functions of time and scale presented as a surface plot. The beat rate is shown as a black line. Red vertical lines indicate the change of rest/drive sections. (a) Subject01 that does not show noticeable differences between the segments. (b) Subject08 that shows clear anticorrelations on scales 10-20 in the rest sections that are not present in the drive section.

the second rest section. However, Subject08 shows noticeable change in the 10-20 scale range in the alpha values: the rest sections show clear anticorrelations that disappear instantly when the rest period ends and the drive section begins. At the start of the second rest period these anticorrelations appear again.

Figures 14-16 show shorter segments taken from Fig. 13. Figure 14 exemplifies the first rest period of Subject08, and Fig. 15 is an excerpt from the first rest period of Subject12. Strong anticorrelations in the RR intervals can be seen in Subject08 on scales 10-20. In particular, the beat rate steadily increases for about 10 consecutive beats until it starts to decrease for another 10 beats. This pattern repeats through the whole rest period. On the other hand, Subject12 shows more complex behavior of the beat rate. The RR intervals change constantly without a clearly visible pattern.

When inspecting the drive sections of these subjects shown in Fig. 16, the behavior for both of the subjects is similar to the behavior of Subject12 in rest sections. There are no

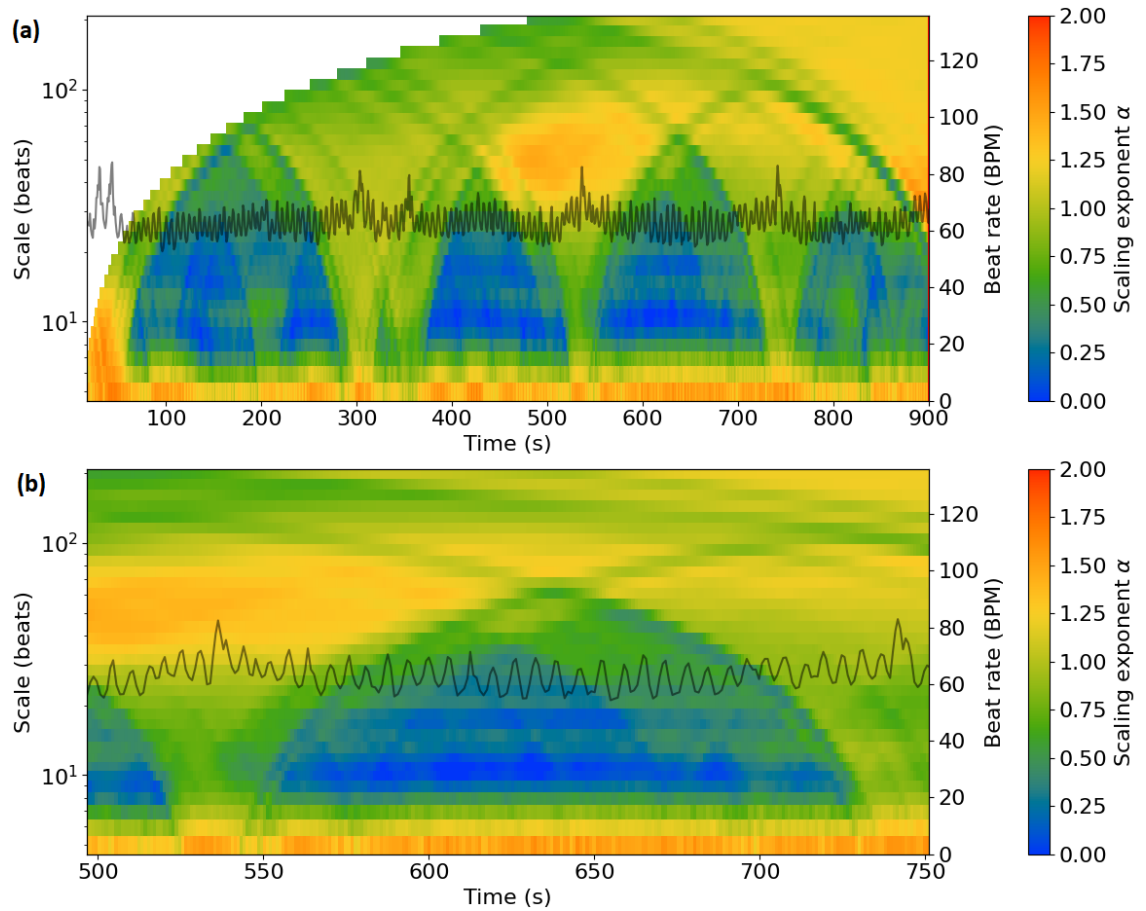


Figure 14: Zoomed plots of DDFA alpha values of Subject08 in the first rest section. (a) Whole rest section. (b) 250 seconds from the middle of the section. The RR intervals (beat rate) show clear anticorrelations.

clear patterns, and the HRV seems random and complex, which is normal and expected for healthy humans.

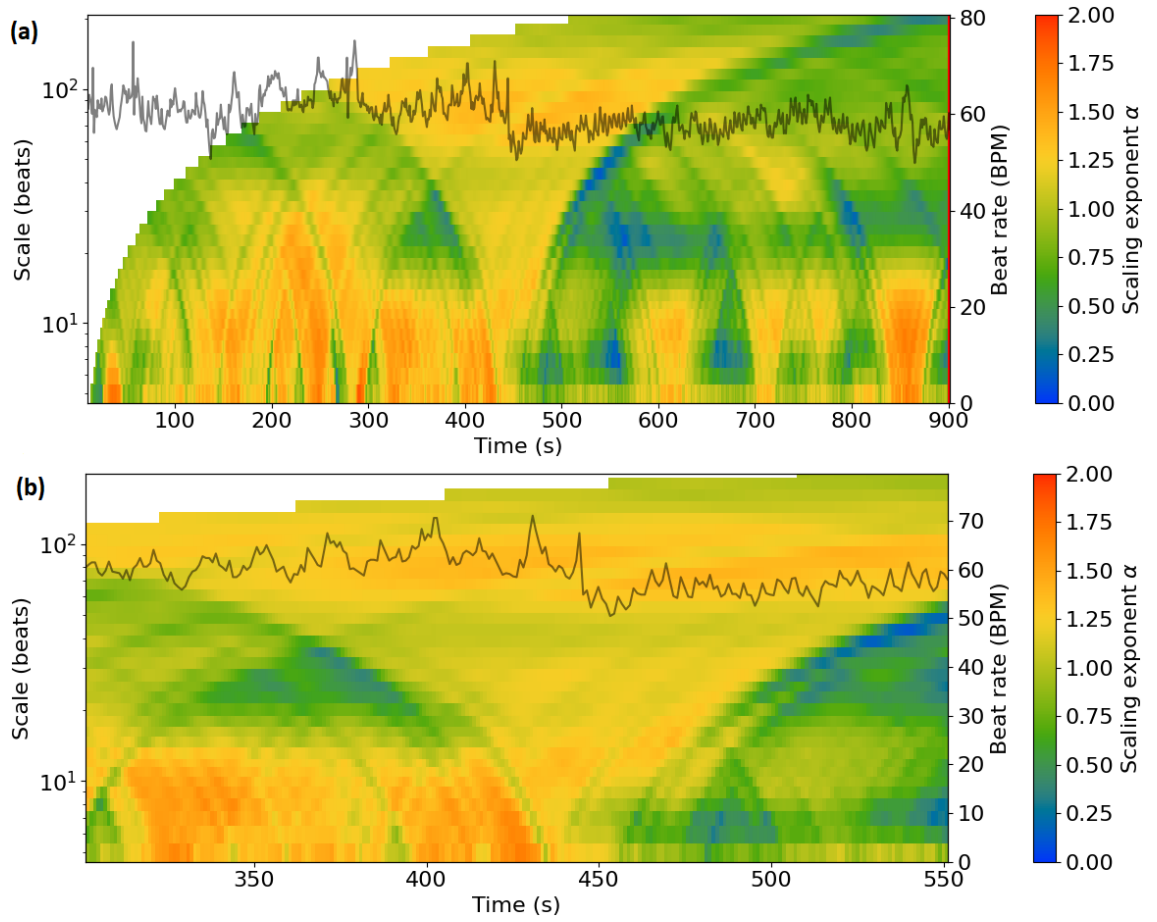


Figure 15: Zoomed plots of DDFA alpha values of Subject12 in the first rest section. (a) Whole rest section. (b) 250 second segment of the section.

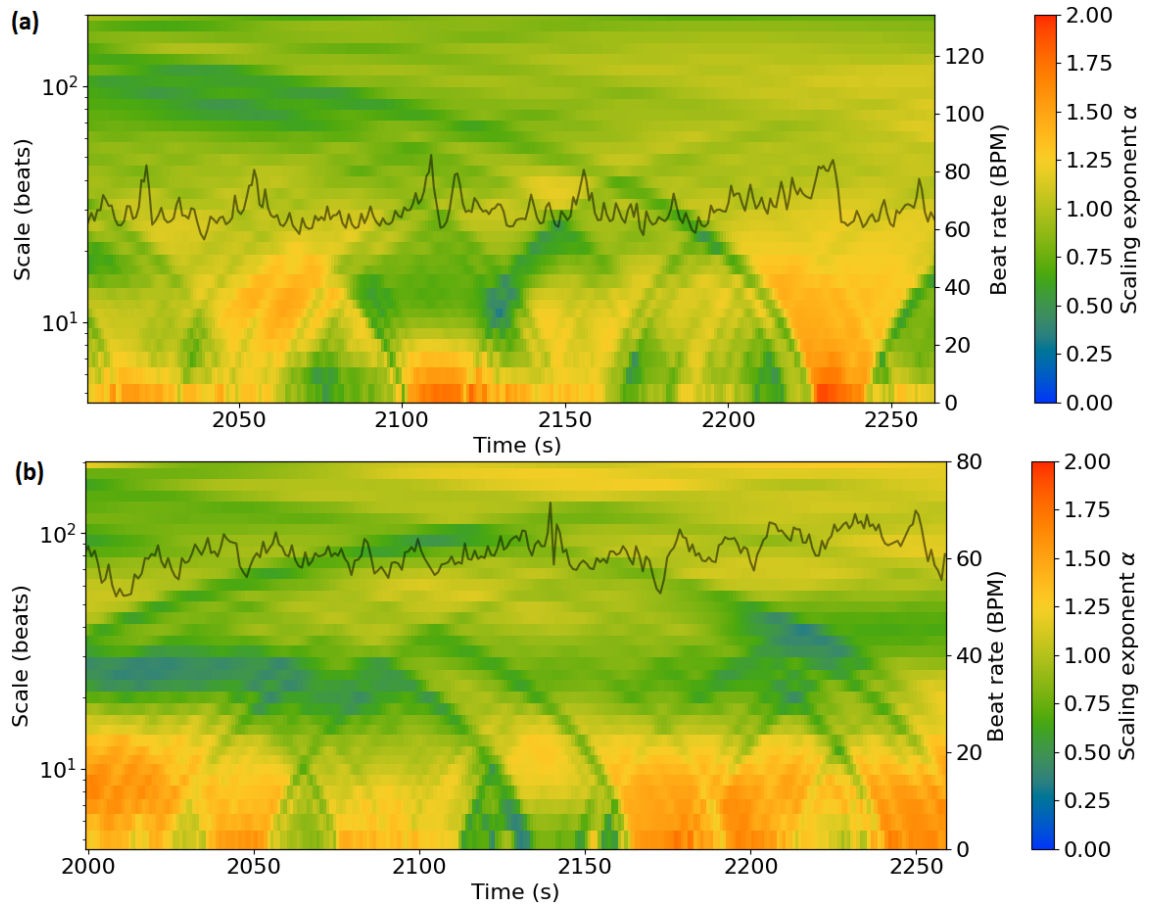


Figure 16: Zoomed DDFA alpha values in drive segments for (a) Subject08 and (b) Subject12. No clear anticorrelations are found in the data in contrast with the rest section of Subject08 (see Fig. 14).

5.2.1 DDFA alpha distribution

Figures 17 and 18 show examples of DDFA alpha distributions as defined in Sec. 4.2.1. Figure 17 shows the aggregated distribution over all the subjects. The scaling exponents are rather evenly distributed, and the only noticeable difference is the slightly more compact distribution during the rest sections in larger scales. This might be caused by the steady long-range behavior of the HRV during rest, that leads to consistent behavior of the dynamic segments calculated for larger scales. Subject13 shows anticorrelations similarly to Subject08 above. Figure 17 shows this anticorrelated behavior in the alpha distribution. The distribution of alpha values is more condensed in rest than during driving. The anticorrelations are most visible at scales 10-20, where the distribution is clearly concentrated on alpha values around 0.25. At smaller scales there are high nonstationary alpha values that quickly decrease into anticorrelated regime as the scale increases. These high nonstationary alpha values can be causally connected to the anticorrelated behavior: when the data is so highly anticorrelated at scales 10-20, it can

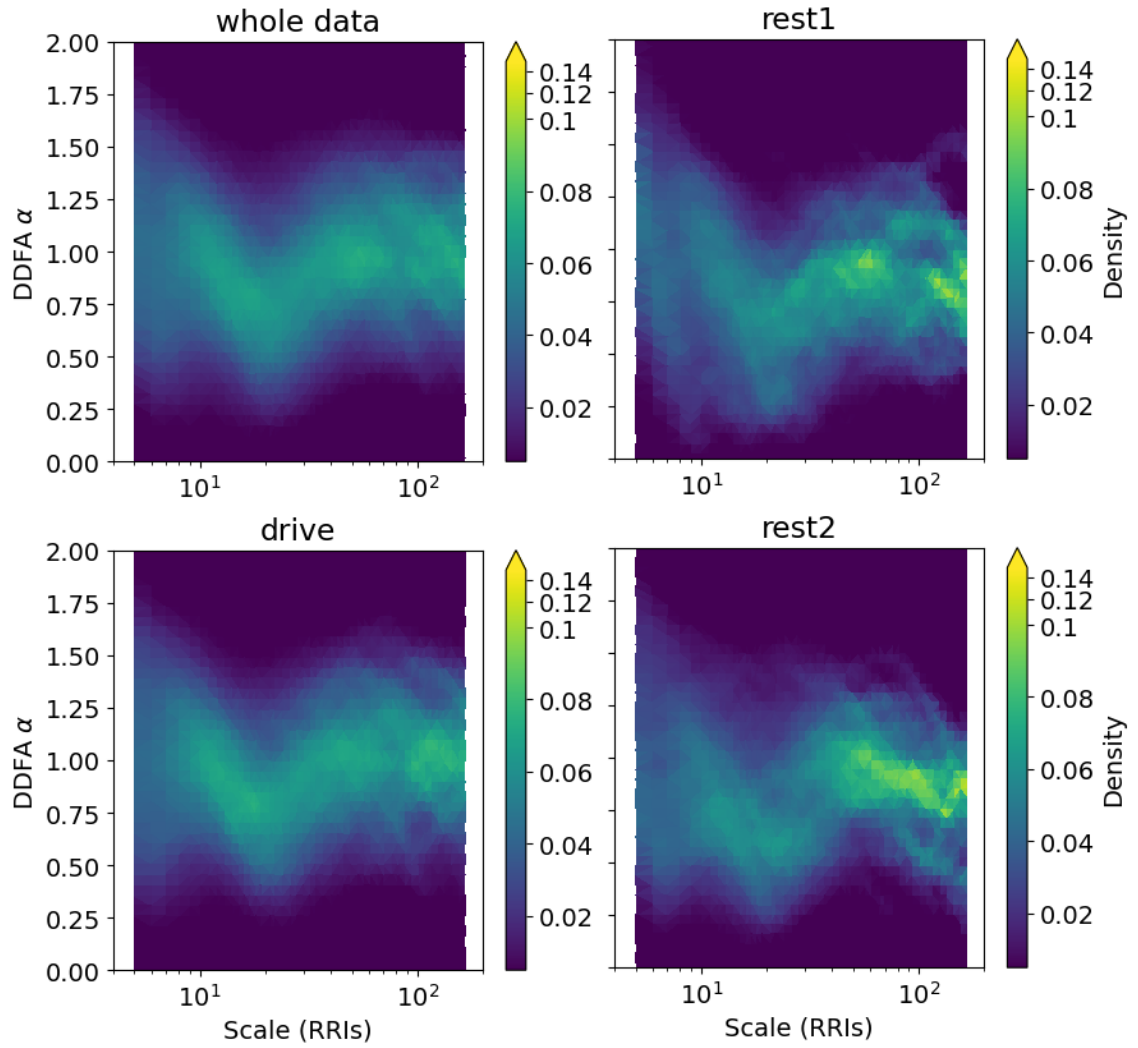


Figure 17: Aggregated distribution of DDFA scaling exponents as function of scale for the whole data (upper left) and each segment separately. The scales are identical in every section for easier interpretation. The distribution is visualized as a surface plot of density showing which proportion of the alpha values fall into each measurement bin. The scale of density is linear for densities 0–0.1 and exponential for values larger than 0.1.

have these upward and downward trends leading into nonstationary results when looking at shorter scales. These nonstationary periods do not also have any high frequency and low amplitude anticorrelations and the short scale correlations are evidently visible.

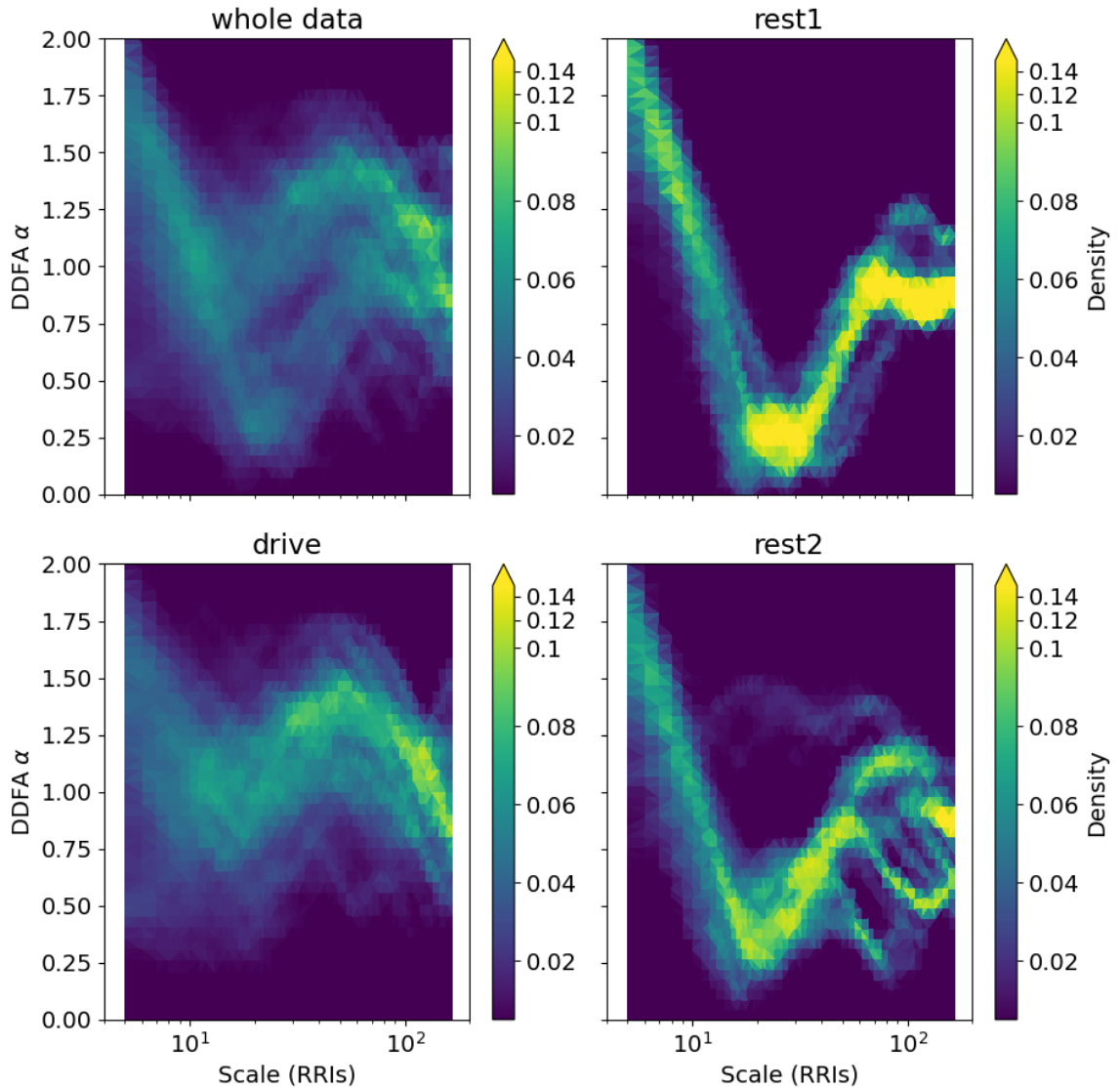


Figure 18: Distribution of DDFA scaling exponents for Subject13 as function of scale for the whole data (upper left) and each segment separately. The scales are identical in every section for easier interpretation. The distribution is visualized as a surface plot of density showing what proportion of the alpha values fall into each measurement bin. The scale of density is linear for densities 0-0.1 and exponential for values greater than 0.1.

5.2.2 Significance comparison of different scales

This section focuses on the comparison of the normalized alpha values calculated as described in Sec. 4.2.2. According to Figs. 19 and 20, there are no clearly distinguishable scales that would give better separation than others either for the mean or the standard deviation. But when studying the overall trend, the values in the drive section are larger than in the rest section across all the scales for both the mean and standard deviation. This is in accordance with the results from normal alpha-1 values presented in Sec. 5.1. The most distinctiveness results are the standard deviation of alphas within small scales. In these small scales, the distribution over all the subjects is narrow for the drive sections, with higher alpha values than in the rest sections.

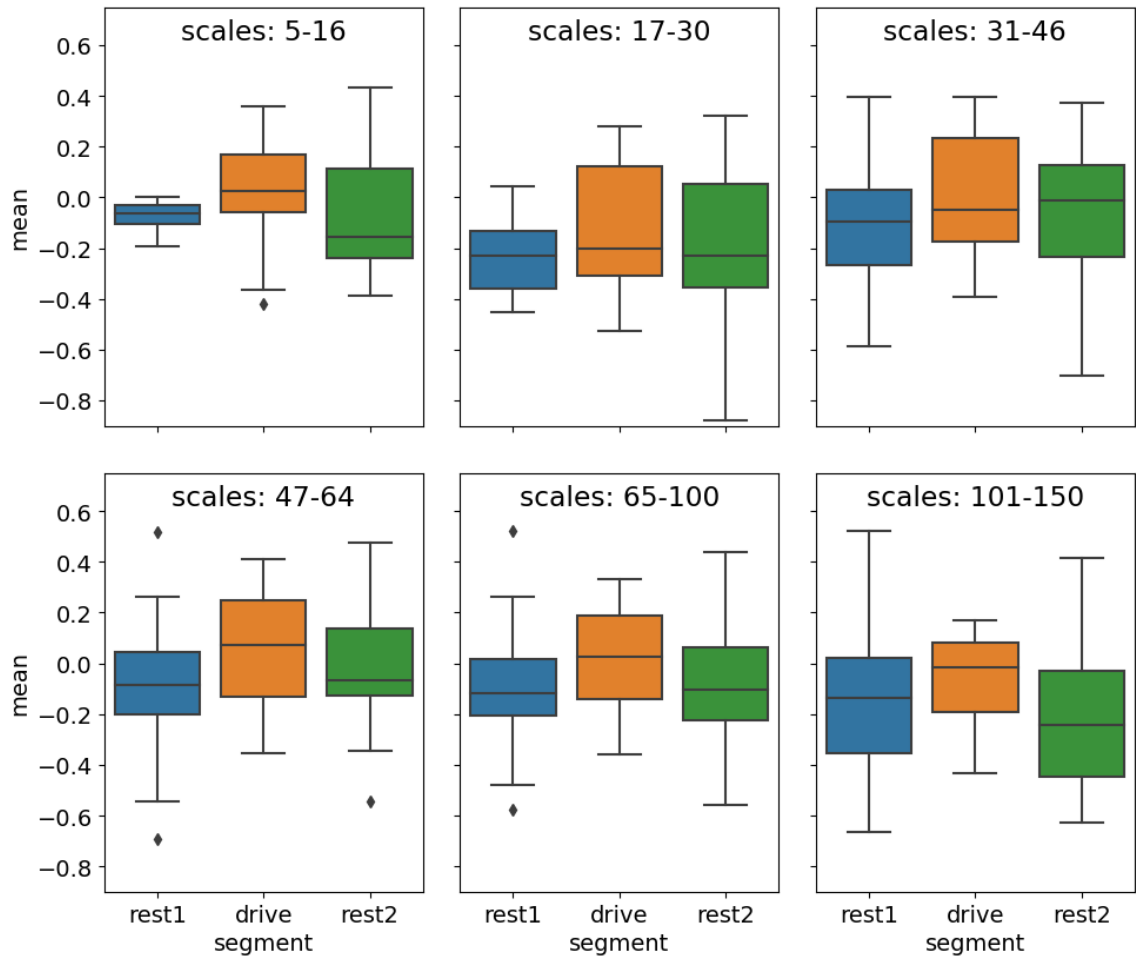


Figure 19: Aggregation box plot of normalized alpha mean values at different scale ranges in rest and drive sections. Each box plot shows the mean values of the scaling exponent calculated over all the subjects.

However, there are significant differences between individual subjects. In particular, there are some scale ranges that give a clear distinctiveness to certain subjects. For example, looking at Subject04 shown in Fig. 21, the standard deviation does not show clear changes between the sections and neither does the mean for small scales. However, the differences in the mean for scales over 50 are evident. The normalized alpha mean values change from -0.5 at scales 101-150 in the rest sections towards zero in the drive section.

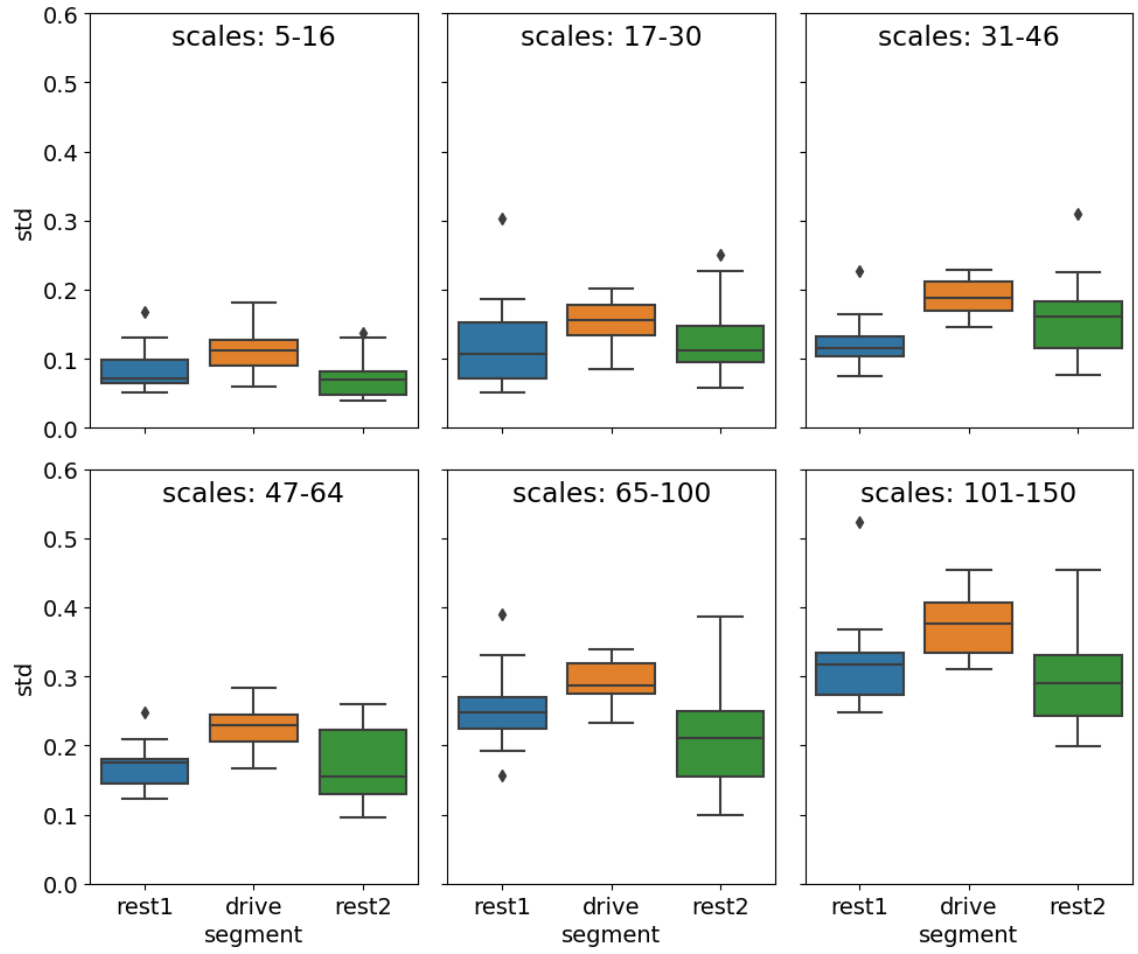


Figure 20: Aggregation box plot of normalized alpha standard deviations at different scale ranges in rest and drive sections. Each box plot shows the standard deviation values of the scaling exponent calculated over all the subjects.

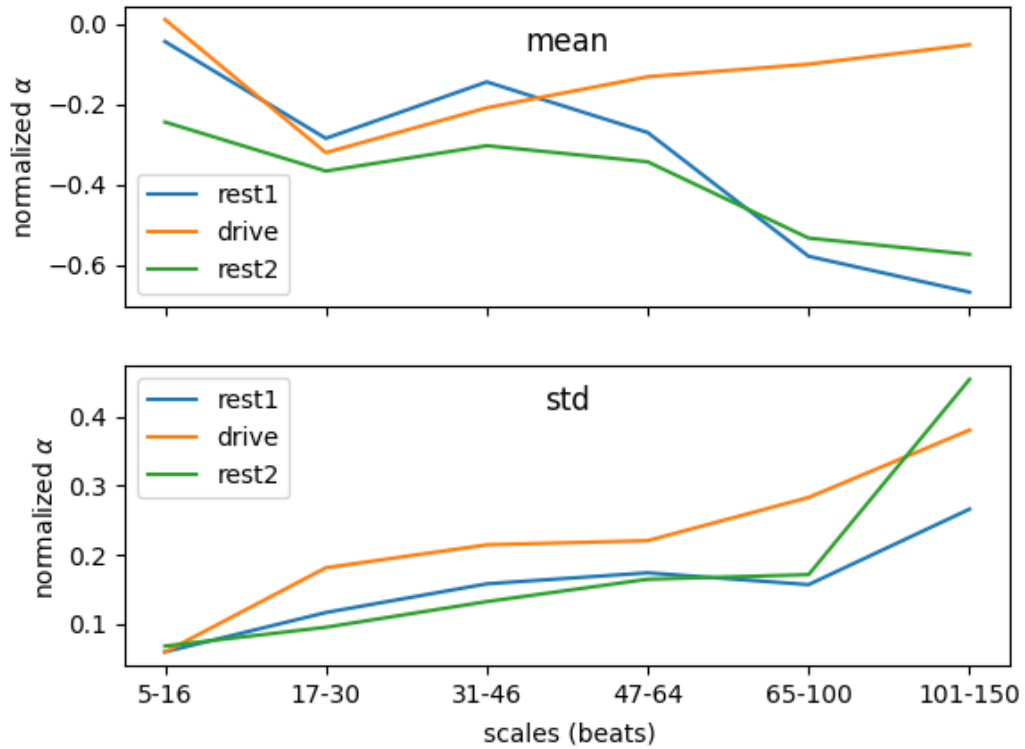


Figure 21: Mean (upper panel) and standard deviation (lower panel) of the normalized DFA scaling exponent α for Subject04 at different scales. This plot shows very consistent behavior between the two rest sections, but the mean value in the drive section is significantly different in larger scales.

5.3 Classification

Classification as described in Sec. 4.3 is carried out with both the conventional features and DDFA features. For the DDFA the classification includes the following features: mean and standard deviations of all the 20 scales (5, 6, 7, 8, 9, 11, 13, 15, 18, 21, 24, 28, 33, 39, 45, 53, 62, 73, 85 and 100). Conventional features used in the classification are mRR, rmssdRR, pRR20 and pRR50 from the time-domain measures and alpha-1 and alpha-2 from the DFA. The time-domain measures are chosen since the results in Sec. 5.1 are fairly consistent. The DFA is chosen to give diversity into the features, while also making the comparison between the conventional and DDFA methods more relevant. The AUC calculations are used to compare the ability of different features in classifying the rest and the drive sections.

The results show that the differences between the subjects are significant. As seen in Fig. 22, AUC calculated from the mean values of the DDFA scaling exponents for different scales range from 0.5 to 1 for almost all the scales. On the other hand, the AUC

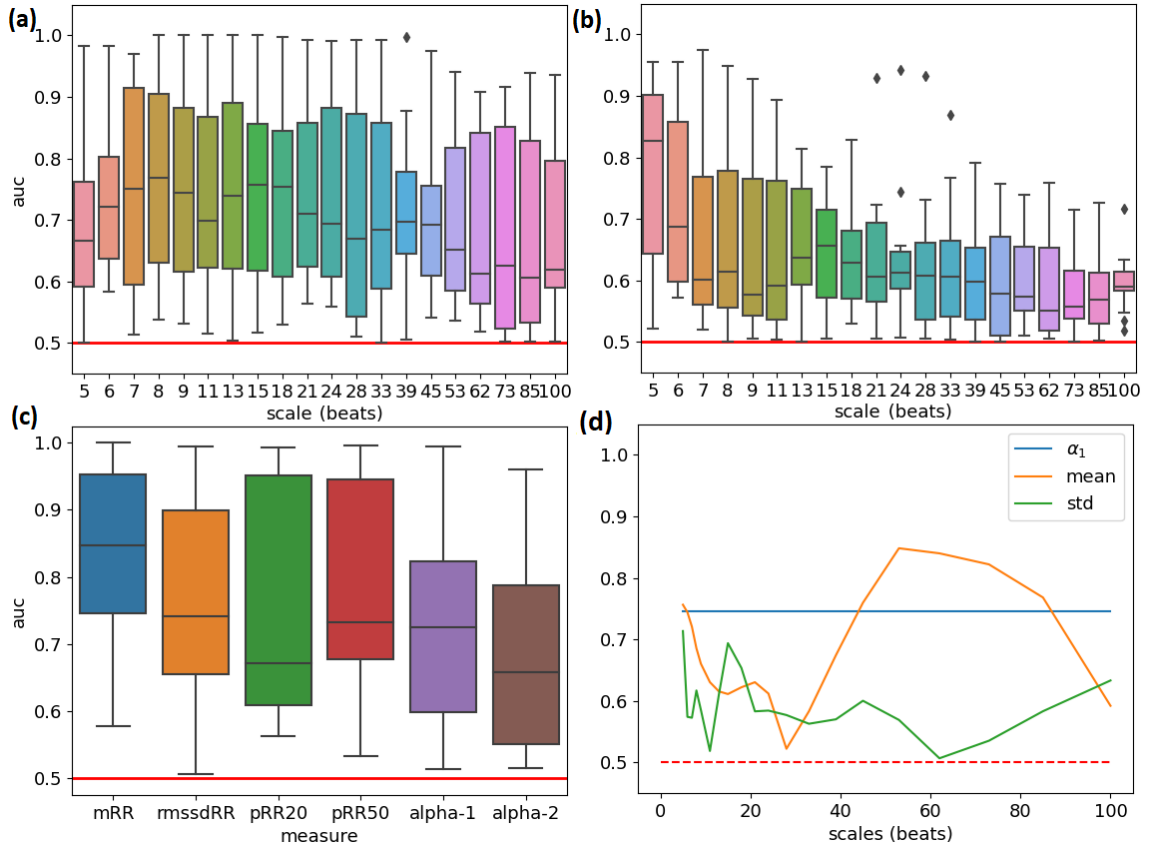


Figure 22: Area under curve (AUC) values for different features. (a) Mean of the area under curve calculations for DDFA scaling exponent at different scales presented as box plot over all the subjects. (b) Standard deviation of the AUC calculations for DDFA scaling exponent at different scales. (c) AUC calculations for different conventional measures. (d) AUC of DDFA scaling exponent mean and standard deviations of Subject12 at different scales. Also including the best of the conventional methods used in classification, which was DFA alpha-1 for Subject12.

values for the standard deviations range from 0.5 to 1 for small scales but the AUC values become lower when the scale increases. This makes the standard deviation of DDFA scaling exponent at high scales a poor classifier compared to its mean values. The conventional measures show similar results compared to the mean value of the DDFA scaling exponents, mRR is the best conventional measure with a high median of 85 % and the lowest values at 58%.

Since the AUC values over all subjects include values from the whole scale from 0.5 to 1 for both conventional measures and the mean values of the DDFA scaling exponent these results alone are not sufficient to show the performance of the DDFA results. However, the subject specific AUC curves like exemplified in Fig. 22 (d) show the possibilities of DDFA. Certain subjects have some scales, where the DDFA results are better at classifying than the conventional methods used in this classification. For example, the mean values of the DDFA alpha for scales 50 to 80 beats reach AUC values higher than the conventional methods. This shows that DDFA can perform better than ordinary DFA and some time-domain measures in classification.

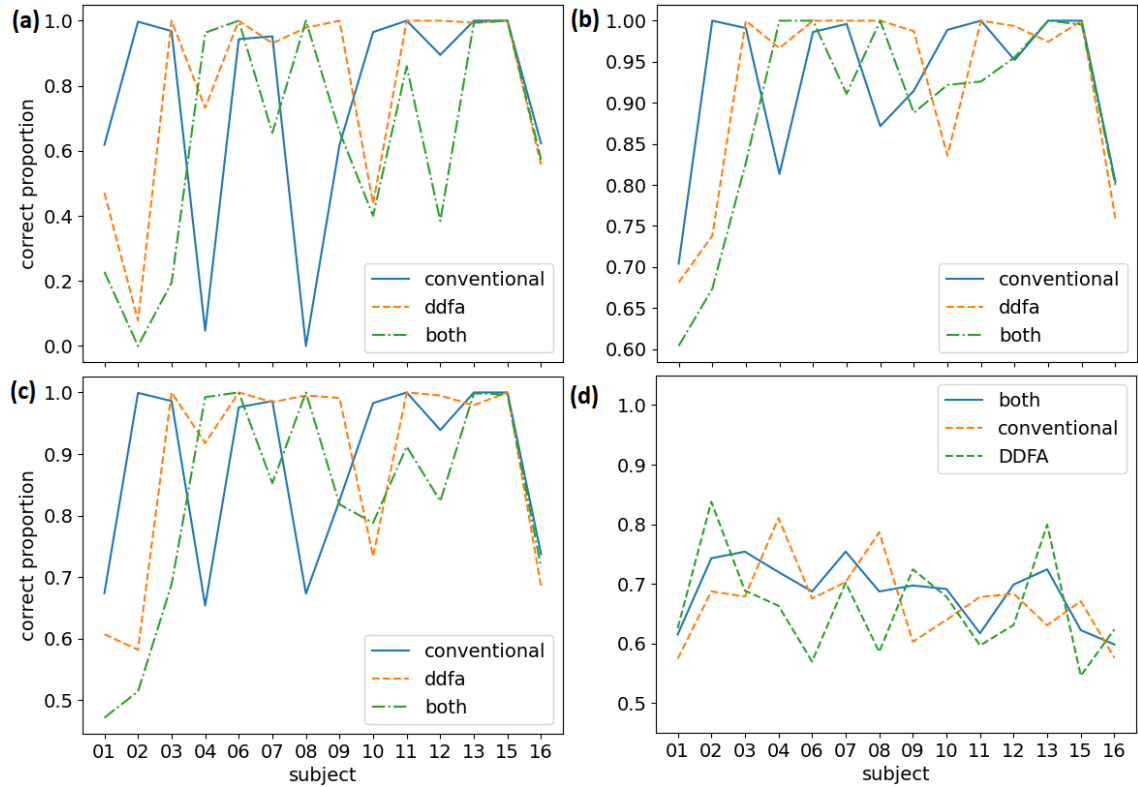


Figure 23: Correct classification proportions of the support vector machine classification algorithm. For (a) rest sections, (b) drive section and (c) both combined, (total correct proportion shown). The leave-one-subject-out method results are shown in d) for all the subjects.

The results from the classification calculations are presented in Fig. 23. Both the subject-specific and the leave-one-subject-out classifications are done separately for conventional features, DDFA features and for both combined. The Subject-specific classification is also done separately for the different rest and drive sections.

The subject-specific classification gives significant results with 12 out of the 14 subjects reaching over 95 % classification accuracy with some combination of features. However, the best combination of features changes between the subjects making the results less useful when comparing different subjects. For some subjects using both conventional and DDFA features results in worse classification than the features alone. This is probably caused by increased features that do not separate between the rest and drive sections. These features can conceal the good features and thus reduce the classification performance. This problem can probably be solved with more advanced machine learning algorithms and better feature selection. Also, Fig. 23, shows some mislabeled results (Subjects: 02, 04 and 08) in the rest percentages.

The classification with DDFA performs better than with the conventional measures in six out of 14 subjects. In addition, the performance is similar for two subjects, both being close to 100% accuracy. In the rest sections, the DDFA performs better than the conventional methods in eight subjects and similarly in two.

When using the leave-one-subject-out method the results are more consistent between the subjects. A large training data with a lot of different subjects reduce the accuracy of the classification for some specific subjects that perform very well in classifications above. On the other hand, the subjects performing poorly in previous classifications do not significantly suffer from the different training data. This difference in the performance between different subjects is probably caused by the differences in the DDFA results in rest and drive sections. There are some subjects such as Subject08, where the difference in DDFA results is remarkable between the rest and drive sections, whereas certain subjects such as Subject01 does not show clearly distinguishable differences. This can also be seen in subject-specific classification results in Fig. 23, where DDFA has classification accuracy of 100% for Subject08 and 60% for Subject01. When these DDFA results are combined into the leave-one-out method, the poor classification data from certain subjects such as 01 is hindering the results for some subjects such as 08. On the other hand, the data with good classification does not really affect the performance of the already almost undistinguishable subjects.

Adding the DDFA features into conventional features increases the classification accuracy for 10 out of 14 subjects. When comparing the DDFA features to conventional features, DDFA performs better in six of the subjects and similarly in two. The best features for the leave-one-out method are again subject-specific.

The kernels and C parameters are also subject-specific in both classification methods. The best parameters show a lot of different combinations of different kernel functions and C parameters. The rbf kernel and C parameters 0.1 and 100 are the most prominent, especially in the subject-specific classifications.

Based on both AUC and SVM results, DDFA performs well against the conventional methods used and, in some cases, even outperforming them. This backs up the use of scaling exponents calculated with DDFA as a HRV measure and classification feature.

5.4 Comparison to previous studies

The dataset used in this thesis has been previously utilized in two studies on stress during driving [18, 54]. In the original publication of the data in *“Detecting Stress During Real-World Driving Tasks Using Physiological Sensors”* [18] the HRV measures from frequency domain and the mRR and stdRR measures from the time domain performed well in detecting stress. GSR was the only measure that performed better than the HRV measures in the study. The significant differences between the subjects were also noted [18]. In *“Driver Stress Level Detection Using HRV Analysis”* [54], different HRV measures were classified with various algorithms. SVM with RBF kernel function showed

the best results for both the time-domain measures and conventional DFA measures. This is in agreement with the use of SVM classification in this thesis.

In general, the previous results [18, 54] are in accordance with the results presented in this thesis. On the other hand, the further improvements with the utilization of the DDFA methods are promising. The dynamic approach of DDFA enables us to notice the changes in HRV over time, while also bringing more useful features for classification. In particular, the sections can be classified better than with conventional methods and the visual presentation of DDFA alpha values shows the dynamical changes between different sections for some subjects. The performance of the DDFA is also compatible with previous studies that highlight the possibilities of DDFA in classification sleep stages and studying running [7, 8].

6. CONCLUSION

In this thesis we have studied heart rate variability (HRV) of 16 different subjects while driving and resting. The aim of the study was to find changes in the HRV during different tasks. The HRV was studied with several different methods. They included conventional methods from both time and frequency domains, but the main focus was on a new nonlinear method called dynamic detrended fluctuation analysis (DDFA). This method allowed us to study the scaling exponents as functions of both scale and time.

The methods used in the thesis showed promising capability in getting insight into physiological effects of driving. DDFA showed a very clear difference between the rest and drive sections that the conventional methods were not able to distinct for certain subjects. The mean and standard deviation of the DDFA scaling exponents are generally higher during the drive than in the rest sections across all the scales. However, some subjects show clear differences at certain scales, while the others show similar values in the different sections across all the scales.

The differences in the results between different subjects can be at least partly explained by the difference in how driving affects different people. Some people can be very relaxed and calm while driving. On the other hand, some people with less driving experience, for example may be stressed while driving. Due to these individual differences, universally applicable classifications are not straightforward.

However, when looking at the differences in the individual level, the subjects that showed clear changes in their HRV during the rest and drive sections performed well in the classification. The changes in the scaling exponent are easily noticeable, and with other HRV data about the specific subject, classification of driving and resting with HRV is possible with high accuracy. The classification across subjects is also promising: it is more consistent than the subject-specific classification, but with lower classification accuracy. The correct classes can be found with accuracy between 62% and 82% for all the subjects.

In summary, there are valid reasons to study the DDFA scaling exponents while driving to find the fundamental reasons behind the observed changes in the HRV. A reasonable next step would be to further improve the classification and then move into analyzing larger data sets with labeled sections of different activities to find out more information about the physiological effects of driving and other activities.

REFERENCES

1. A.H. Khandoker, H.F. Jelinek, M. Palaniswami, Identifying diabetic patients with cardiac autonomic neuropathy by heart rate complexity analysis, Biomedical engineering online, 1, 2009, <https://doi.org/10.1186/1475-925x-8-3>
2. J. Dong, The role of heart rate variability in sports physiology, Experimental and therapeutic medicine, 5, 2016, <https://doi.org/10.3892/etm.2016.3104>
3. H. Kim, E. Cheon, D. Bai, Y.H. Lee, B. Koo, Stress and heart rate variability: a meta-analysis and review of the literature, Psychiatry investigation, 3, 2018, <https://doi.org/10.30773/pi.2017.08.17>
4. M. Karthaus, M. Falkenstein, Functional Changes and Driving Performance in Older Drivers: Assessment and Interventions, Geriatrics (Basel), 2, 2016, <https://doi.org/10.3390/geriatrics1020012>
5. T.A. Dingus, F. Guo, S. Lee, J.F. Antin, M. Perez, M. Buchanan-King, J. Hankey, Driver crash risk factors and prevalence evaluation using naturalistic driving data, Proceedings of the National Academy of Sciences - PNAS, 10, 2016, <http://dx.doi.org/10.1073/pnas.1513271113>
6. F. Shaffer, J.P. Ginsberg, An Overview of Heart Rate Variability Metrics and Norms, Frontiers in public health, 2017, <https://doi.org/10.3389/fpubh.2017.00258>
7. M. Molkkari, G. Angelotti, T. Emig, E. Räsänen, Dynamical heart beat correlations during running, Scientific reports, 1, 2020, <http://dx.doi.org/10.1038/s41598-020-70358-7>
8. M. Molkkari, M. Tenhunen, A. Tarniceriu, A. Vehkaoja, S. Himanen, E. Rasanen, Non-Linear Heart Rate Variability Measures in Sleep Stage Analysis with Photoplethysmography, CIC, Sep 2019, pp1-4. <http://dx.doi.org/10.22489/CinC.2019.287>
9. R. McCraty, F. Shaffer, Heart Rate Variability: New Perspectives on Physiological Mechanisms, Assessment of Self-regulatory Capacity, and Health Risk, Global Advances in Health and Medicine, 2015, pp46-61. <https://doi.org/10.7453/gahmj.2014.073>
10. F. Shaffer, R. McCraty, C.L. Zerr, A healthy heart is not a metronome: an integrative review of the heart's anatomy and heart rate variability, Frontiers in psychology, 2014, <https://doi.org/10.3389/fpsyg.2014.01040>
11. L.K. McCorry, Physiology of the Autonomic Nervous System, American journal of pharmaceutical education, 4, 2007, <https://doi.org/10.5688/aj710478>
12. A.M. Friis, J.J. Sollers, Yoga Improves Autonomic Control in Males, Journal of evidence-based complementary & alternative medicine, 3, 2013, <https://doi.org/10.1177%2F2156587212470454>
13. W. Palma, time series analysis, John Wiley & Sons, Incorporated, 2016, <https://doi.org/10.1007/s00362-016-0858-4>

14. M. Pickup, introduction to time series analysis, 2015, pp1-18.
<https://dx.doi.org/10.4135/9781483390857>
15. R.H.D. Townsend, Fast Calculation of the Lomb-Scargle Periodogram Using Graphics Processing Units, The Astrophysical journal. Supplement series, 2, 2010,
<https://doi.org/10.1088/0067-0049/191/2/247>
16. M.P. Tarvainen, P.O. Ranta-aho, P.A. Karjalainen, An advanced detrending method with application to HRV analysis, TBME, 2, 2002,
<https://doi.org/10.1109/10.979357>
17. A.L. Goldberger, L.A.N. Amaral, L. Glass, J.M. Hausdorff, P.C. Ivanov, R.G. Mark, J.E. Mietus, G.B. Moody, C. Peng, H.E. Stanley, PhysioBank, PhysioToolkit, and PhysioNet: Components of a New Research Resource for Complex Physiologic Signals, Circulation, 23, 2000, <https://doi.org/10.1161/01.CIR.101.23.e215>
18. J.A. Healey, R.W. Picard, Detecting Stress During Real-World Driving Tasks Using Physiological Sensors, IEEE Transactions on Intelligent Transportation Systems, 2, 2005, <https://doi.org/10.1109/TITS.2005.848368>
19. B. Moody George, WFDB Applications Guide, 2019,
<https://www.physionet.org/physiotools/wag/>
20. M. Valentini, G. Parati, Variables Influencing Heart Rate, Progress in cardiovascular diseases, 1, 2009, <https://doi.org/10.1016/j.pcad.2009.05.004>
21. A. J. Camm, M. Malik, J. T. Bigger, G. Breithardt, S. Cerutti, R. Cohen, et al., Heart rate variability. Standards of measurement, physiological interpretation, and clinical use. Task Force of the European Society of Cardiology and the North American Society of Pacing and Electrophysiology, European heart journal, 3, 1996,
<https://doi.org/10.1161/01.CIR.93.5.1043>
22. R.E. Kleiger, J.P. Miller, J.T. Bigger, A.J. Moss: , Decreased heart rate variability and its association with increased mortality after acute myocardial infarction, The American journal of cardiology, 4, 1987, [http://dx.doi.org/10.1016/0002-9149\(87\)90795-8](http://dx.doi.org/10.1016/0002-9149(87)90795-8)
23. F. Yasuma, J. Hayano, Respiratory sinus arrhythmia: why does the heartbeat synchronize with respiratory rhythm? Chest, 2, 2004,
<https://doi.org/10.1378/chest.125.2.683>
24. J. Vescovi, Intra-Individual Variation of HRV during Orthostatic Challenge in Elite Male Field Hockey Players, J Med Syst, 12, 2019, <https://doi.org/10.1007/s10916-019-1478-z>
25. A. Flatt, Improving HRV Data Interpretation with the Coefficient of Variation, 2017,
<https://elitehrv.com/improving-hrv-data-interpretation-coefficient-variation>, retrieved 11.1.2021
26. K. Umetani, D.H. Singer, R. McCraty, M. Atkinson, Twenty-Four Hour Time Domain Heart Rate Variability and Heart Rate: Relations to Age and Gender Over Nine Decades, Journal of the American College of Cardiology, 3, 1998,
[http://dx.doi.org/10.1016/S0735-1097\(97\)00554-8](http://dx.doi.org/10.1016/S0735-1097(97)00554-8)

27. K.E. Barrett, S. Boitano, S.M. Barman, Ganong's Review of Medical Physiology (23rd Edition), McGraw-Hill Professional Publishing, 2010, pp.588.
28. C.K. Peng, S.V. Buldyrev, S. Havlin, M. Simons, H.E. Stanley, A.L. Goldberger, Mosaic organization of DNA nucleotides, Physical review. E, 2, 1994, <https://doi.org/10.1103/physreve.49.1685>
29. C. K. Peng, S. Havlin, H.E. Stanley, A.L. Goldberger, Quantification of scaling exponents and crossover phenomena in nonstationary heartbeat time series, Chaos (Woodbury, N.Y.), 1, 1995, <http://dx.doi.org/10.1063/1.166141>
30. Z. Chen, P.C. Ivanov, K. Hu, H.E. Stanley, Effect of nonstationarities on detrended fluctuation analysis, Physical review. E, Statistical, nonlinear, and soft matter physics, 4 Pt 1, 2002, <https://doi.org/10.1103/physreve.65.041107>
31. K. Hu, P.C. Ivanov, Z. Chen, P. Carpena, H.E. Stanley: , Effect of trends on detrended fluctuation analysis, Physical review. E, Statistical, nonlinear, and soft matter physics, 1 Pt 1, 2001, <https://doi.org/10.1103/physreve.64.011114>
32. J.W. Kantelhardt, E. Koscielny-Bunde, H.H.A. Rego, S. Havlin, A. Bunde, Detecting long-range correlations with detrended fluctuation analysis, Physica A, 3, 2001, [http://dx.doi.org/10.1016/S0378-4371\(01\)00144-3](http://dx.doi.org/10.1016/S0378-4371(01)00144-3)
33. A.K. Golińska, Detrended Fluctuation Analysis (DFA) in biomedical signal processing: selected examples, Grammar and Rhetoric, 29.2012,
34. P.A. Absil, R. Sepulchre, A. Bilge, P. Gérard, Nonlinear analysis of cardiac rhythm fluctuations using DFA method, Physica A, 1, 1999, [http://dx.doi.org/10.1016/S0378-4371\(99\)00295-2](http://dx.doi.org/10.1016/S0378-4371(99)00295-2)
35. G.M. Viswanathan, C.K. Peng, H.E. Stanley, A.L. Goldberger, Deviations from uniform power law scaling in nonstationary time series, Physical review. E, Statistical physics, plasmas, fluids, and related interdisciplinary topics, 1, 1997, <https://doi.org/10.1103/physreve.55.845>
36. J. Scargle, Studies in astronomical time series analysis. II: Statistical aspects of spectral analysis of unevenly spaced data, Astrophysical Journal, 1982, pp.835-853, <http://dx.doi.org/10.1086/160554>
37. P. Virtanen, R. Gommers, T.E. Oliphant, M. Haberland, T. Reddy, D. Cournapeau, E. Burovski, P. Peterson, W. Weckesser, J. Bright, van der Walt, Stéfan J, M. Brett, J. Wilson, K.J. Millman, N. Mayorov, A.R.J. Nelson, E. Jones, R. Kern, E. Larson, C.J. Carey, Í Polat, Y. Feng, E.W. Moore, J. VanderPlas, D. Laxalde, J. Perktold, R. Cimrman, I. Henriksen, E.A. Quintero, C.R. Harris, A.M. Archibald, A.H. Ribeiro, F. Pedregosa, P. van Mulbregt, SciPy 1.0: fundamental algorithms for scientific computing in Python, Nature methods, 3, 2020, <https://doi.org/10.1038/s41592-019-0686-2>
38. K. Kiyono, Y. Tsujimoto, Nonlinear filtering properties of detrended fluctuation analysis, Physica A, 2016, <http://dx.doi.org/10.1016/j.physa.2016.06.129>

39. F. Pedregosa, G. Varoquaux, A. Gramfort, V. Michel, B. Thirion, O. Grisel, M. Blondel, P. Prettenhofer, R. Weiss, V. Dubourg, J. Vanderplas, A. Passos, D. Cournapeau, M. Brucher, M. Perrot, É Duchesnay, Scikit-learn: Machine Learning in Python, Journal of machine learning research, 2011, <https://hal.inria.fr/hal-00650905>
40. S. Raschka, V. Mirjalili, Python machine learning, Packt, 2019,
41. E. Alpaydın, Introduction to machine learning, MIT Press, 2010, pp.21-386.
42. R. Amami, D.B. Ayed, N. Ellouze, Practical Selection of SVM Supervised Parameters with Different Feature Representations for Vowel Recognition, 2015, <https://arxiv.org/abs/1507.06020>
43. S. Narkhede, Understanding AUC - ROC curve, 2018, <https://towardsdatascience.com/understanding-auc-roc-curve-68b2303cc9c5>, retrieved 22.04.2021
44. I.T. Jolliffe, J. Cadima, Principal component analysis: a review and recent developments, Philosophical transactions of the Royal Society of London. Series A: Mathematical, physical, and engineering sciences, 2065, 2016, <https://doi.org/10.1098/rsta.2015.0202>
45. A. Hyvärinen, Principal component analysis, 2009, https://www.mv.helsinki.fi/home/amoaning/movies/uml/pca_handout.pdf
46. Z. Gniazdowski, New Interpretation of Principal Components Analysis, Zeszyty Naukowe Warszawskiej Wyższej Szkoły Informatyki, 16, 2017, <http://dx.doi.org/10.26348/znwwsi.16.43>
47. Scikit-learn Support Vector Machines, <https://scikit-learn.org/stable/modules/svm.html>, retrieved 22.04.2021
48. A. Mechelli, S. Vieira, Machine learning, Academic Press, 2020, pp.101-108.
49. I. Syarif, A. Prugel-Bennett, G. Wills, SVM Parameter Optimization using Grid Search and Genetic Algorithm to Improve Classification Performance, Telkomnika, 4, 2016, <http://dx.doi.org/10.12928/telkomnika.v14i4.3956>
50. J. Meseguer, J. Meseguer, C. Calafate, C. Calafate, J. Cano, J. Cano, On the Correlation Between Heart Rate and Driving Style in Real Driving Scenarios, Mobile Netw Appl, 1, 2018, <https://doi.org/10.1007/s11036-017-0833-x>
51. B. Choi, S. Choi, J. Jeong, J. Lee, S. Shu, N. Yu, S. Ko, Y. Zhu, Ambulatory heart rate of professional taxi drivers while driving without their typical psychosocial work stressors: a pilot study, Annals of occupational and environmental medicine, 1, 2016, <https://doi.org/10.1186/s40557-016-0139-7>
52. A. Lanata, G. Valenza, A. Greco, C. Gentili, R. Bartolozzi, F. Bucchini, F. Frendo, E.P. Scilingo: , How the Autonomic Nervous System and Driving Style Change With Incremental Stressing Conditions During Simulated Driving, IEEE Transactions on Intelligent Transportation Systems, 3, 2015, <https://doi.org/10.1109/TITS.2014.2365681>

53. J.W. Tukey, exploratory data analysis, Addison-Wesley, 1977, pp.39-42.,
<https://doi.org/10.1002/bimj.4710230408>

54. N. Munla, M. Khalil, A. Shahin, A. Mourad, Driver stress level detection using HRV analysis, ICABME, Sep 2015, pp61-64.
<http://dx.doi.org/10.1109/ICABME.2015.7323251>

APPENDIX A: DDFA ALPHA SURFACE PLOTS

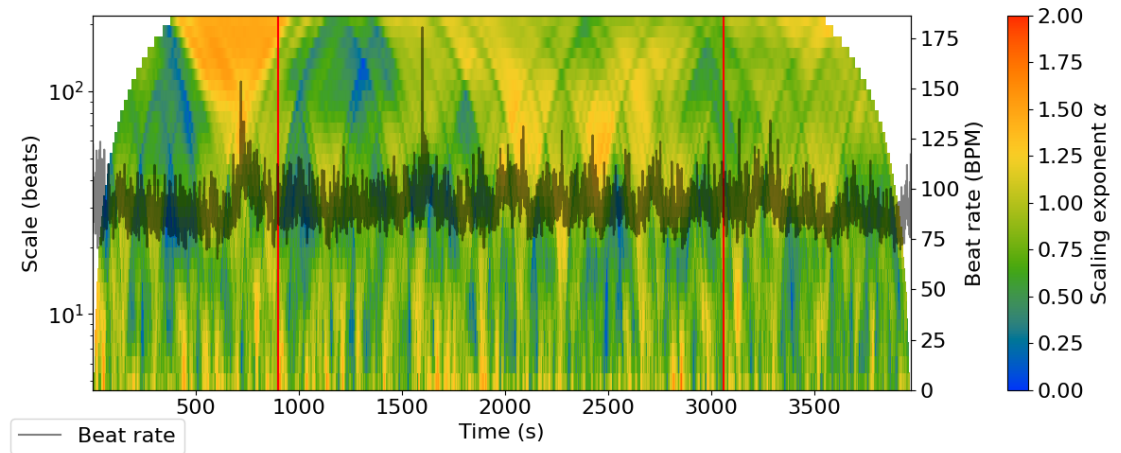


Figure A.1 Subject01: DDFA alpha surface plot.

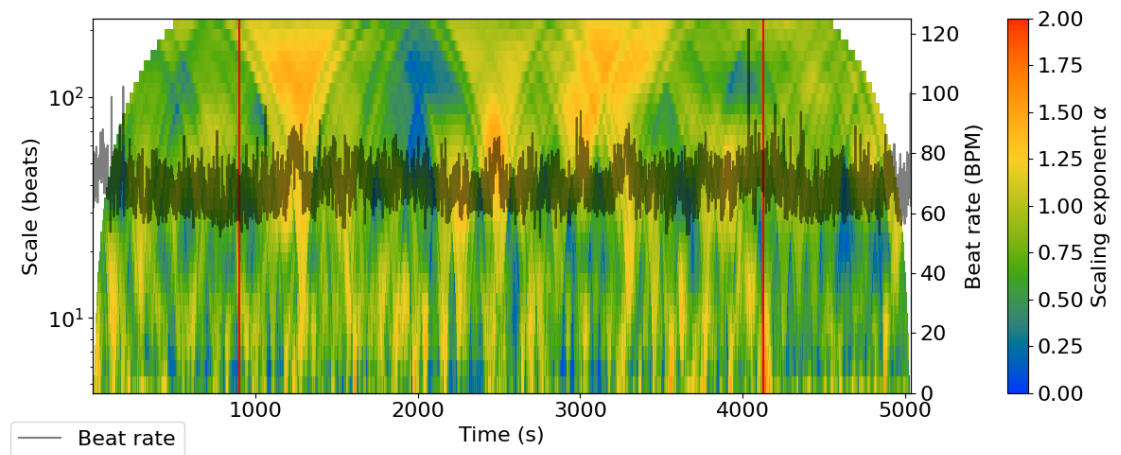


Figure A.2 Subject02: DDFA alpha surface plot.

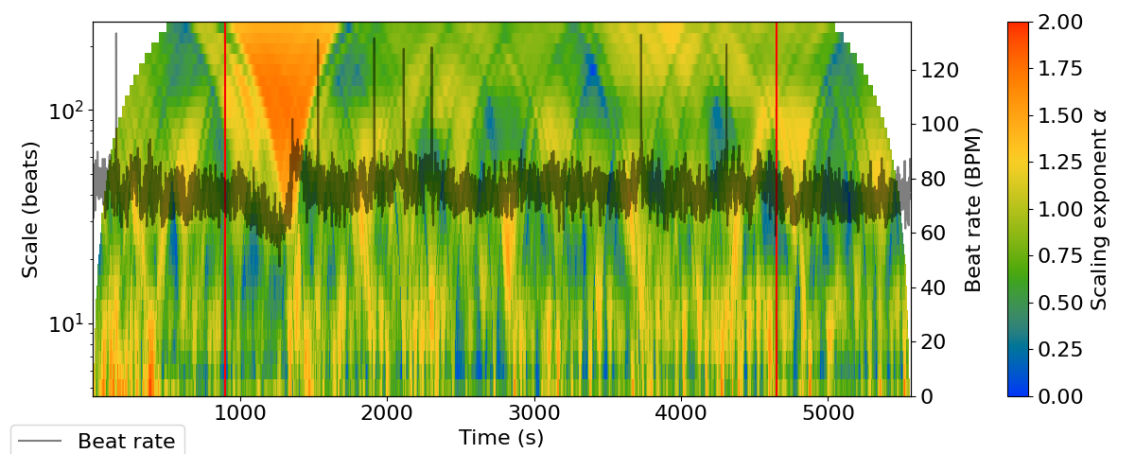


Figure A.3 Subject03: DDFA alpha surface plot.

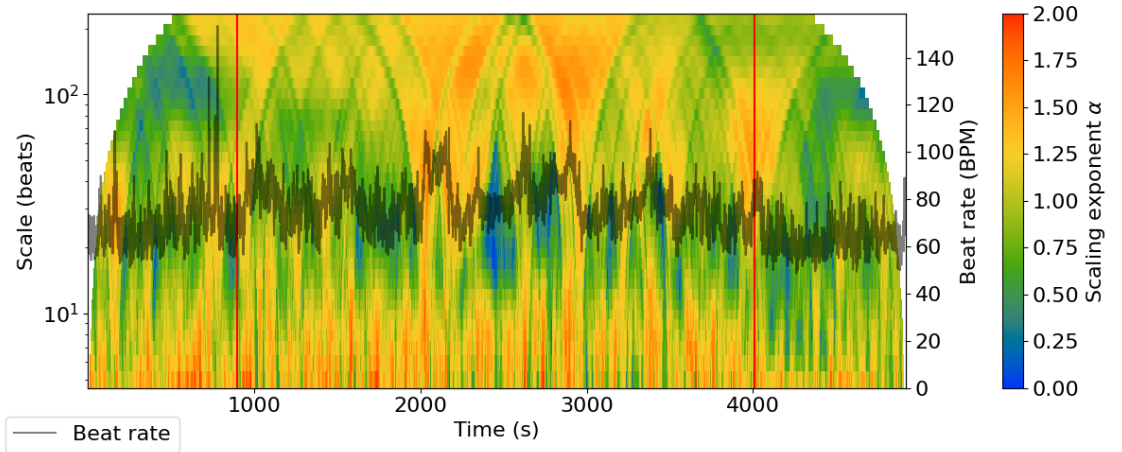


Figure A.3 Subject04: DDFA alpha surface plot.

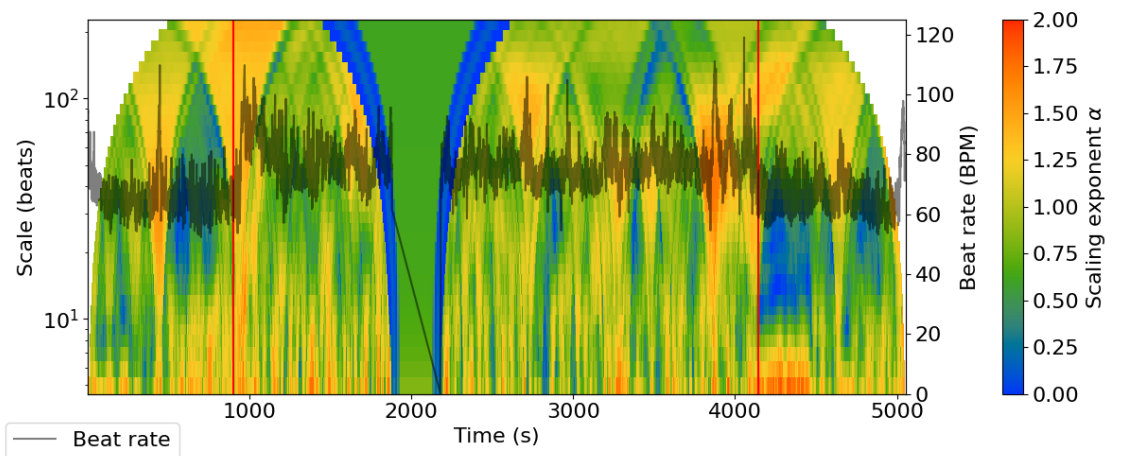


Figure A.5 Subject05: DDFA alpha surface plot.

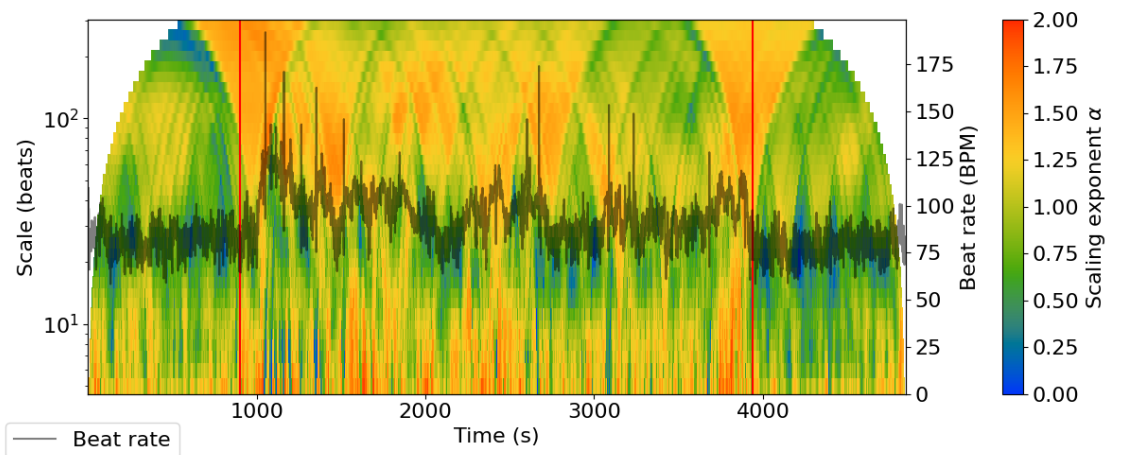


Figure A.6 Subject06: DDFA alpha surface plot.

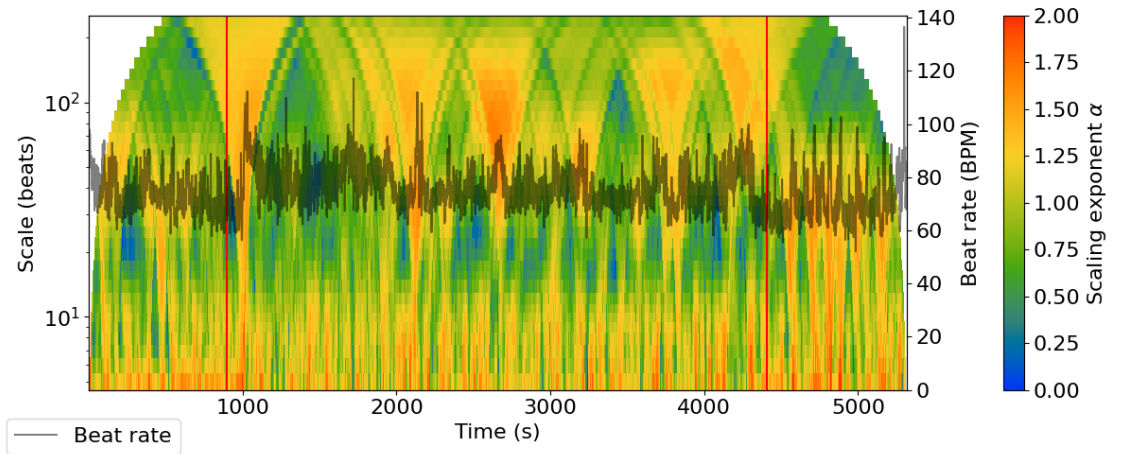


Figure A.7 Subject07: DDFA alpha surface plot.

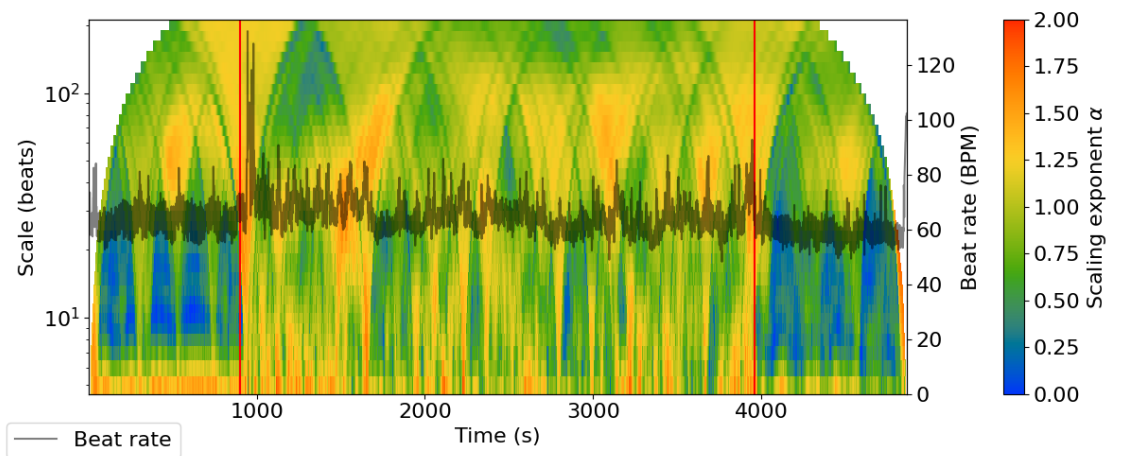


Figure A.8 Subject08: DDFA alpha surface plot.

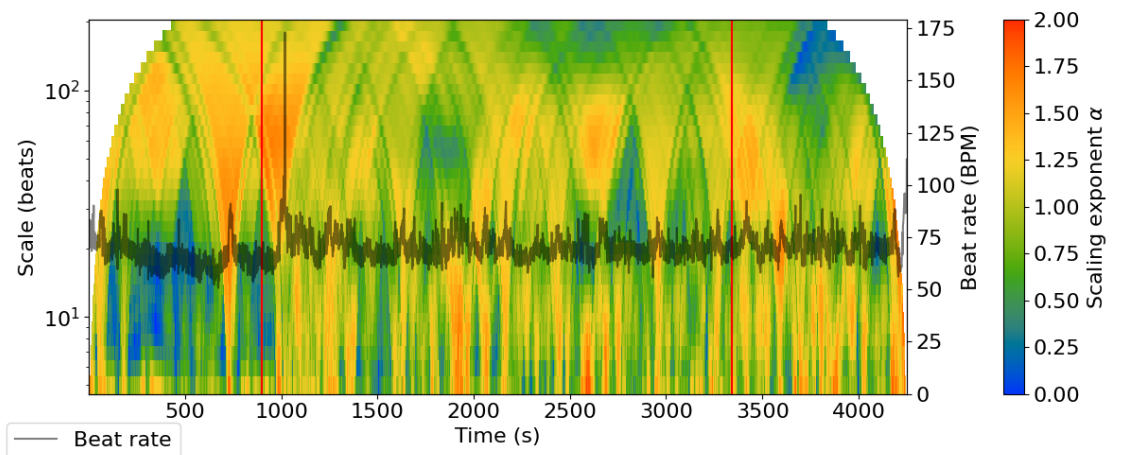


Figure A.9 Subject09: DDFA alpha surface plot.

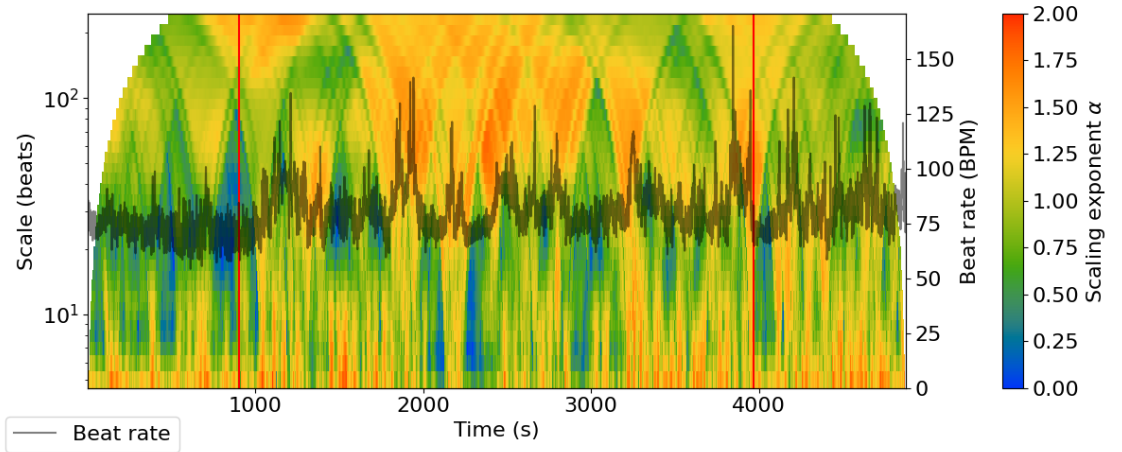


Figure A.10 Subject10: DDFA alpha surface plot.

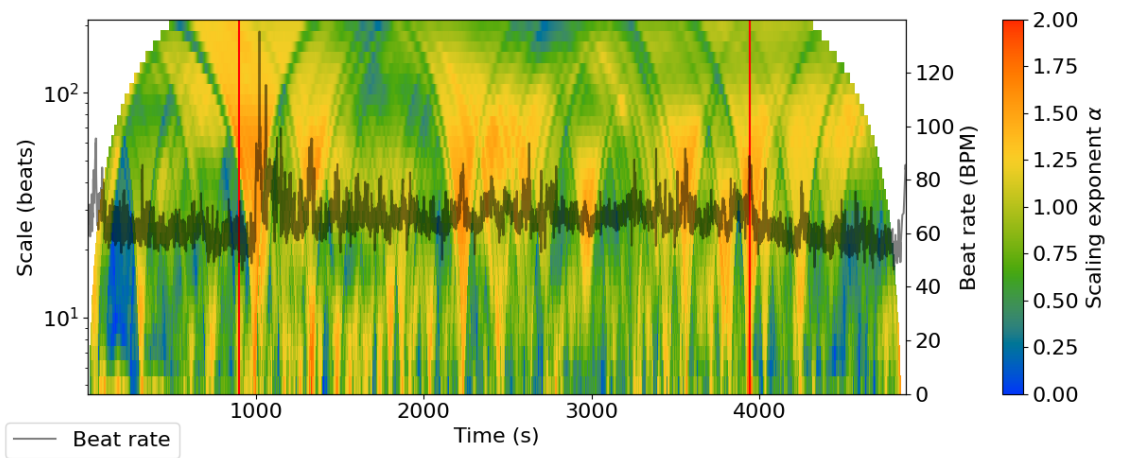


Figure A.11 Subject11: DDFA alpha surface plot.

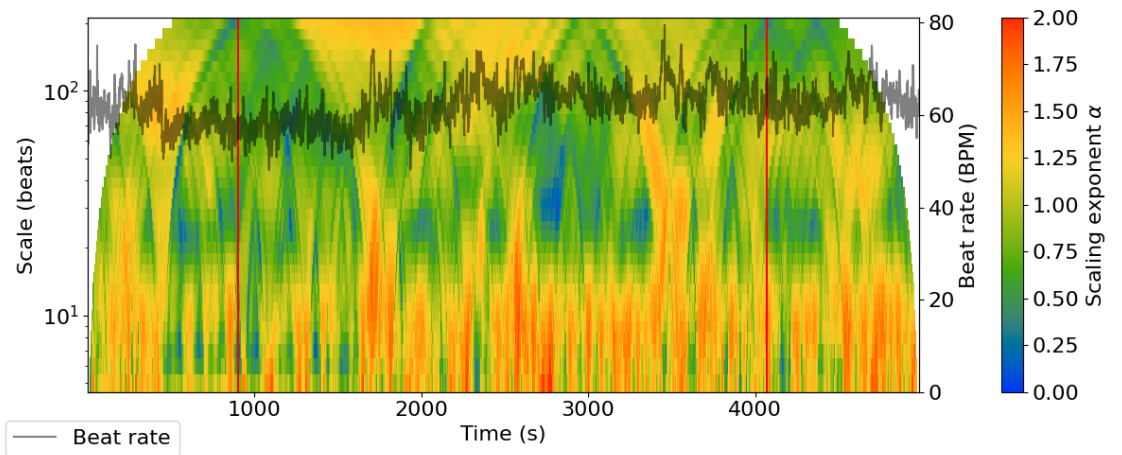


Figure A.12 Subject12: DDFA alpha surface plot.

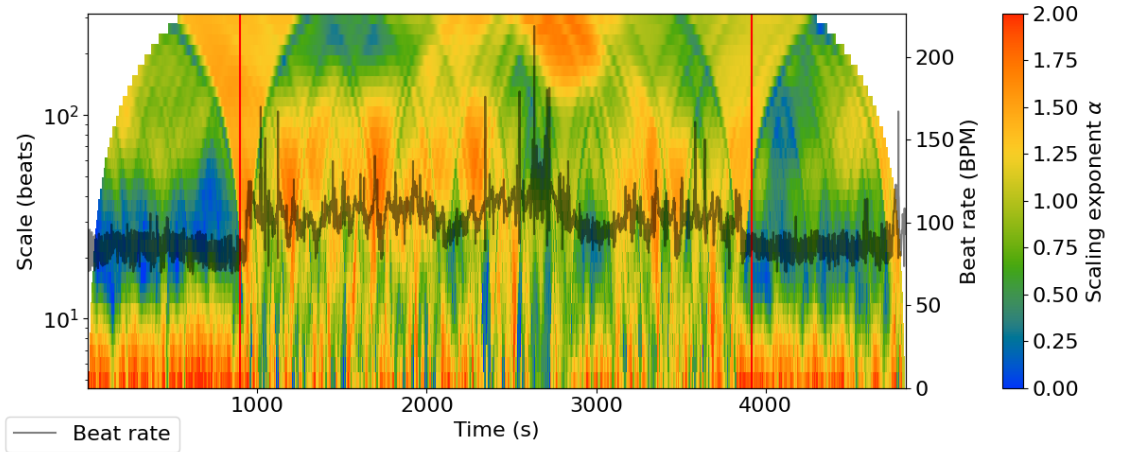


Figure A.13 Subject13: DDFA alpha surface plot.

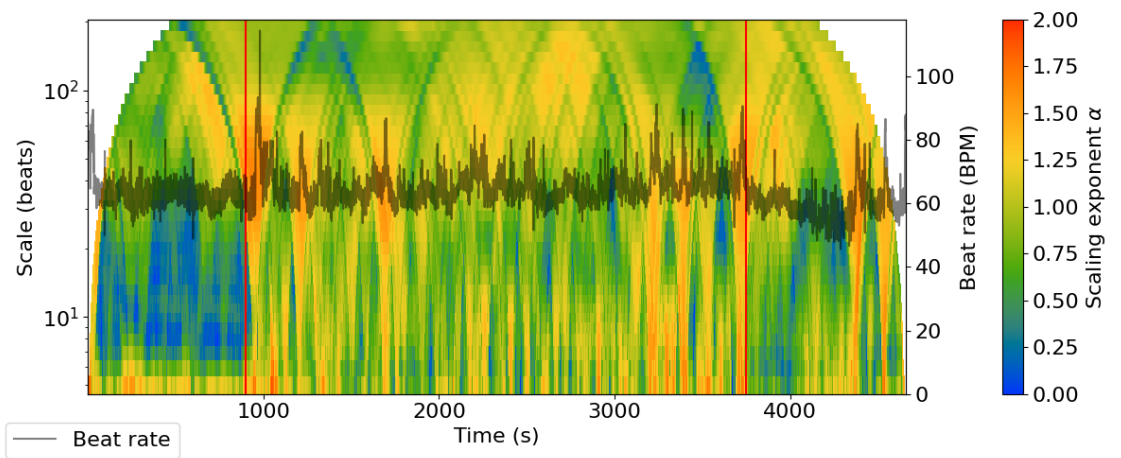


Figure A.15 Subject15: DDFA alpha surface plot.

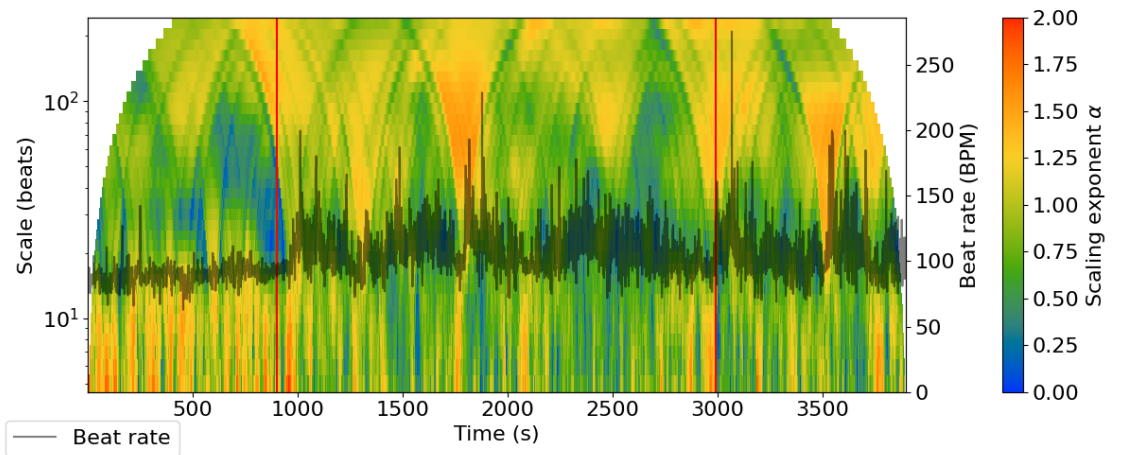


Figure A.16 Subject16: DDFA alpha surface plot.

APPENDIX B: DDFA ALPHA DISTRIBUTION

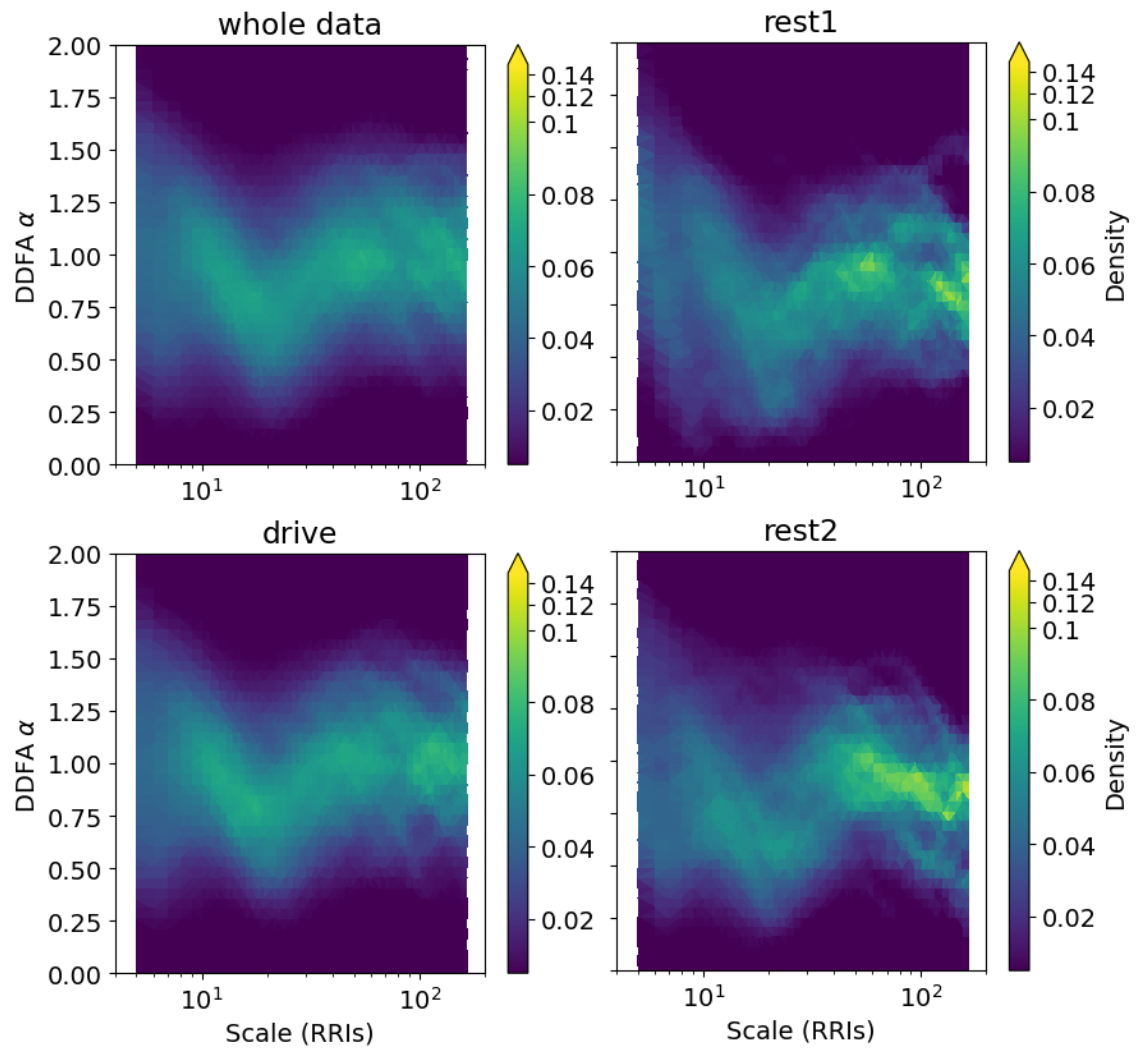


Figure B.1 Aggregation DDFA alpha distribution.

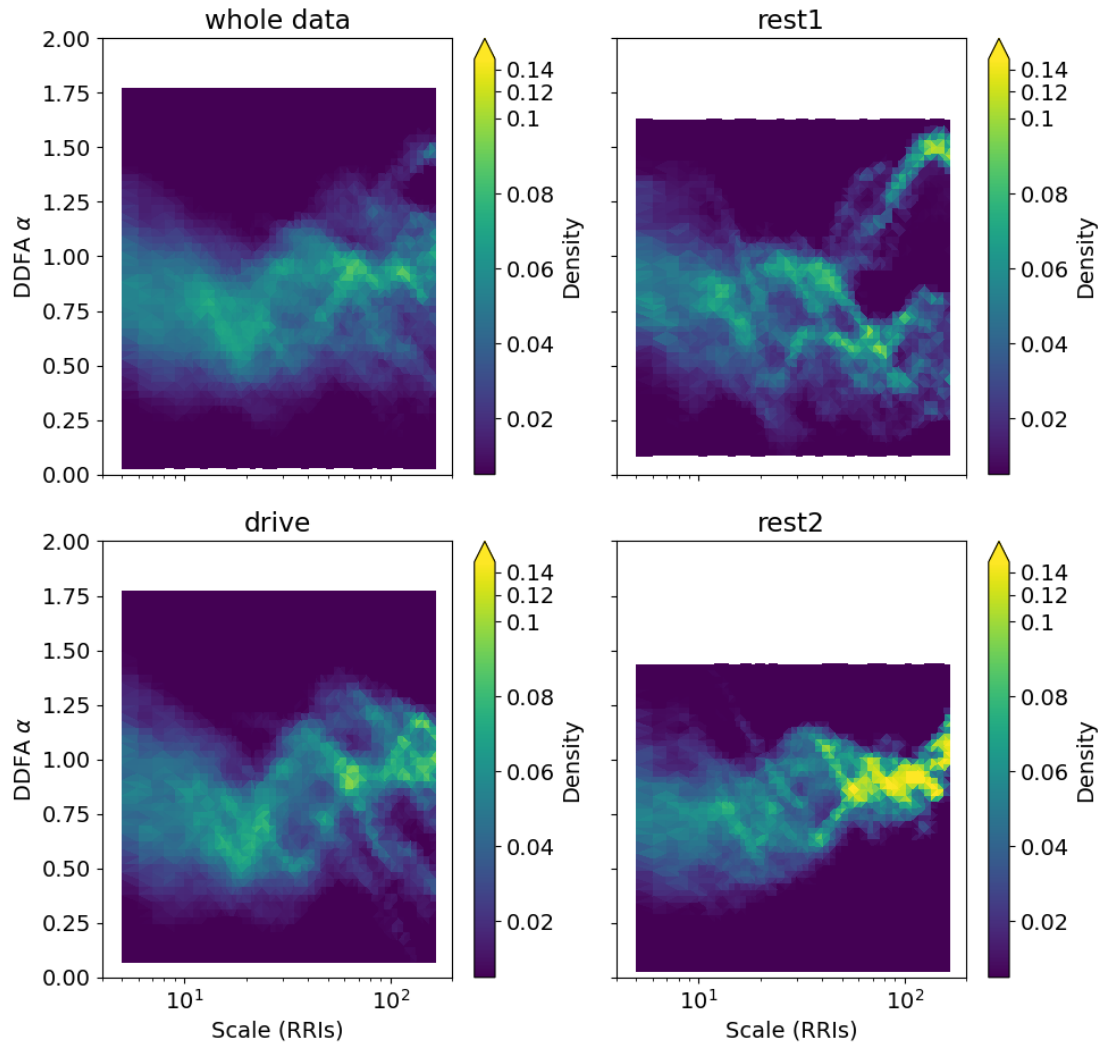


Figure B.2 Subject01: DDFA alpha distribution.

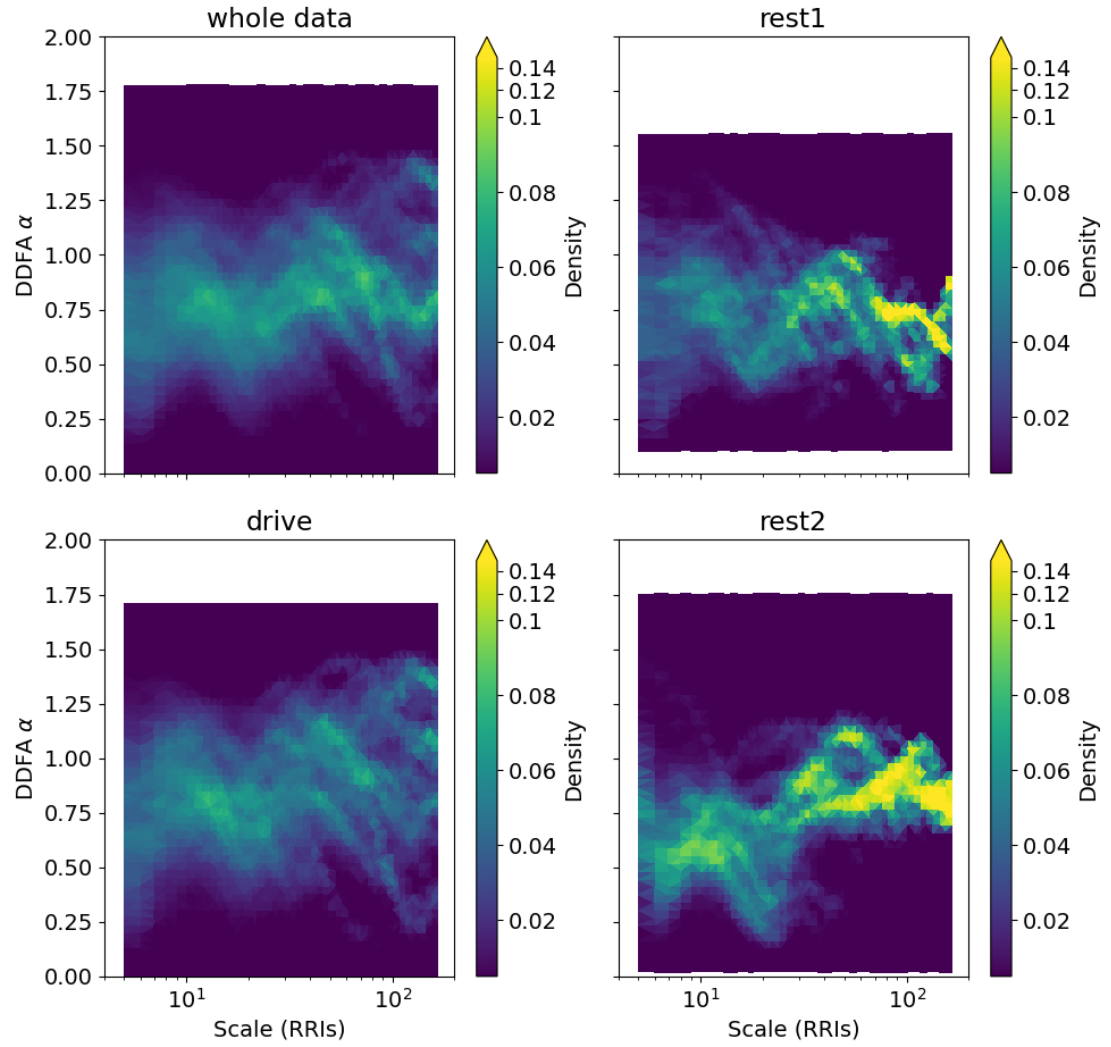


Figure B.3 Subject02: DDFA alpha distribution.

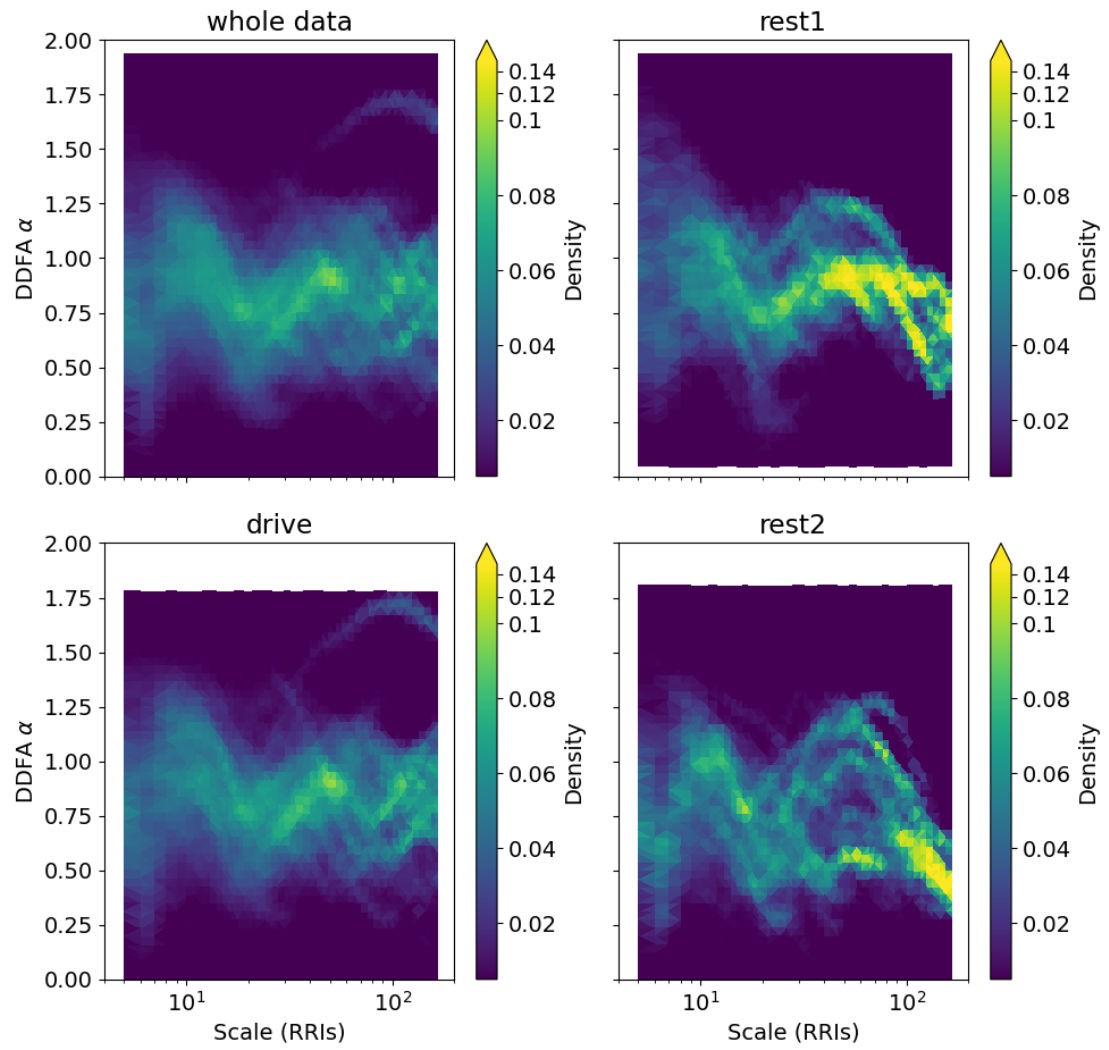


Figure B.4 Subject03: DDFA alpha distribution.

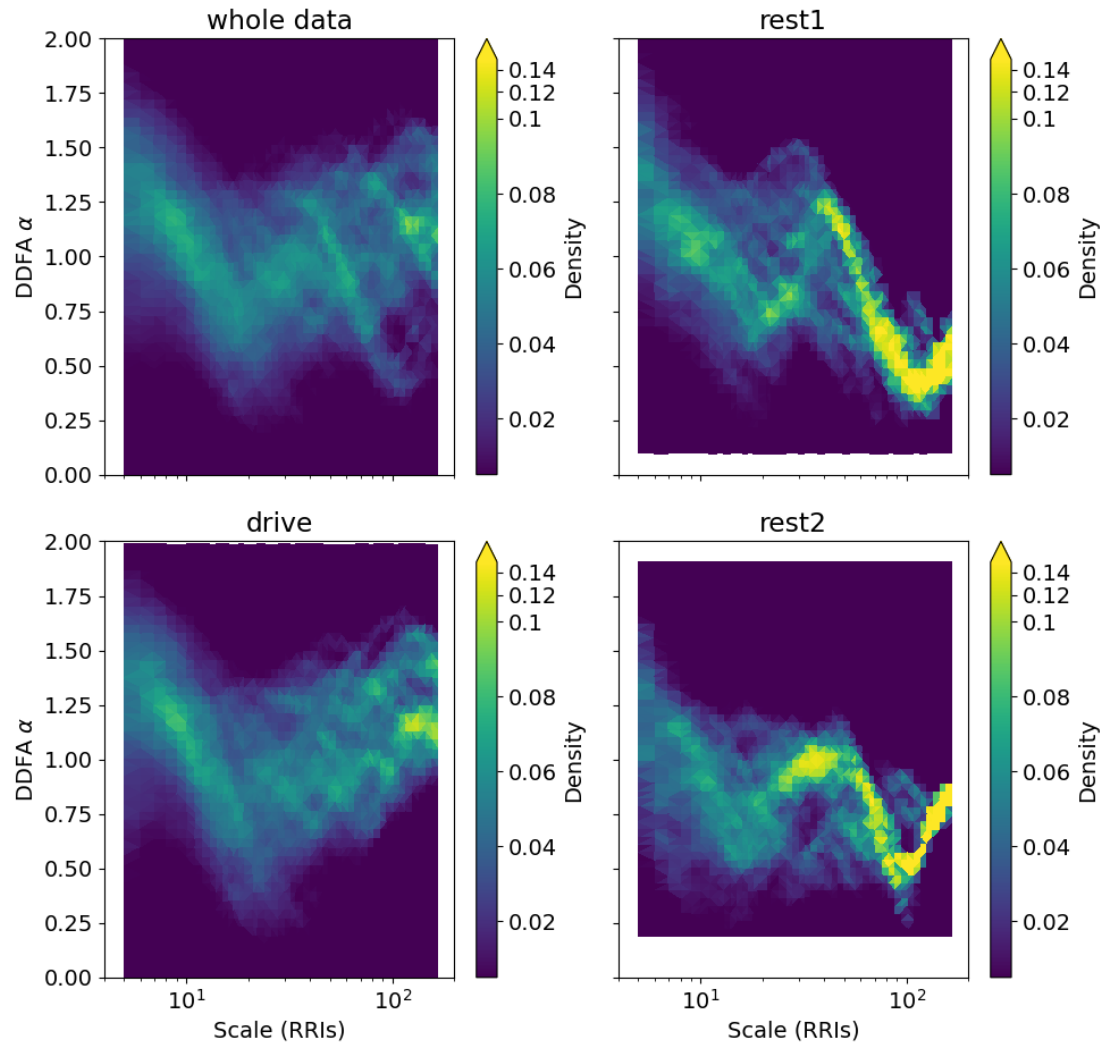


Figure B.5 Subject04: DDFA alpha distribution.

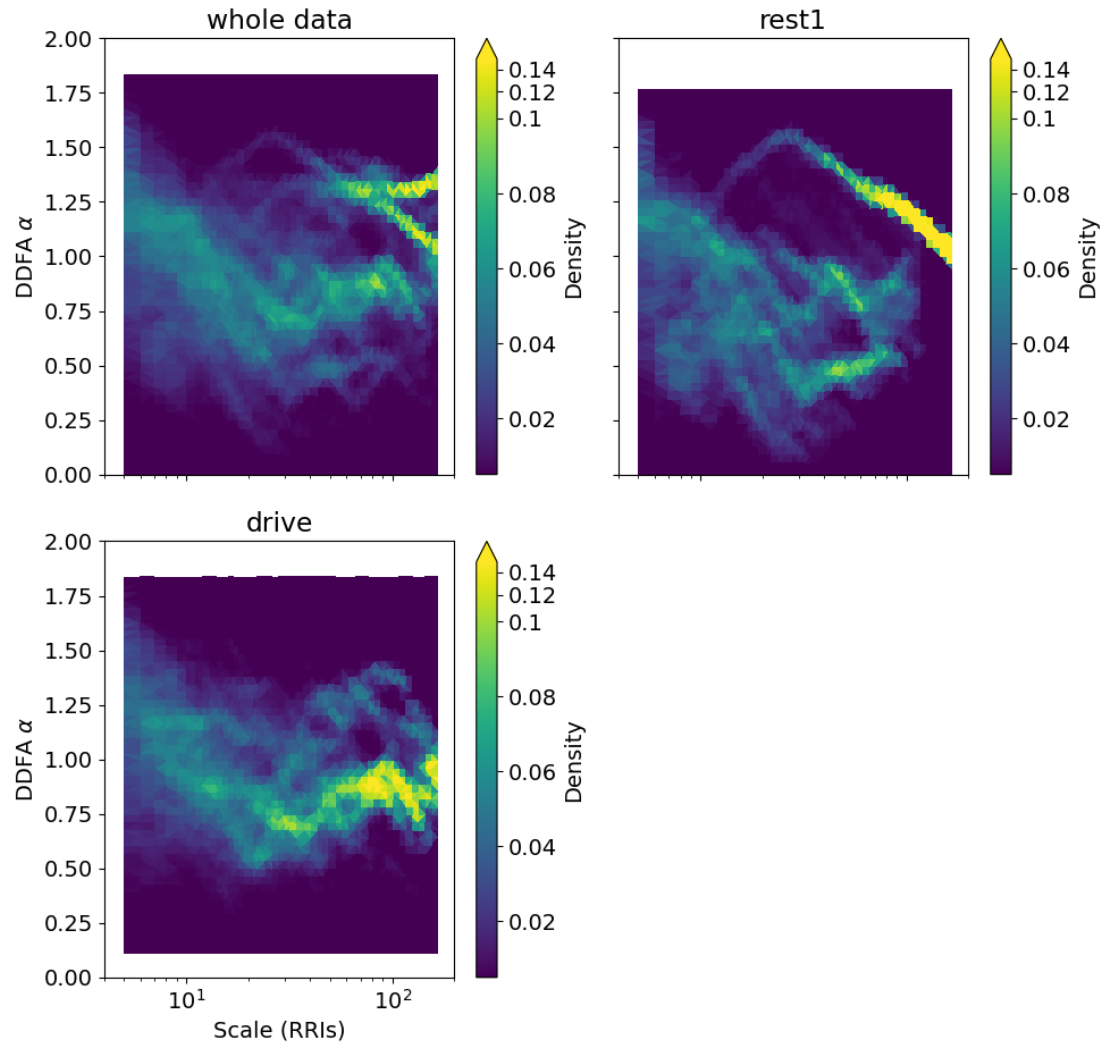


Figure B.6 Subject05a: DDFA α distribution.

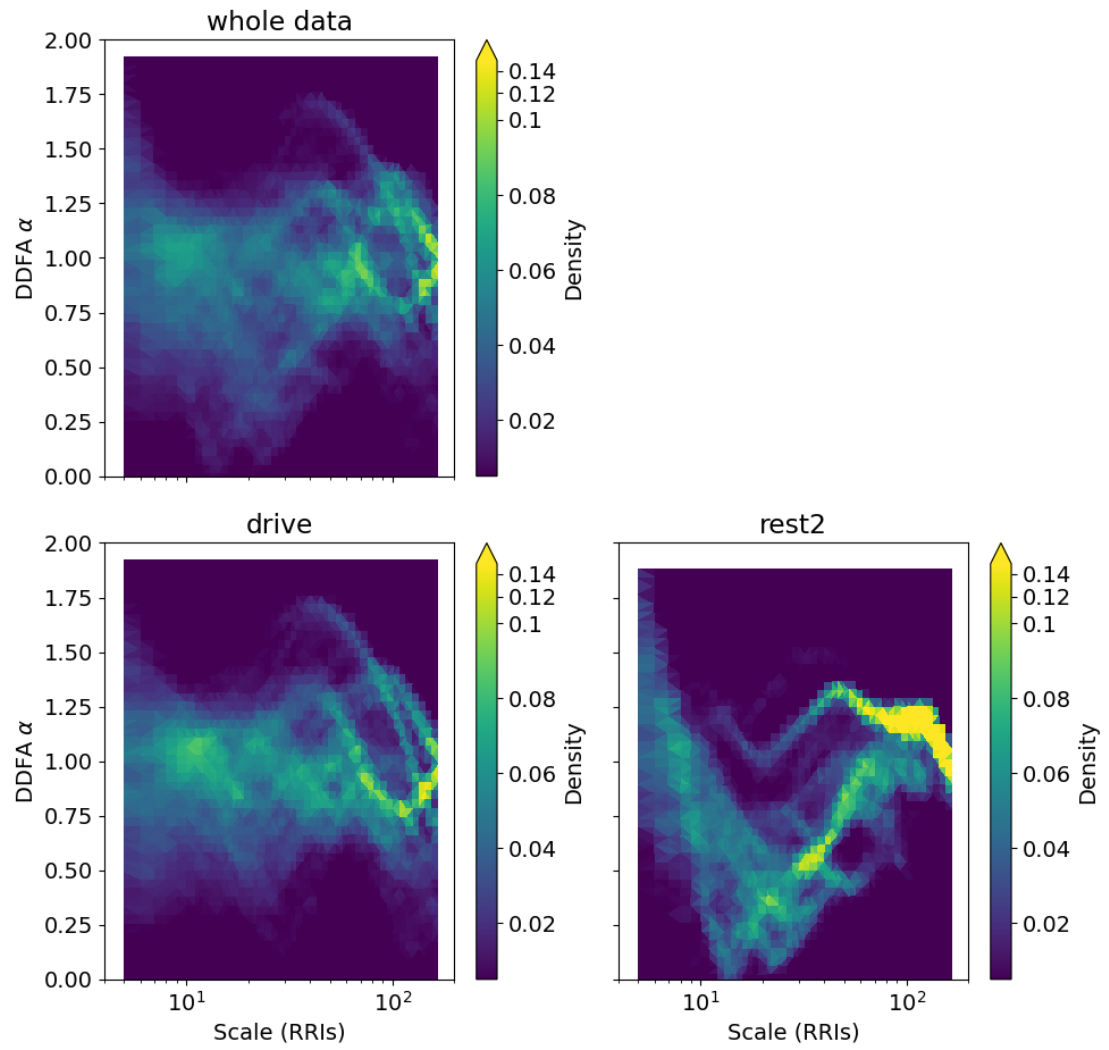


Figure B.7 Subject05b: DDFA alpha distribution.

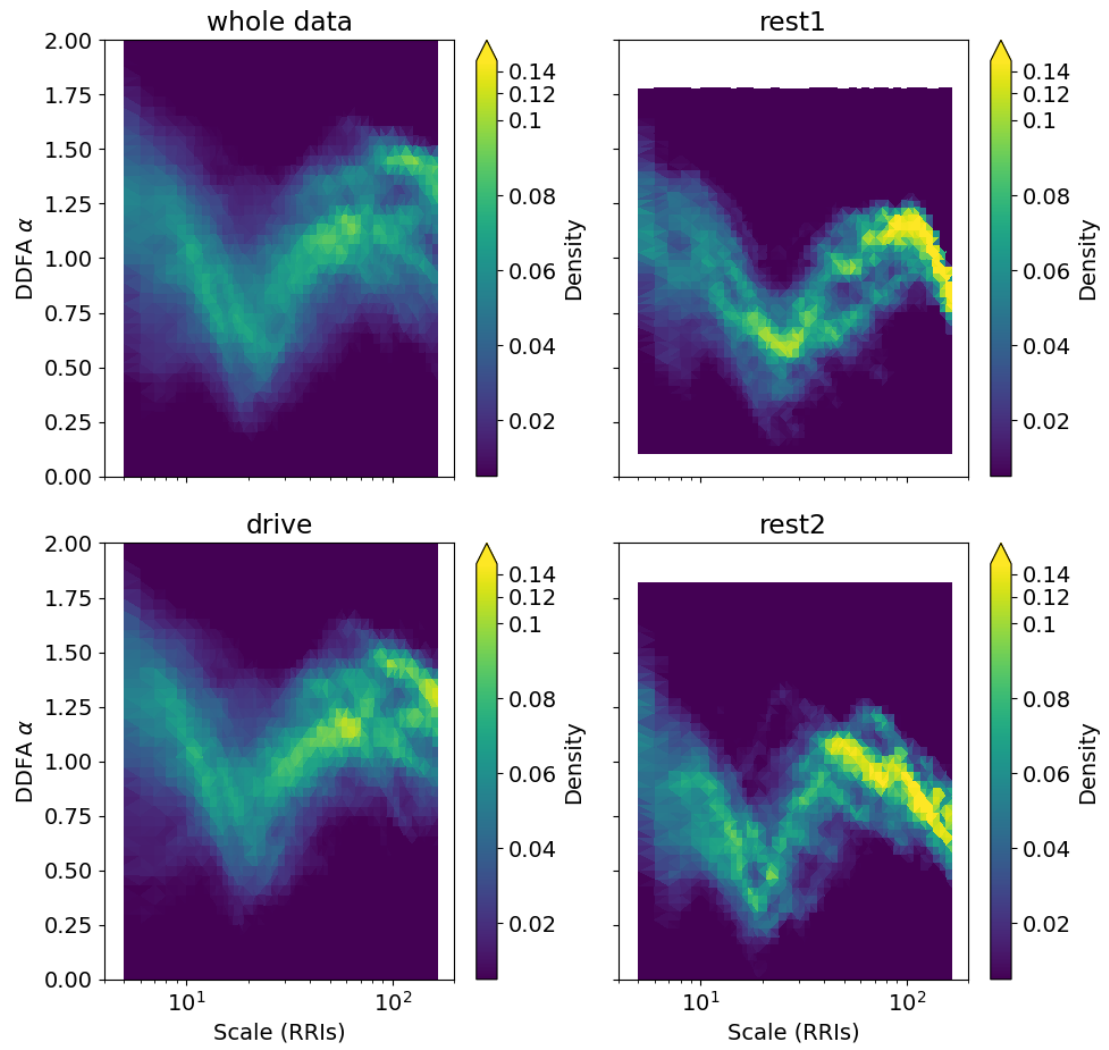


Figure B.8 Subject06: DDFA alpha distribution.

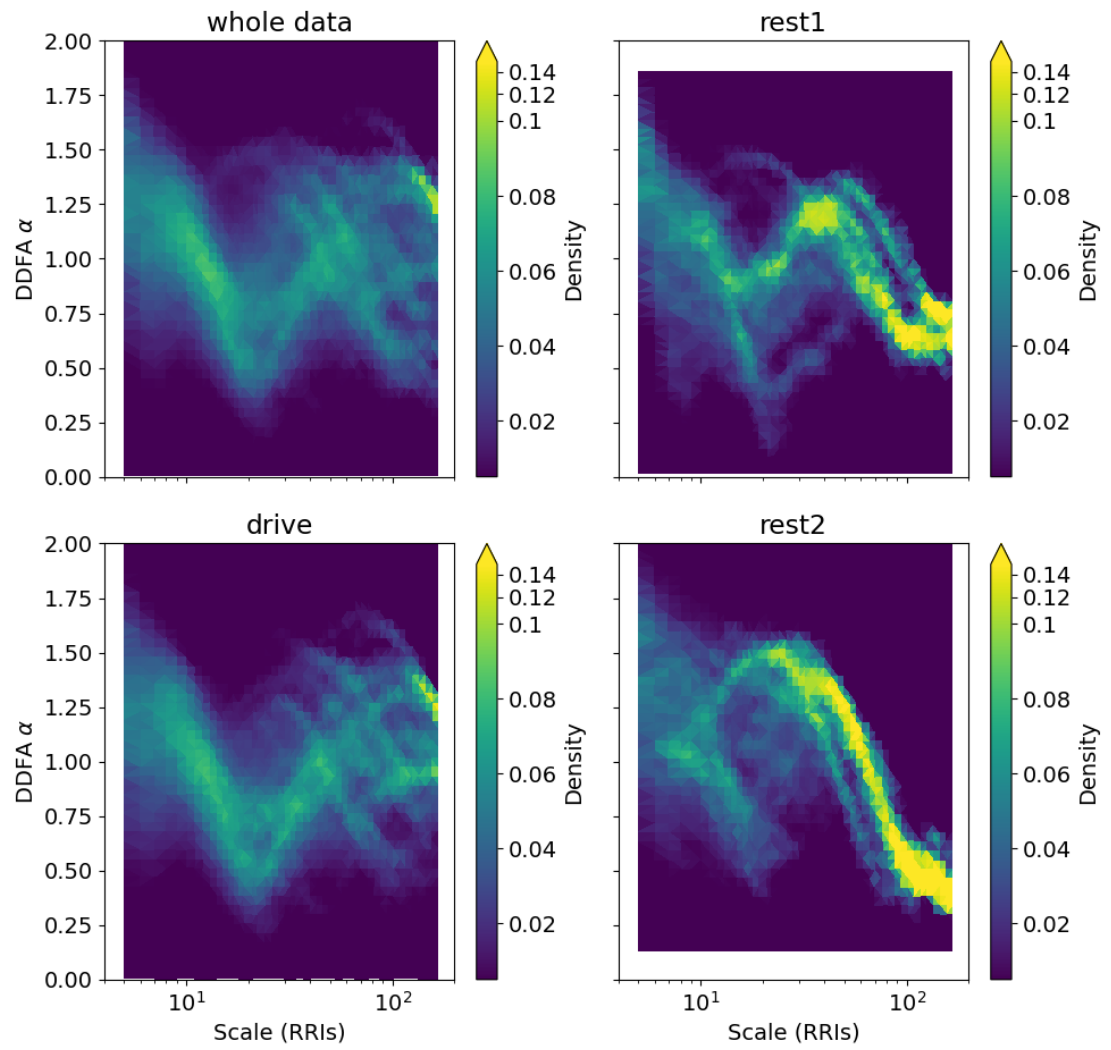


Figure B.9 Subject07: DDFA alpha distribution.

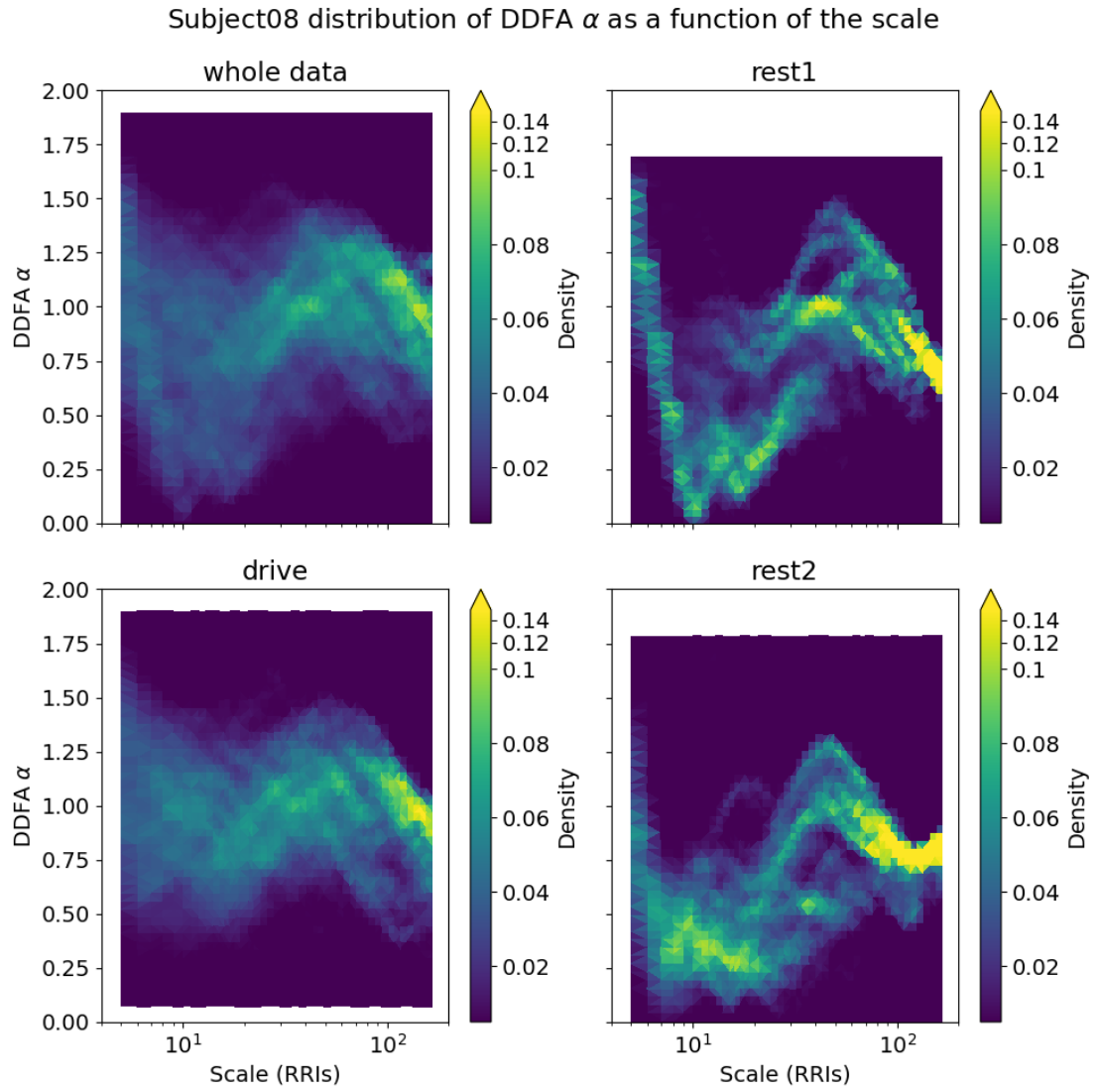


Figure B.10 Subject08: DDFA α distribution.

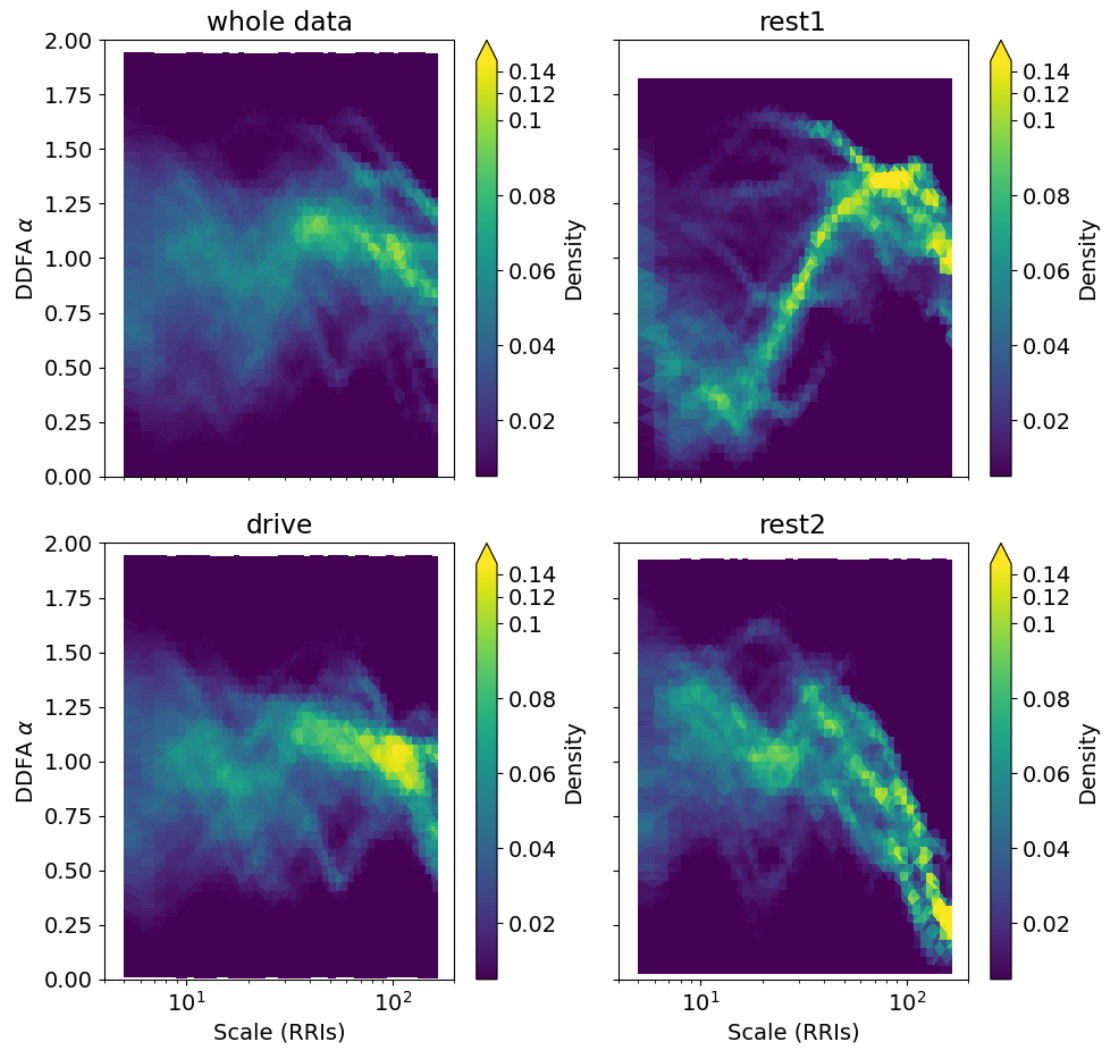


Figure B.11 Subject09: DDFA alpha distribution.

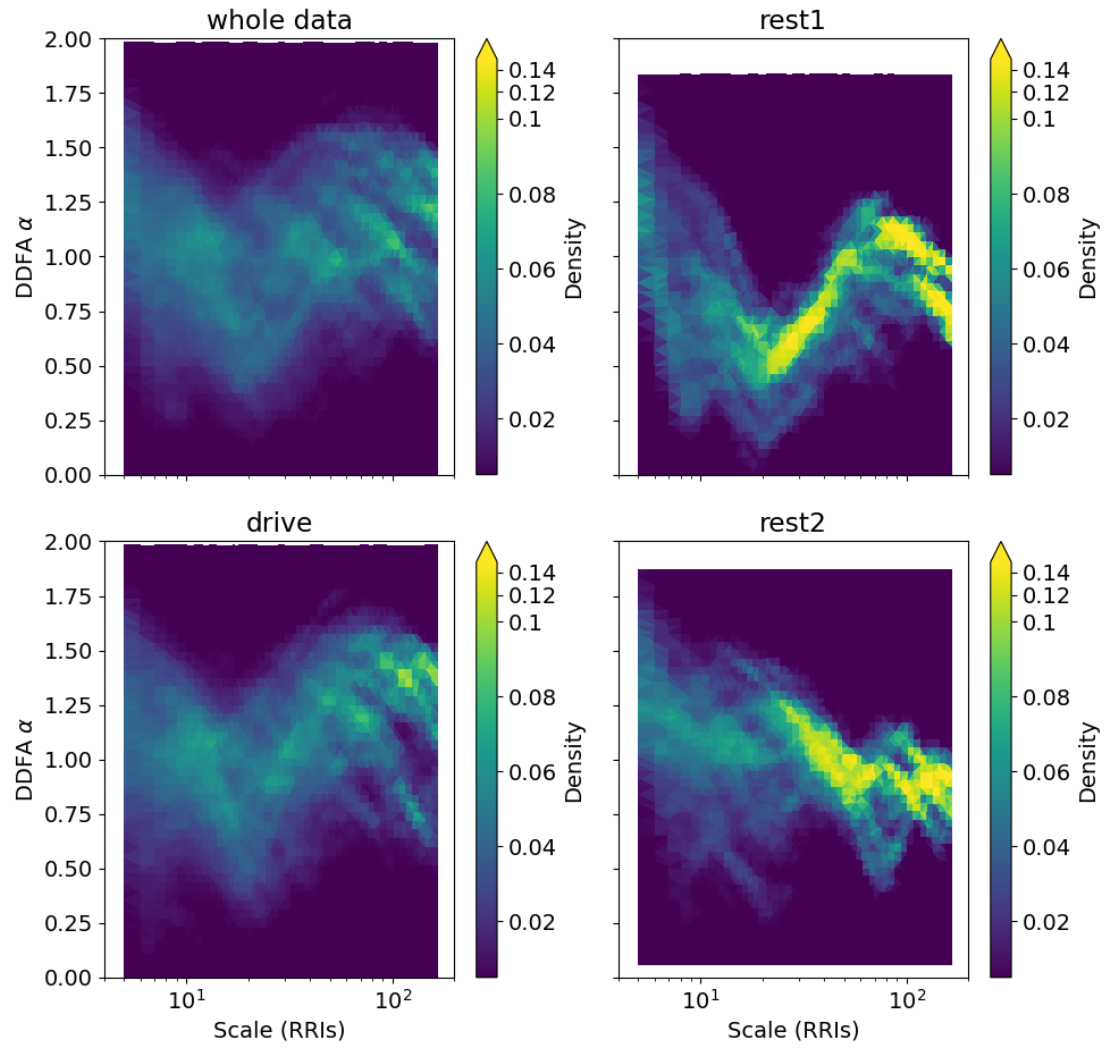


Figure B.12 Subject10: DDFA alpha distribution.

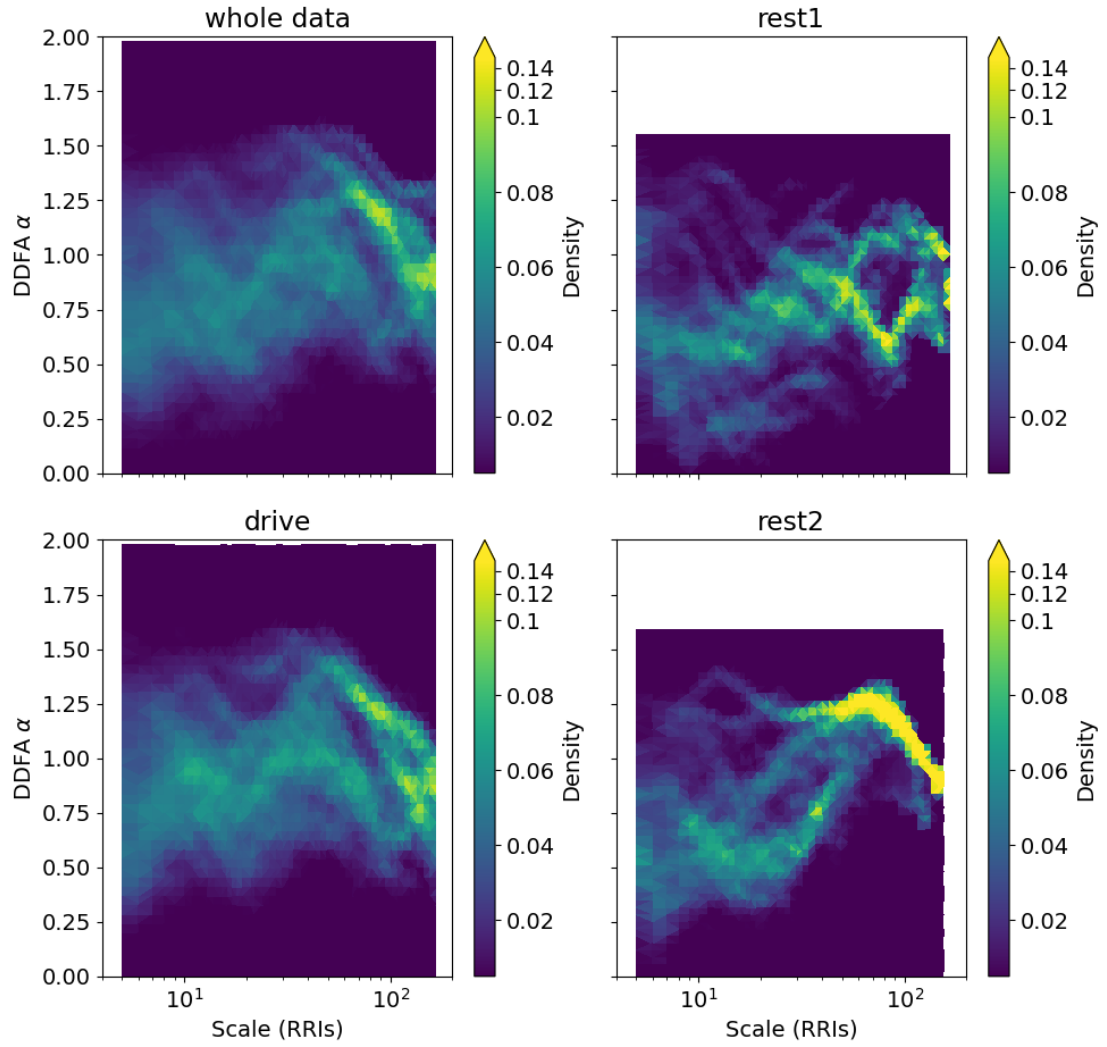


Figure B.13 Subject11: DDFA alpha distribution.

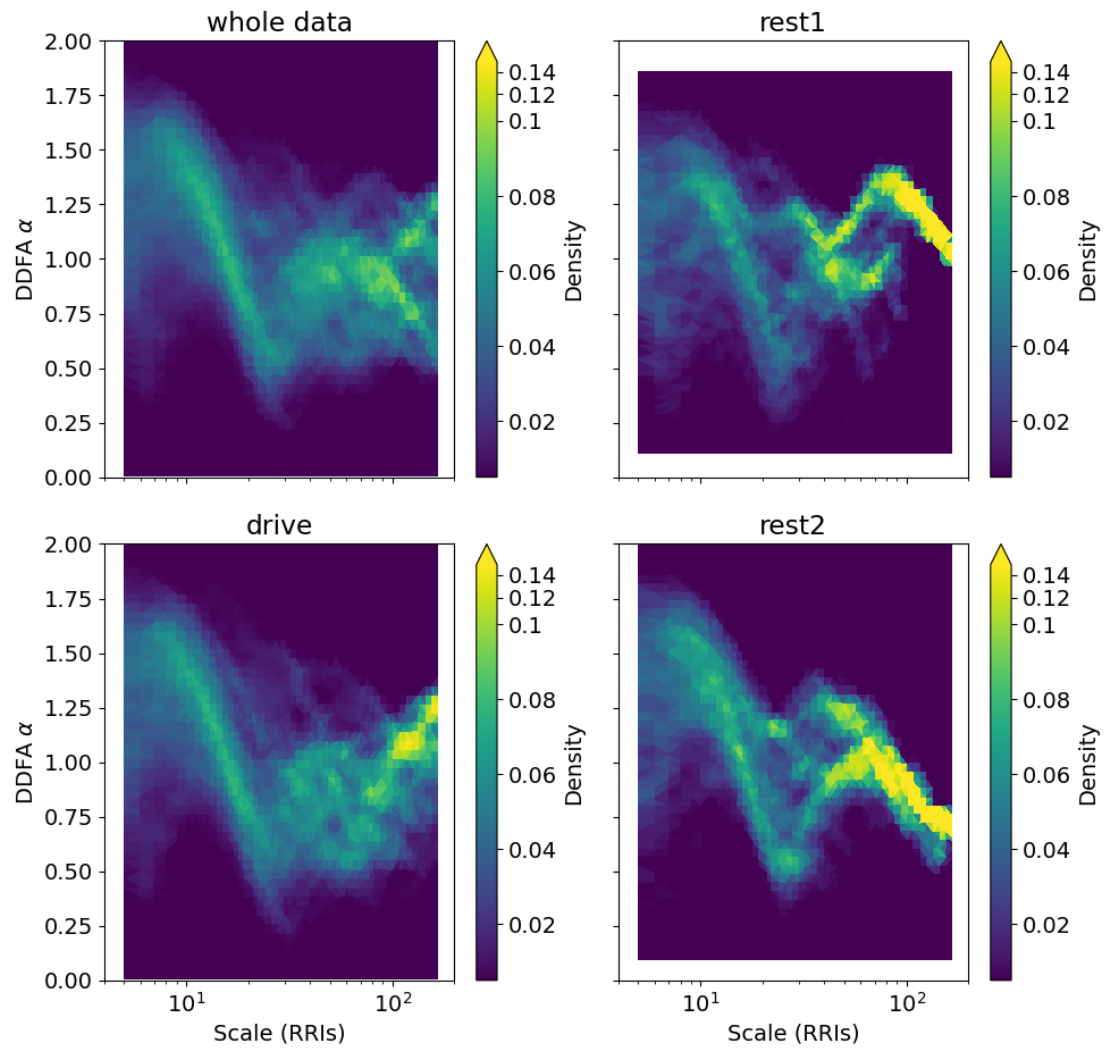


Figure B.14 Subject12: DDFA alpha distribution.

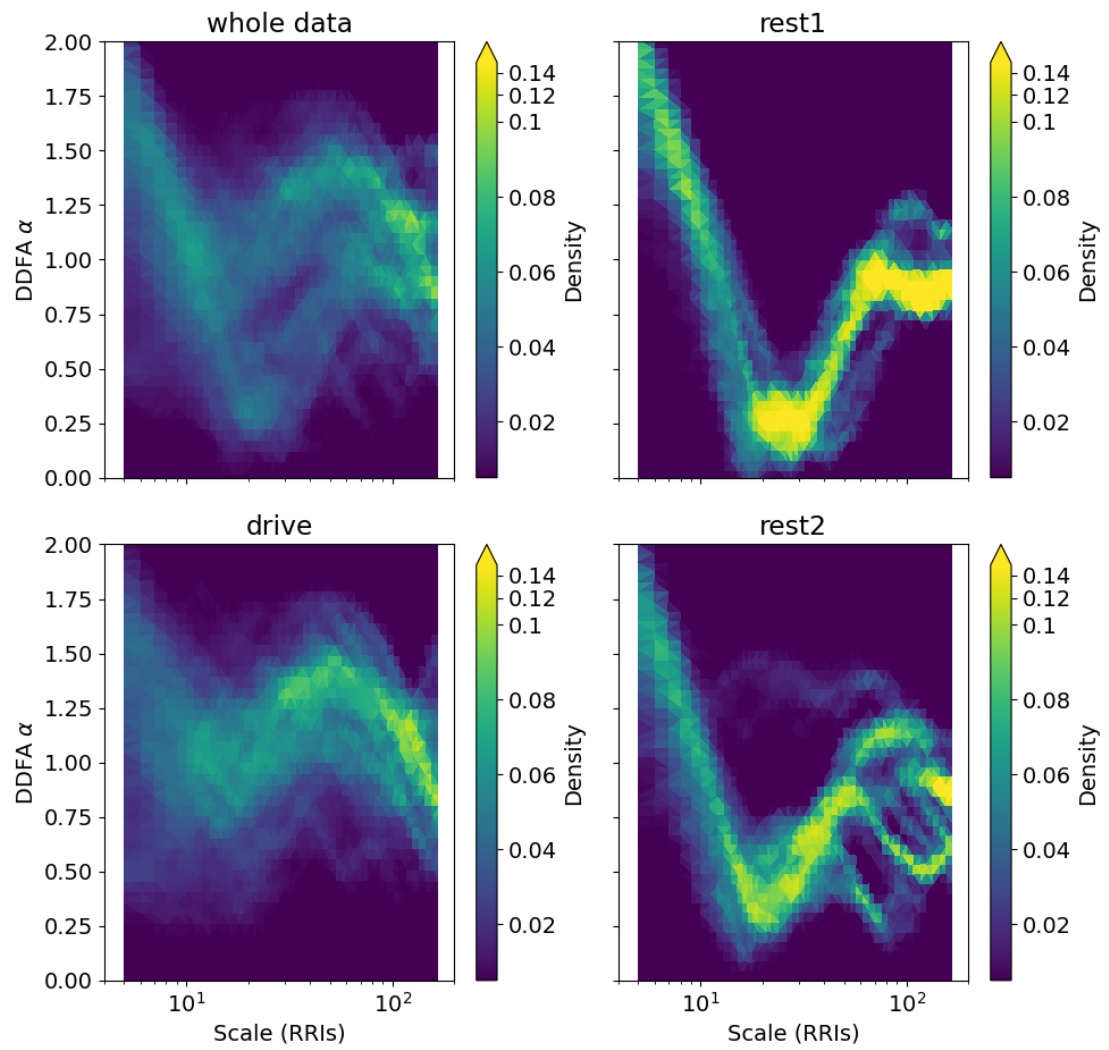


Figure B.15 Subject13: DDFA alpha distribution.

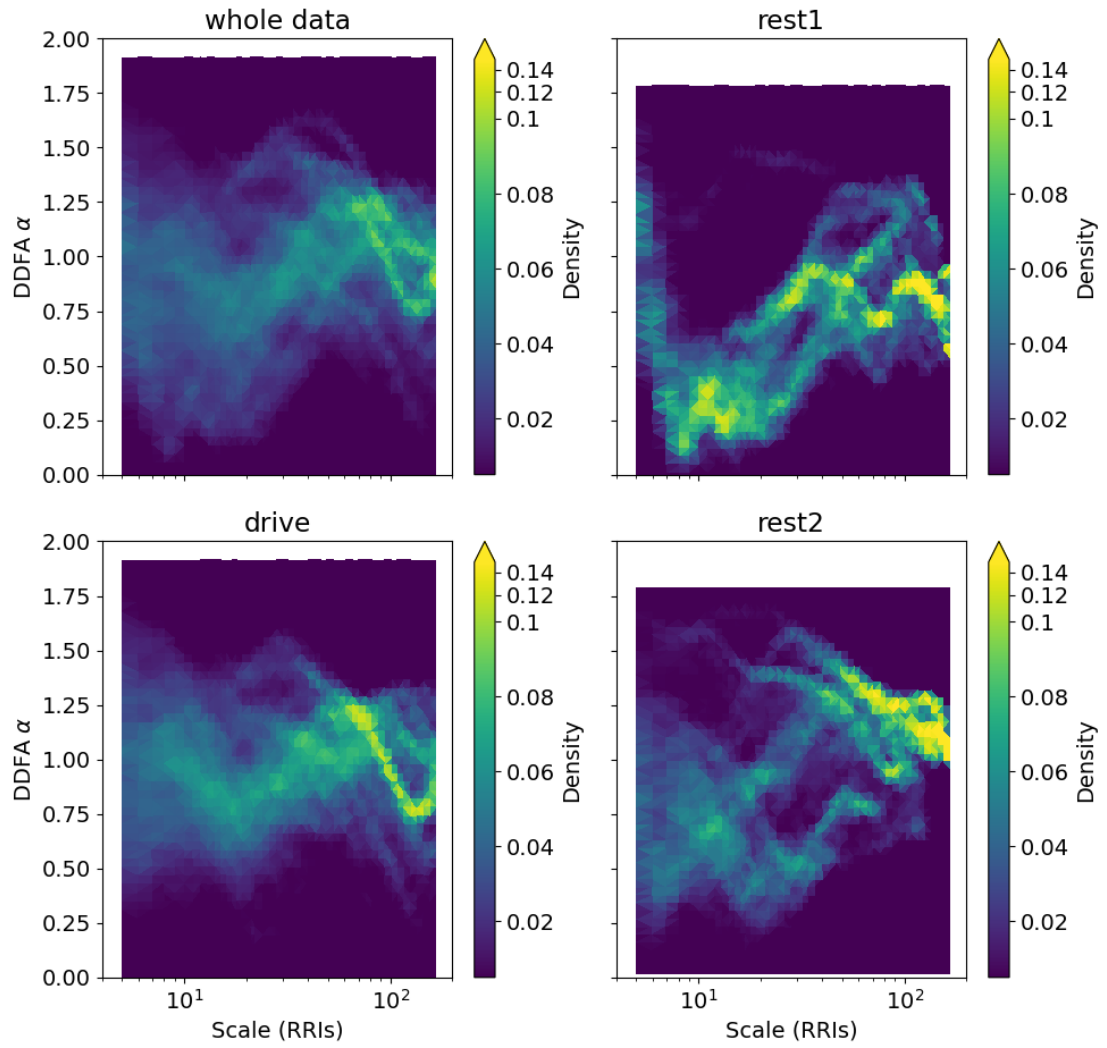


Figure B.16 Subject15: DDFA alpha distribution.

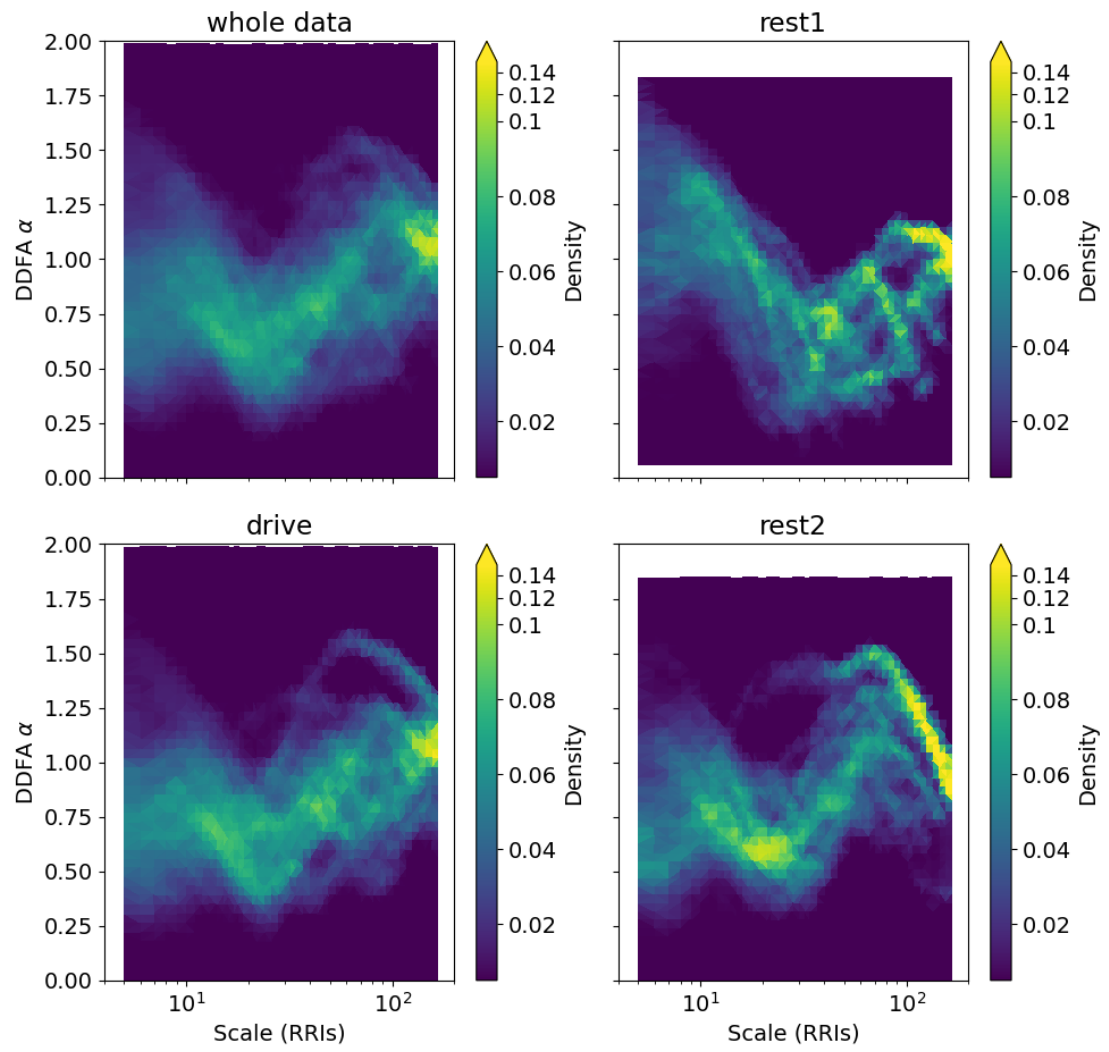


Figure B.17 Subject16: DDFA α distribution.

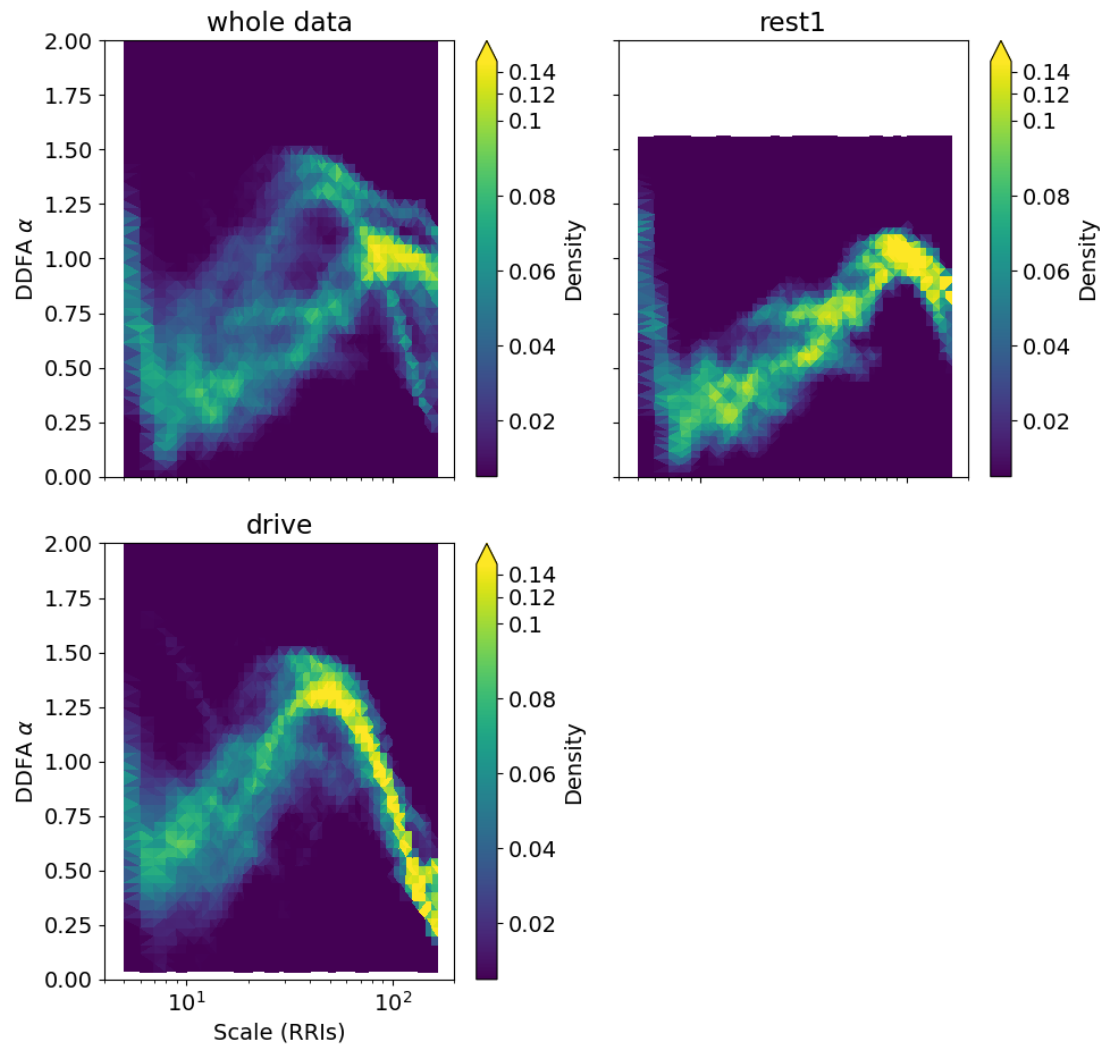


Figure B.18 Subject17a: DDFA alpha distribution.

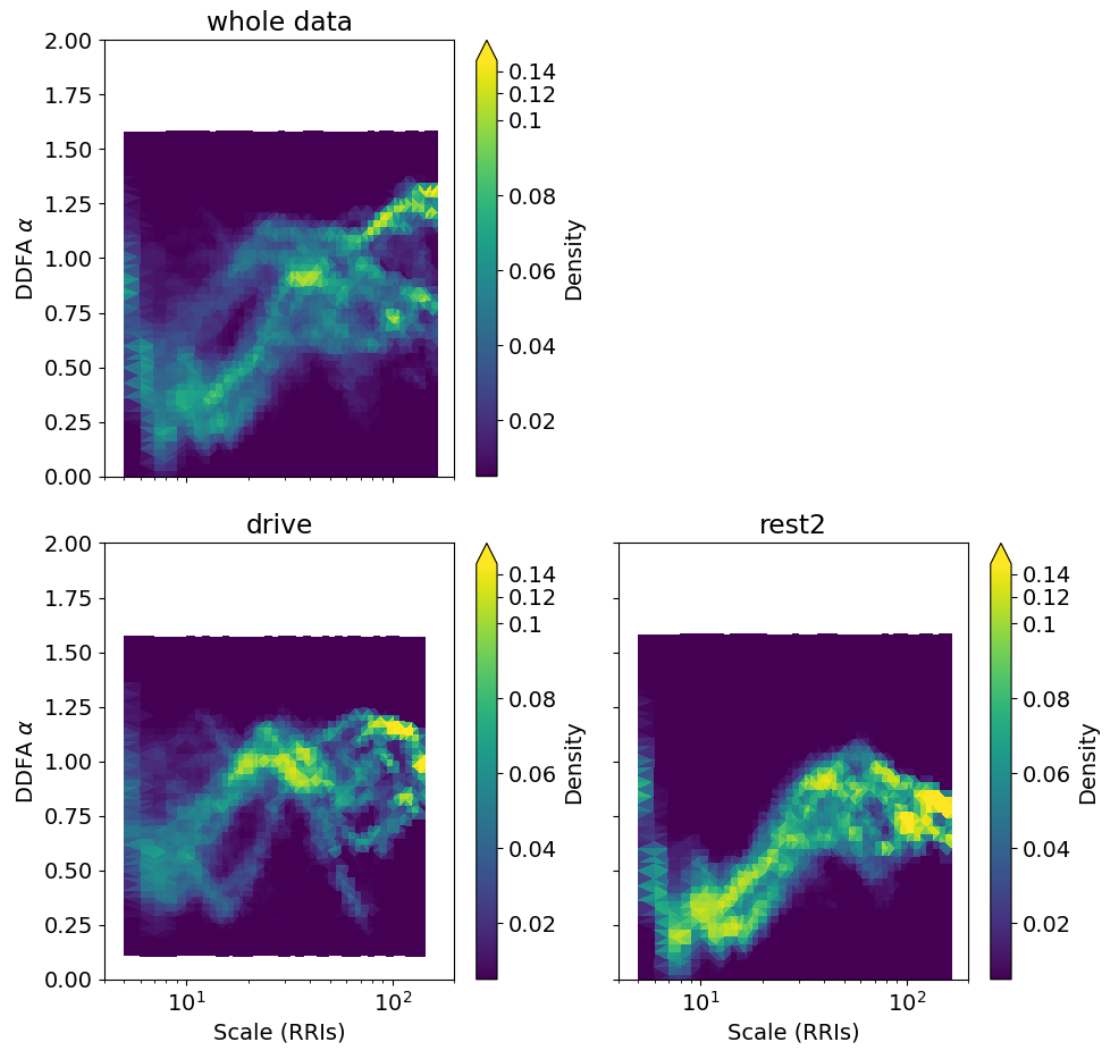


Figure B.19 Subject17b: DDFA alpha distribution.

APPENDIX C: DDFA ALPHA MEAN AND STANDARD DEVIATION AS FUNCTION OF SCALE

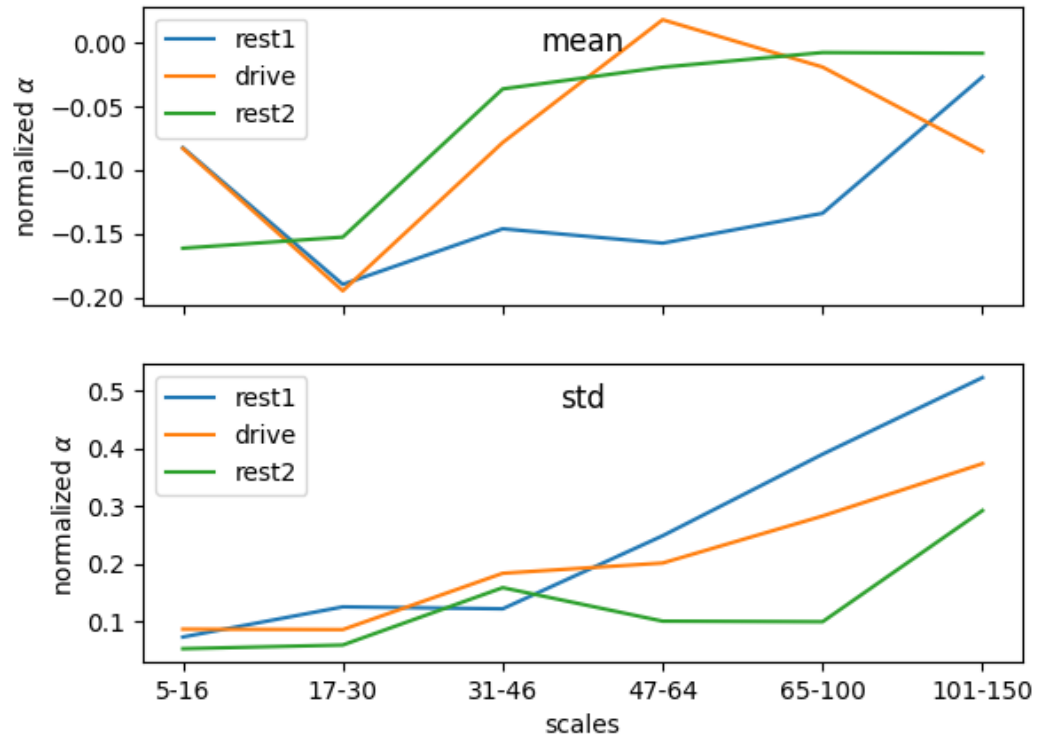


Figure C.1 Subject01: normalized DDFA alpha mean and standard deviation as function of scale.

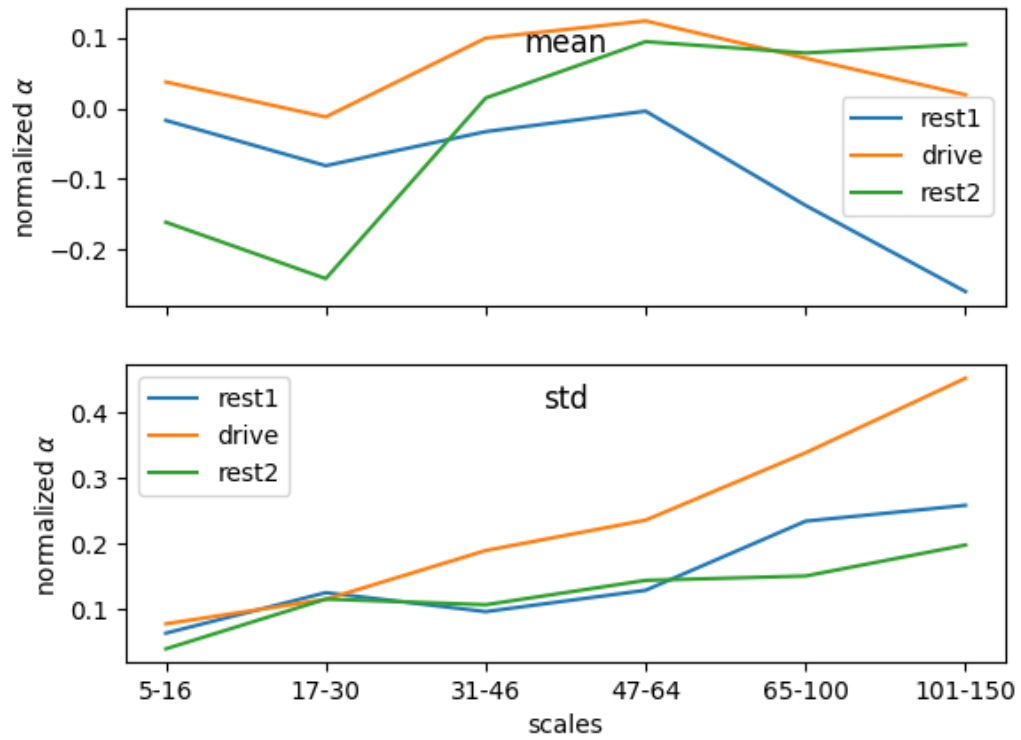


Figure C.2 Subject02: normalized DDFA alpha mean and standard deviation as function of scale

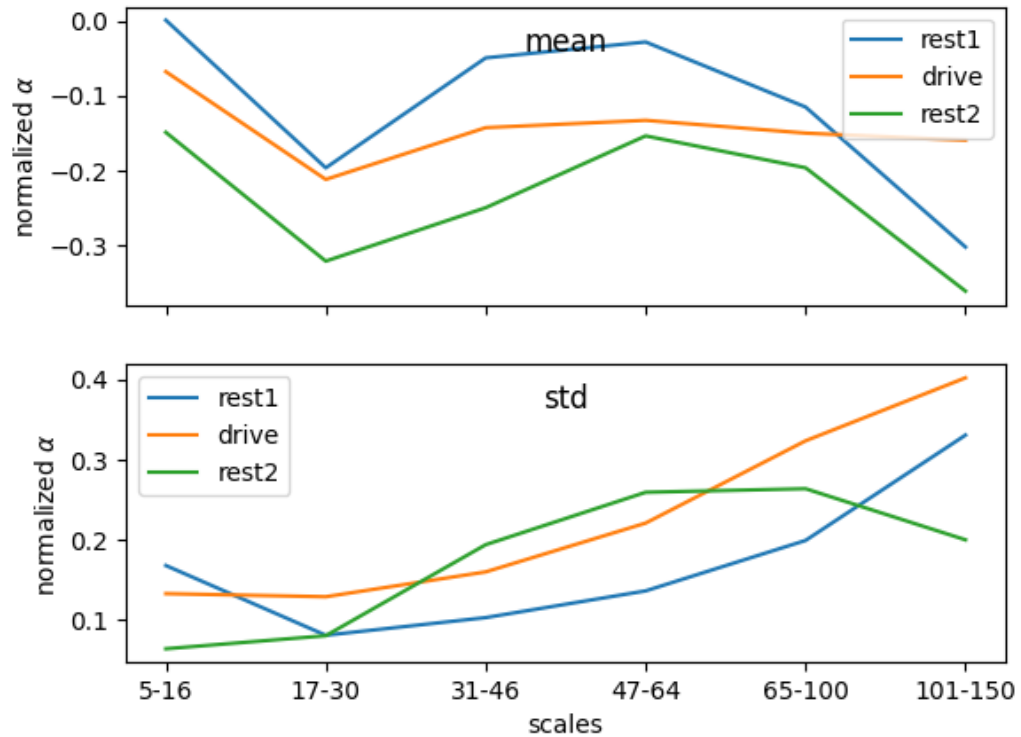


Figure C.3 Subject03: normalized DDFA alpha mean and standard deviation as function of scale.

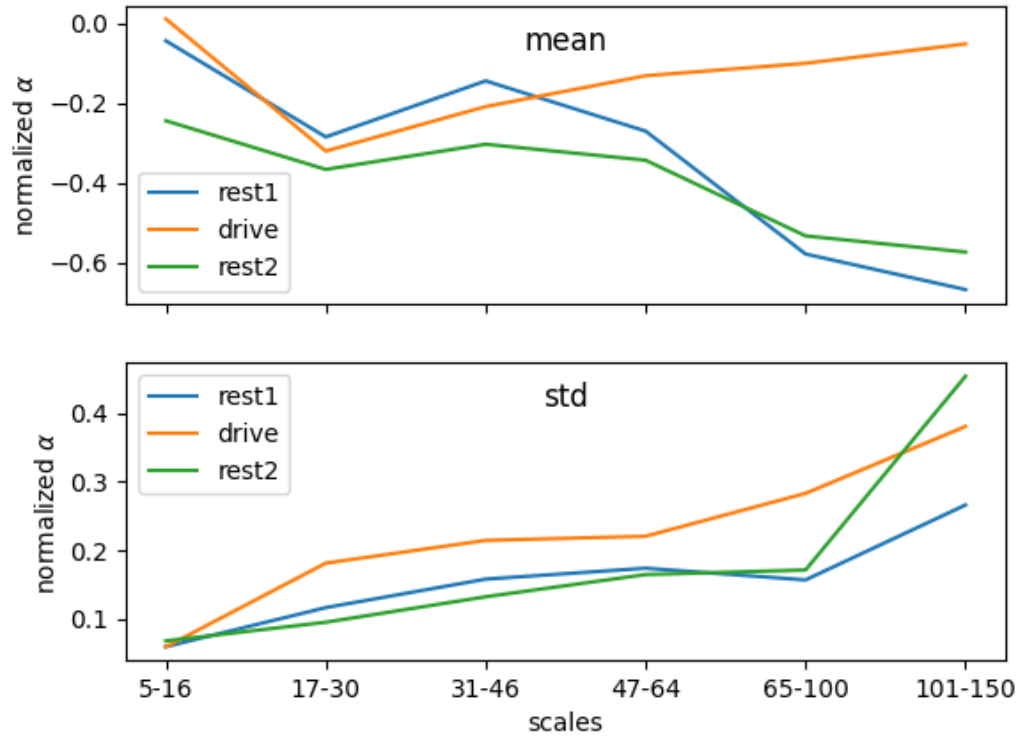


Figure C.4 Subject04: normalized DDFA alpha mean and standard deviation as function of scale.

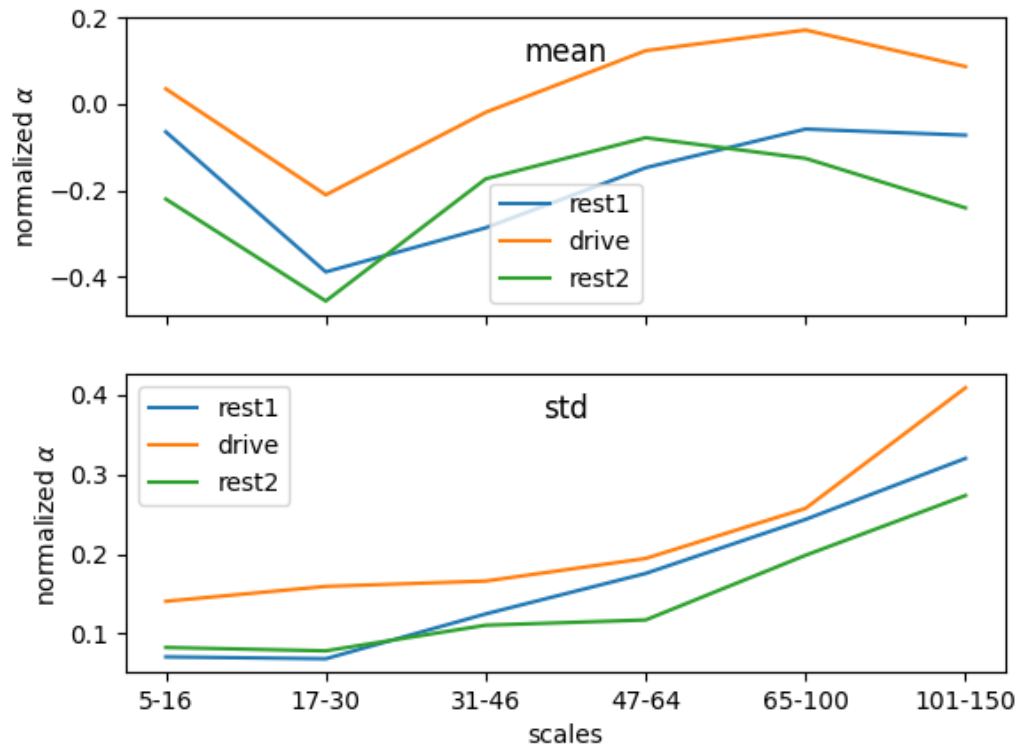


Figure C.5 Subject06: normalized DDFA alpha mean and standard deviation as function of scale.

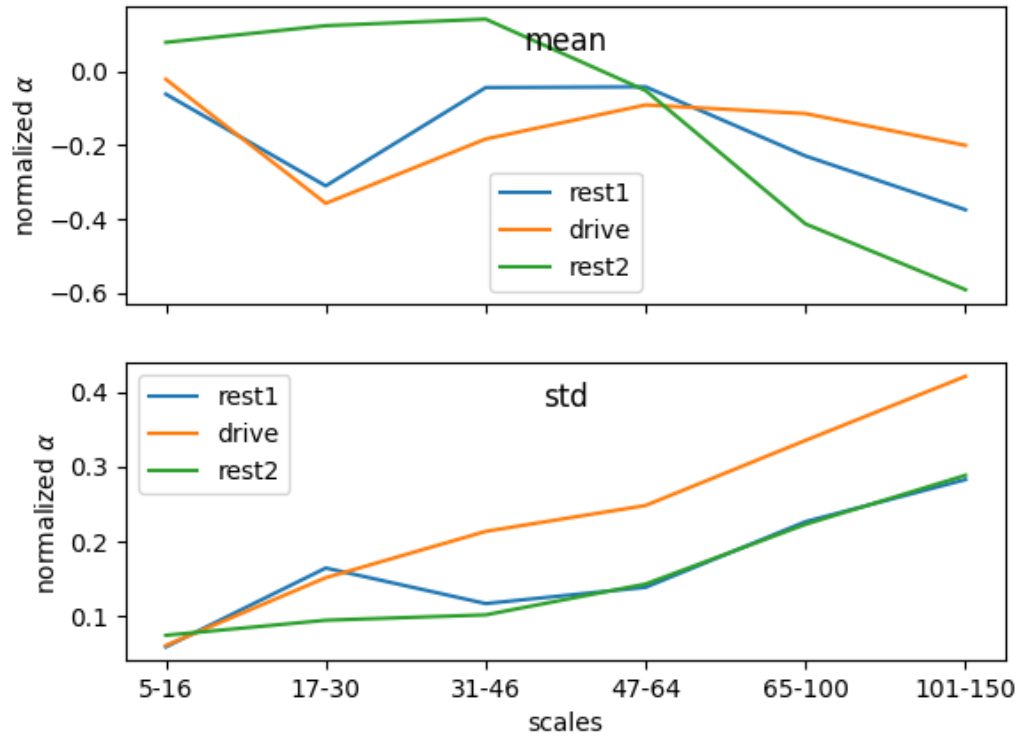


Figure C.6 Subject07: normalized DDFA alpha mean and standard deviation as function of scale.

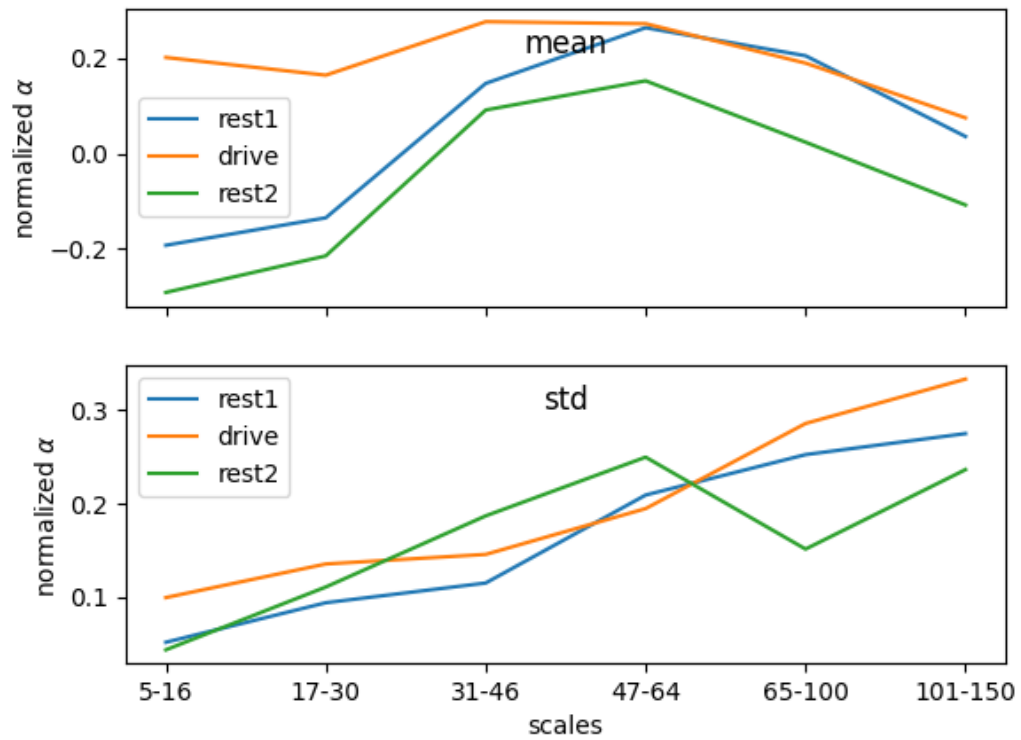


Figure C.7 Subject08: normalized DDFA alpha mean and standard deviation as function of scale.

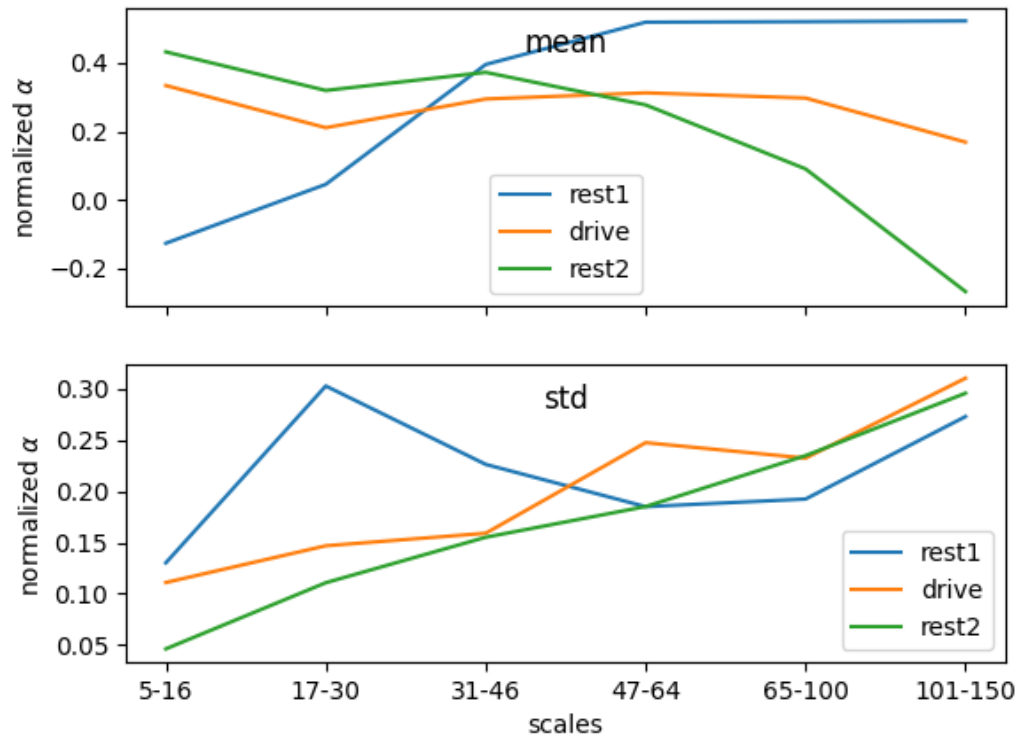


Figure C.8 Subject09: normalized DDFA alpha mean and standard deviation as function of scale.

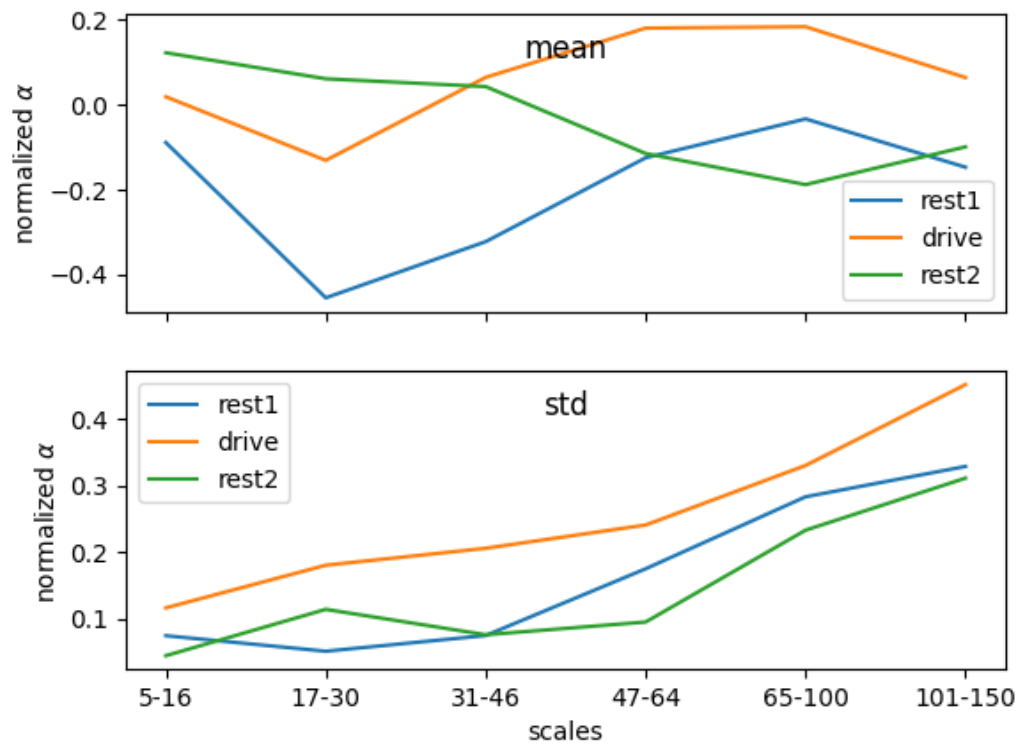


Figure C.9 Subject10: normalized DDFA alpha mean and standard deviation as function of scale.

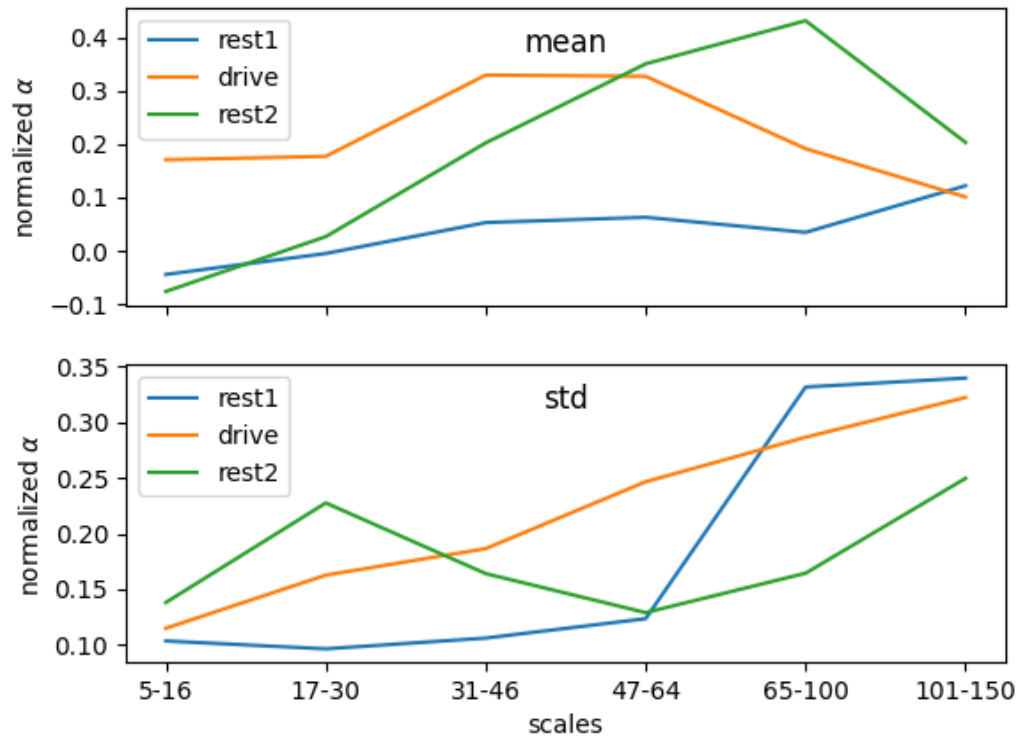


Figure C.10 Subject11: normalized DDFA alpha mean and standard deviation as function of scale.

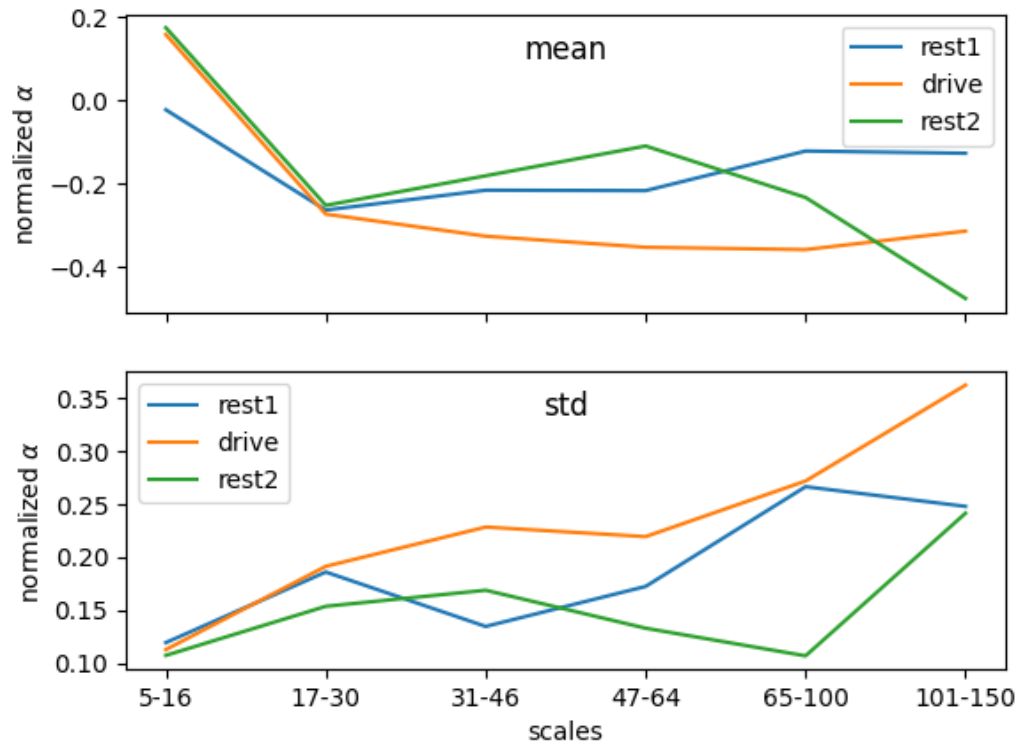


Figure C.11 Subject12: normalized DDFA alpha mean and standard deviation as function of scale.

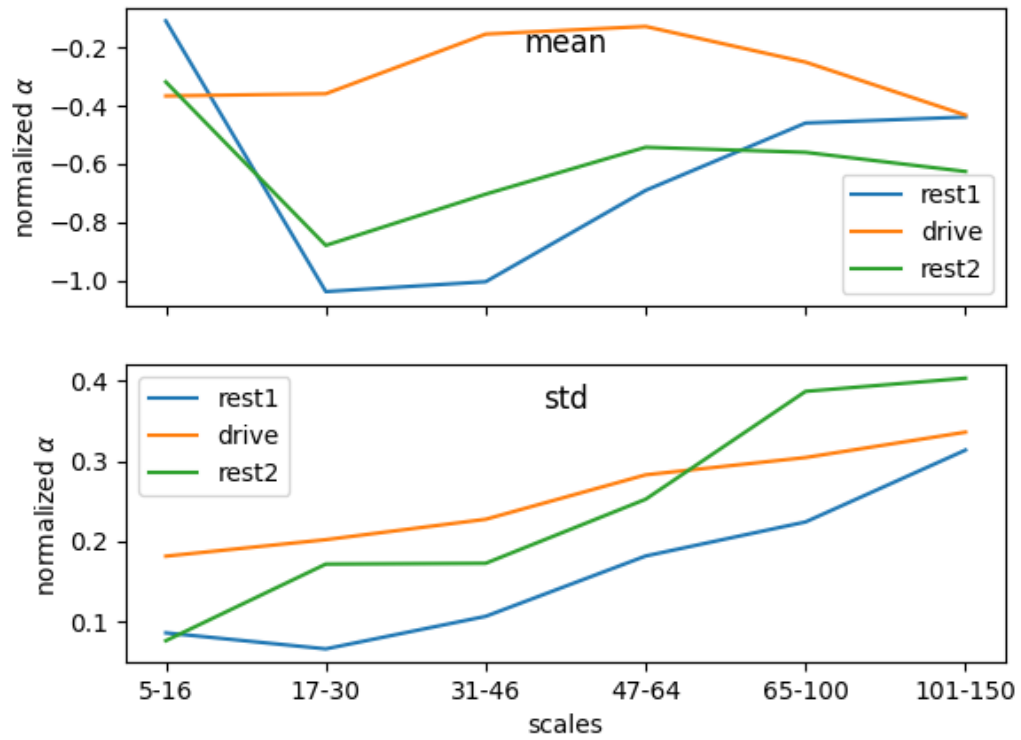


Figure C.12 Subject13: normalized DDFA alpha mean and standard deviation as function of scale.

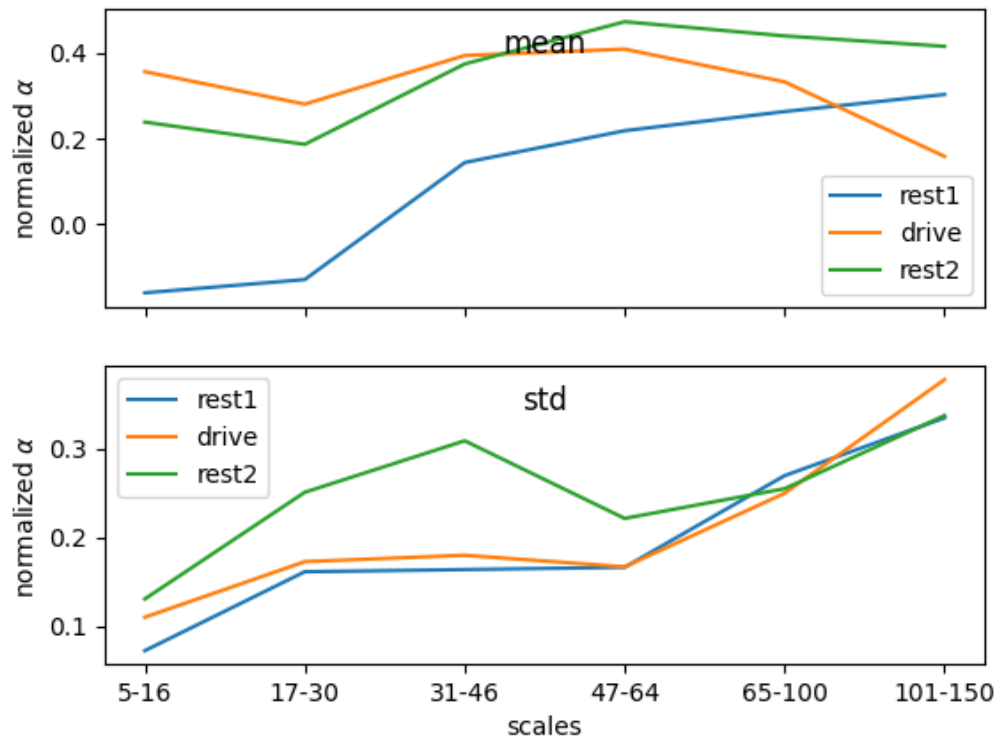


Figure C.13 Subject15: normalized DDFA alpha mean and standard deviation as function of scale.

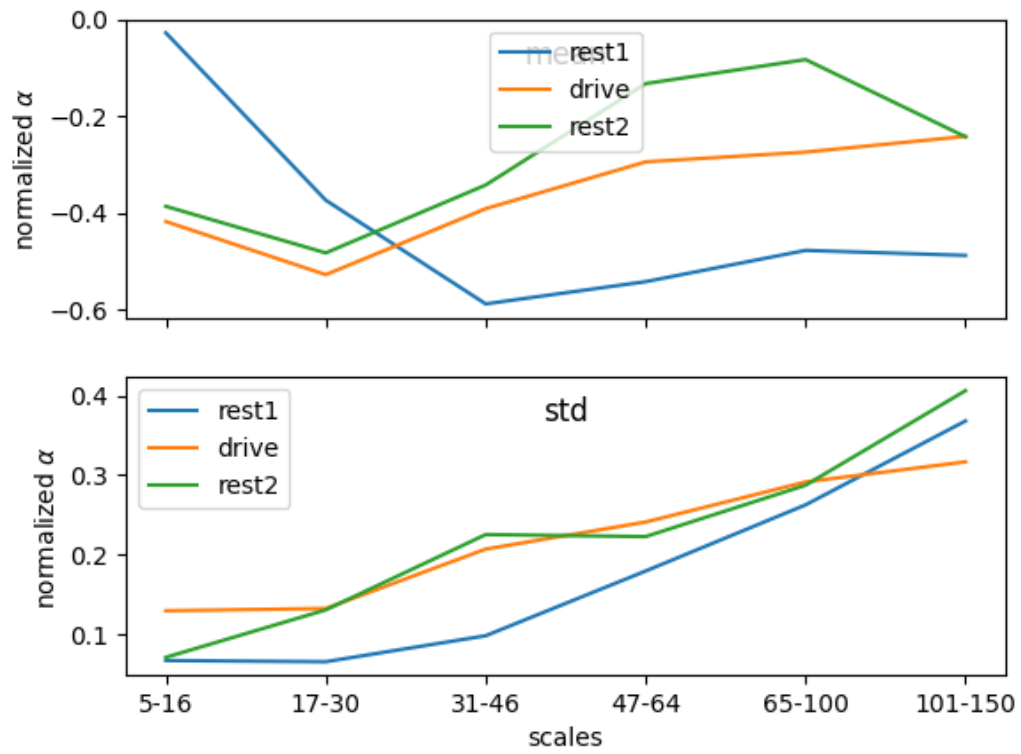


Figure C.14 Subject16: normalized DDFA alpha mean and standard deviation as function of scale.